Kinetic Investigation of Selective Alkane Activation

vorgelegt von

Diplom-Chemiker

Christian Schulz

ORCID: 0000-0002-8573-6759

Von der Fakultät II – Mathematik und Naturwissenschaften

der Technischen Universität Berlin

zur Erlangung des akademischen Grades

Doktor der Naturwissenschaften

- Dr. rer. nat. -

genehmigte Dissertation

Promotionsausschuss:

Vorsitzender: Prof. Dr. Reinhard Schomäcker

Gutachter: Prof. Dr. Matthias Drieß

Gutachter: Prof. Dr. Erhard Kemnitz

Tag der wissenschaftlichen Aussprache: 20.09.2019

Berlin 2019

Danksagung

An dieser Stelle möchte ich mich bei allen Personen bedanken, die mich während meiner Promotion unterstützt und maßgeblich zum Gelingen dieser Arbeit beigetragen haben.
Zuerst möchte ich mich recht herzlich bei Dr. Rosowski und Prof. Dr. Drieß für die Möglichkeit bedanken, meine Dissertation am BasCat BASF UniCat JointLab anzufertigen. Es war sehr spannend, ein Teil der ersten Generation von Doktoranden an einem neuen Jointlab zu sein und die damit verbundene Möglichkeiten zu erhalten ein Labor mitzugestalten. Es war eine außerordentlich schöne und lehrreiche Zeit, die ich nicht missen möchte. Insbesondere möchte ich mich für das entgegengebrachte Vertrauen sowie die guten Diskussionen bedanken. Prof. Dr. Kemnitz danke ich herzlich für die Übernahme des Zweitgutachtens. Prof. Dr. Schomäcker möchte ich für die Übernahme des Prüfungsvorsitzes danken.
Mein außerordentlicher Dank gilt Prof. Dr. Glaum und seiner Arbeitsgruppe. Ohne die gute Zusammenarbeit wäre diese Arbeit nicht möglich gewesen.
Und natürlich gilt ein großer Dank meinen Kollegen und Freunden am BasCat. Die vergangenen Jahre wären ohne eure Unterstützung nicht so angenehm und ohne unsere Salatgruppe deutlich weniger lustig gewesen. Dabei möchte ich ein paar Personen besonders hervorheben. Da wären zuerst meine Kolleginnen Stephanie Linke und Verena Strempel. Ich danke euch für die großartige Zeit mit vielen lustigen Gesprächen. Julia Bauer möchte ich für die witzige und angenehme Zeit in unserem Büro danken. Es war immer schön zu wissen, dass man gegenüber jemanden sitzen hat, mit dem man fachlich wie privat sehr gut reden kann. Ein weiterer Dank geht an Dr. Raoul Naumann d'Alnoncourt und Dr. Michael Geske. Eure Expertise im Anlagenbau und Katalyse war von unverzichtbarem Wert für diese Arbeit war. Des Weiteren möchte ich Dr. Benjamin Frank für die fachlichen, sehr spannenden Diskussionen und die gute Betreuung danken.
Prof. Dr. Schlögl und den Mitarbeitern des FHI möchte ich für die gute Kooperation danken. Ein besonderer Dank gilt dem Elektroniklabor, welches mich bei der Sicherheitstechnik gut unterstützt hat, sowie Gudrun von der Waydbrink für die Unterstützung bei der Planung und Umsetzung des Katalysatorteststands.
Lars Paasche möchte ich für den kompetenten Rat und Hilfe in allen elektrotechnischen sowie privaten Belangen danken, insbesondere für die stets offene Tür sowie die guten Gespräche beim Mittagessen.
Zum Schluss danke ich den wichtigsten Menschen in meinem Leben. Da wären meine Eltern und Geschwister, die mich immer unterstützt haben und mir diesen Weg ermöglicht haben. Meiner Freundin Julia möchte ich von ganzem Herzen danken, ohne sie wäre ich nicht so weit gekommen.

Abstract

Since the discovery of vanadyl pyrophosphate $(VO)_2P_2O_7$ (VPP) based catalysts in the 1970s, major efforts were put in understanding the reaction network of the selective oxidation of *n*-butane to maleic anhydride (MAN). Although a significant improvement of the yield could be realized since then by advanced synthesis protocols, the selectivity of MAN is limited to 70 % at an industrially relevant conversion of 80-85 %. No breakthrough could be obtained within the past decades. The main reason is the limited understanding of the active site. Further, VPP is the only catalyst, which was discussed and studied in detail. Therefore, the thermodynamically stable structure motif of vanadyl pyrophosphate was the starting point of most research efforts (Fig. 1, left).

For a basic understanding of structure reactivity relations, new structure motifs, which are different from VPP as well as catalytically active, are inevitable. One promising way to access novel crystal structures are new synthesis methods like solution combustion syntheses. With this method, metastable vanadium phosphorus oxides and mixed metal phosphate solid solutions with new structure types were synthesized, tested and compared to vanadyl pyrophosphate and β-$VOPO_4$. A fundamental requirement for selectivity of MAN was the presence of vanadium, phosphorus and oxygen. Surprisingly, the most active and selective materials were not stable under reaction conditions. XRD studies of spent materials revealed the formation of VPP as by-phase. The most promising materials were $(V_{1-x}W_x)OPO_4$ with α_{II}-$VOPO_4$ structure type (Fig. 1, right), which were found to be more active and selective in the oxidation of *n*-butane compared to β-$VOPO_4$. By adjusting the tungsten content the oxidation state of vanadium in $(V_{1-x}W_x)OPO_4$ can be tuned between 4.74 and 4.99. Stability under reaction conditions was confirmed by XRD. VPP, β-$VOPO_4$ and α_{II}-$(V_{1-x}W_x)OPO_4$ form a series of materials, which differ in structure motifs, oxidation state as well as catalytically performance (Table 1). The diversity in crystal structure and catalytic activity is an ideal starting point for a basic understanding of the reaction mechanism as well as the active site.

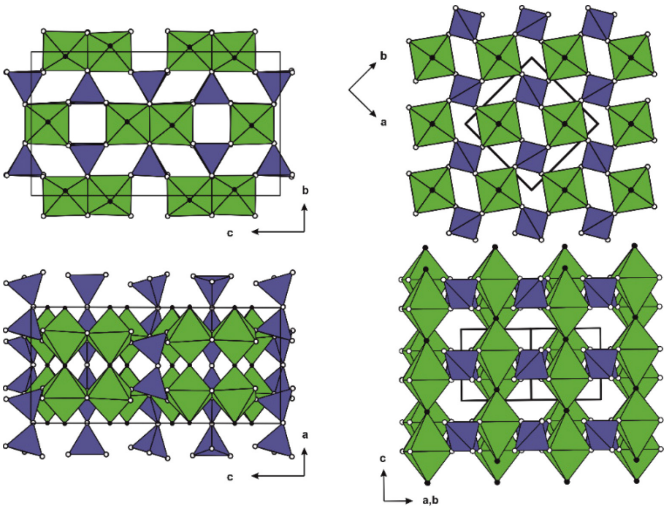

Figure 1 – Crystal structure of VPP (left) and α_{II}-$VOPO_4$ (right) with VO_6 units (green) and PO_4 units (blue). Oxygen atoms from phosphate groups are given as ○, vanadyl oxygen atoms as ●.

Table 1 – Properties of different vanadium phosphorous catalysts

Catalyst	Oxidation State of Vanadium	Space Group	S(MAN) / %
β-$VOPO_4$	5.0	*Pnma*	22
α_{II}-$V_{0.8}W_{0.2}OPO_4$	4.8	*P4/n*	30
VPP	4.0	$Pca2_1$	70

Therefore, the reaction network of *n*-butane selective oxidation was comparatively analyzed over α_{II}-$V_{0.8}W_{0.2}OPO_4$ and VPP by parameters field studies as well as co-feed and pulse experiments with presumed reaction intermediates. For VPP the selectivity to MAN is particularly sensitive to the reaction temperature, *n*-butane concentration, and the amount of co-fed H_2O. Interestingly, the selectivity to MAN over the W-containing catalyst is almost independent of all reaction parameters. However, the product spectrum is identical for both catalysts. Probing of the reaction network by pulsing of possible C4 intermediates indicates that their desorption from the catalyst surface is detrimental to MAN selectivity. The consecutive reaction of acetylene with H_2O can lead to acetic acid, whereas all other by-products are predominantly formed directly from *n*-butane. The stability of both samples was confirmed by repeated catalyst performance test under reference conditions, XRD, and SEM. A formal kinetic model including *n*-butane, MAN, CO, CO_2, acetic acid, and acrylic acid was developed, in which the acids were found to be less relevant on the $V_{0.8}W_{0.2}OPO_4$ catalyst. However, the main reaction pathways were found to be similar over both catalysts, which differ mainly in product selectivity.

If the product pattern and kinetic aspects of a catalyst under certain reaction conditions can be regarded as a sensitive fingerprint for the nanostructure of the active site of a catalyst, then the apparent similarities between VWPO and VPP point at a similarly structured active domain. Therefore, VPP is chosen as a reference system for detailed analysis with ^{18}O isotope labeling studies (Fig. 2), which gives a deeper insight in the participation of surface and subsurface oxygen as well as the contribution of bulk and amorphous phases. Further, kinetic analyses of the activation of gas-phase oxygen and the dynamics of oxygen species on the VPP surface and in the bulk were done. The results indicate the existence of at least two catalytically relevant surface oxygen species responsible for selective and unselective activation of *n*-butane, which are formed by adsorption and consecutive dissociation of O_2 at the active site. The formation of selective [O] from unselective [O_2] is likely promoted by co-fed H_2O, which increases the MAN selectivity. Regarding the VPP bulk serving as a reservoir for active [O] species it is concluded that the dynamic exchange is limited to the

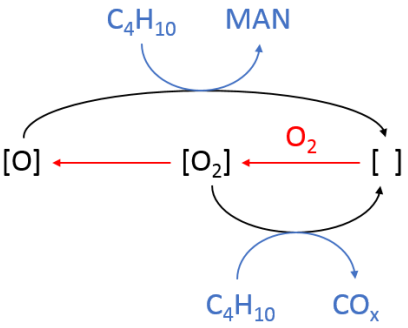

Figure 2 – Reaction scheme for *n*-butane oxidation discriminated from experimental studies.

amorphous surface layer forming under reaction conditions, whereas the crystalline bulk is not involved into the reaction but works as a support. This finding is supported by TEM studies of phase pure VPP catalysts from the literature.

Zusammenfassung

Seit der Entdeckung von Vanadylprophosphat (VPP) als Katalysator für die Butanoxidation zu Maleinsäureanhydrid (MAN) in den 70er Jahren werden der Reaktionsmechanismus sowie das aktive Zentrum kontrovers diskutiert. Industrielle Prozesse basieren heute primär auf diesem Katalysator. Die Selektivität zu MAN zeigt jedoch eine Limitierung bei ca. 70 %. Dies gilt bei industriell relevanten Umsätzen von 80-85 %. Versuche, strukturanaloge, thermodynamisch stabile Katalysatoren zu synthetisieren waren erfolglos, was letztendlich an dem begrenzten Wissen über das aktive Zentrum sowie die geringe Anzahl an Katalysatoren für diese Reaktion liegt. Die meisten Studien über Butanoxidation zu Maleinsäureanhydrid beschäftigen sich daher mit VPP als Katalysator. Dabei ist die thermodynamisch stabile Phase des VPP der Ausgangspunkt für die meisten Katalysatorentwicklungen (Fig. 1). Jedoch blieben in den vergangenen Jahren die erhofften Durchbrüche aus.

Für ein tiefgehendes Verständnis von Struktur-Reaktivität-Korrelationen, sind weitere Materialien, mit unterschiedlichen Kristallstrukturen sowie katalytischen Eigenschaften unumgänglich. Eine Möglichkeit sind daher neue Synthesemethoden, die zu neuen, metastabilen Materialien führen. Eine dieser Synthesemethoden ist die Lösungsverbrennungssynthese. Im ersten Teil dieser Arbeit wurden neue Vanadiumphosphoroxidkatalysatoren sowie Mischmetallphosphatoxide, die mittels der Lösungsverbrennungssynthese hergestellt wurden, getestet und mit den Referenzsystemen VPP und β-$VOPO_4$ verglichen. Die Anwesenheit von Vanadium, Phosphor und Sauerstoff stellte sich als notwendige Bedingung für eine katalytische Aktivität in der MAN-Synthese heraus. Überraschend war dabei, dass einige Materialien, die besonders hohe Selektivitäten zu MAN zeigten, sich unter Reaktionsbedingungen zu VPP umwandelten. Es wurde eine neue Materialklasse gefunden, die unter Reaktionsbedingungen stabil ist. Dabei handelt es sich um $(V_{1-x}W_x)OPO_4$ mit einem α_{II}-$VOPO_4$ Strukturtyp, die eine höhere Aktivität und Selektivität als β-$VOPO_4$ aufweist. Die Oxidationsstufe vom Vanadium konnte dabei durch den Wolframgehalt zwischen 4.74 und 4.99 eingestellt werden. Aus akademischer Sicht stellen VPP, β-$VOPO_4$ und α_{II}-$(V_{1-x}W_x)OPO_4$ eine interessante Serie von Materialien dar, die sich durch Struktur, Aktivität sowie Oxidationsstufe des Vanadiums unterscheiden. Um die Unterschiede zwischen den Reaktionsnetzwerken detaillierter zu untersuchen, wurde eine vergleichende Studie mit $V_{0.8}W_{0.2}OPO_4$ und VPP durchgeführt. Es wurden Parameterfeldtests, Codosierungsstudien sowie Pulsexperimente mit erwarteten Reaktionsintermediaten durchgeführt. Dabei wurde eine Korrelation zwischen der Selektivität von MAN und der Reaktionstemperatur, *n*-Butankonzentration sowie der Menge an dosiertem Wasser für VPP gefunden. Für $V_{0.8}W_{0.2}OPO_4$ hingegen konnte keine Korrelation gefunden werden. Das Produktspektrum war für beide Systeme identisch. Pulsstudien von

potenziellen C4 Intermediaten lieferten erste Hinweise, dass deren Ad-/Desorption an der Katalysatoroberfläche einen negativen Effekt auf die MAN Selektivität hat. Die Stabilität der Katalysatoren wurde durch SEM- und XRD-Messungen bestätigt. Basierend auf den Parameterfelddaten wurde ein formal kinetisches Model entwickelt. Der Einfluss der Säuren war dabei weniger signifikant für $V_{0.8}W_{0.2}OPO_4$ und wurde daher nicht modelliert. Beide Reaktionsnetzwerke zeigten dabei eine hohe Ähnlichkeit miteinander auf, die sich primär nur in der Selektivität für MAN unterscheidet.

Unter der Annahme, dass das Produktspektrum sowie die kinetischen Merkmale eines Katalysators einen Rückschluss auf das aktive Zentrum zulassen, ist es naheliegend, dass beide Katalysatoren ein ähnliches aktives Zentrum haben. Daher wurde VPP als Referenzsystem weitergehend untersucht. Es wurden dabei Isotopenstudien mit $^{18}O_2$ sowie weitere kinetische Analysen aller Sauerstoffspezies (Gasphase, Oberfläche und Kristallgitter) durchgeführt. Dabei wurden Indizien für die Existenz zweier aktiver Sauerstoffspezies gefunden, die durch Adsorption und nachfolgender Dissoziation von Sauerstoff entstehen. Eine Sauerstoffspezies ist dabei für die selektive Umsetzung relevant, wohingegen die andere Spezies zur Bildung von CO_x führt. Die Bildung von selektiven [O] aus unselektiven [O_2] wird in Anwesenheit von Wasser begünstigt, was die Selektivität zu MAN erhöht. Der dynamische Austausch von aktiven Sauerstoffspezies ist dabei auf eine amorphe Grenzschicht an der Oberfläche begrenzt. Das Kristallgitter hingegen ist nicht beteiligt, sondern fungiert als Träger für die Grenzschicht. Diese Theorie wird von aktuellen TEM-Studien von phasenreinen VPP Katalysatoren unterstützt.

Erklärung zur Dissertation

Ich erkläre hiermit, dass ich bislang an keiner anderen Hochschule oder Fakultät meine Promotionsabsicht beantragt habe.
Die vorliegende Dissertation wurde bereits in Form von wissenschaftlichen Publikationen veröffentlicht. Es handelt sich hierbei um die folgenden Veröffentlichungen (chronologisch nach Einreichung):

Paper 1: α_{II}-$(V_{1-x}W_x)OPO_4$ catalysts for the selective oxidation of *n*-butane to maleic anhydride

Christian Schulz, Subrata Chandra Roy, Knut Wittich, Raoul Naumann d'Alnoncourt, Stephanie Linke, Verena Strempel, Benjamin Frank, Robert Glaum, Frank Rosowski

Catalysis Today 333 (**2019**) 113-119
https://doi.org/10.1016/j.cattod.2018.05.040

Eigenteil: Erstautor; In dieser Publikation wurden neue Materialien für die Oxidation von *n*-Butan zu Maleinsäureanhydrid untersucht. Dabei wurden verschiedene Mischmetalloxide basierend auf Vanadium, Molybdän und Wolfram hergestellt und getestet. Dabei zeigten Katalysatoren mit einer Zusammensetzung von $(V_{1-x}W_x)OPO_4$ mit einem α_{II}-$VOPO_4$ Strukturtyp als besonders aktiv. Die Materialien wurden von der Arbeitsgruppe von Prof. Dr. Glaum hergestellt und charakterisiert. Die Katalytische Studie wurde von mir geplant. Die katalytischen Messungen sowie Auswertungen der Daten wurden von mir durchgeführt. Dabei hatte ich die Unterstützung von Dr. Raoul Naumann d'Alnoncourt. Das Manuskript wurde von mir angefertigt. Alle Autoren haben das finale Manuskript diskutiert und der Veröffentlichung zugestimmt.

Paper 2: Selective Oxidation of *n*-Butane over Vanadium Phosphate Based Catalysts: Reaction Network and Kinetic Analysis

Christian Schulz, Felix Pohl, Matthias Driess, Robert Glaum, Frank Rosowski, Benjamin Frank

Industrial & Engineering Chemistry Research **2019**, 58, 7, 2492-2502
https://doi.org/10.1021/acs.iecr.8b04328

Eigenteil: Erstautor; In dieser Publikation wurde das Reaktionsnetzwerk der Oxidation von *n*-Butan zu Maleinsäureanhydrid für VPP und α_{II}-$V_{0.8}W_{0.2}OPO_4$ untersucht. Stoff- und Wärmetransportlimitierung wurde untersucht sowie die Einflüsse der Partialdrücke von *n*-Butan, Sauerstoff, Wasser und der Verweilzeit. Zusätzlich wurden Reaktionsintermediate zum Reaktionsgas über einen kontinuierlichen Fluss oder einem definierten Puls hinzugefügt. Die Studie wurde von mir geplant. Die Reaktionsparametervariation beider Katalysatoren sowie die Pulsstudien über VPP wurden von mir durchgeführt und ausgewertet. Das kinetische Modell wurde von Dr. Benjamin Frank erstellt und gefittet. Das Manuskript habe ich angefertigt. Alle Autoren haben das finale Manuskript diskutiert und der Veröffentlichung zugestimmt.

Paper 3: Selective Oxidation of *n*-Butane over Vanadium-Phosphorus Oxide: Oxygen Activation and Dynamics

Christian Schulz, Ralph Krähnert, Frank Rosowski, Benjamin Frank

ChemCatChem 10 (*23*), **2018**, 5523-5532.
https://doi.org/10.1002/cctc.201801177

Eigenteil: Erstautor; In dieser Veröffentlichung wurde anhand von kinetischen Messdaten ein Mechanismus für die Aktivierung von Gasphasensauerstoff in der Oxidation von *n*-Butan zu Maleinsäureanhydrid für VPP vorgeschlagen. Zudem wurde die Dynamik von Festkörper- und Oberflächensauerstoff mittels Isotopenexperimenten genauer untersucht. Dabei wurde eine amorphe Grenzschicht als katalytisch aktive Phase für VPP identifiziert. Die Studie wurde von mir geplant. Die kinetischen Daten sowie die Isotopenaustauschexperimente wurden von mir durchgeführt und ausgewertet. Das Manuskript habe ich angefertigt. Alle Autoren haben das finale Manuskript diskutiert und der Veröffentlichung zugestimmt.

Jeweils ein Exemplar der hier aufgeführten Publikationen ist dieser Dissertation beigefügt.

_____	_____
Ort, Datum	Christian Schulz

Table of contents

List of Abbreviations

Abbreviation	Description
AceA	Acetic Acid
AcrA	Acrylic Acid
ALD	Atomic Layer Deposition
FID	Flame Ionization Detector
GC	Gas Chromatograph
GHSV	Gas Hourly Space Velocity
HRTEM	High Resolution Transmission Electron Microscopy
MAN	Maleic Anhydride
MFC	Mass Flow Controller
MS	Mass Spectrometer
S	Selectivity
SBA	Santa Barbara Amorphous
SCS	Solution Combustion Synthesis
SEM	Scanning Electron Microscopy
SSITKA	Steady State Isotope Transient Kinetic Analysis
TCD	Thermal Conductivity Detector
TEP	Triethyl Phosphate
THF	Tetrahydrofuran
TPO	Temperature Programmed Oxidation
VPP	Vanadyl Pyrophosphate
VPO	Vanadium Phosphorus Oxide
VWPO	Vanadium Tungsten Phosphorus Oxide
wt	Weight
X	Conversion
XPS	X-ray Photoelectron Spectroscopy
XRD	X-ray Diffraction
Y	Yield

1 Introduction

1.1 Objective

The goal of this research project is a detailed investigation of the selective oxidation of *n*-butane with molecular oxygen to gain a deeper understanding of the reaction pathway for selective oxidation and the nature of the active site. The targeted reaction product is maleic anhydride, which plays an outstanding role in the petrochemical industry[1]. The state of the art catalyst is based on vanadyl pyrophosphate (VPP)[2,3]. Alternative catalysts are poorly described in the literature[4]. Therefore, the first milestone is the identification of novel materials. Different materials are synthesized, tested and compared to VPP. As a second milestone, the most relevant material is used for a more detailed, comparative study. In a first step parameters field studies of the novel catalyst and the industrial VPP are performed as well as pulse studies of promising reaction intermediates. The formal kinetic models are derived from the data and compared. The last milestone is a detailed analysis of the surface dynamics of oxygen. Therefore, isotope labeling studies with $^{18}O_2$ of at least one catalyst are carried out to clarify the role of oxygen.

The crucial requirements for all milestones include planning, construction as well as physical and chemical validation of suitable test setups. Therefore, a commercial parallel test setup is used for the identification of novel materials and parameters field testing. A self-constructed transient test setup is used for the isotope labeling as well as pulse studies. Cofeed studies are conducted on both setups.

1.2 Motivation

One of the main challenges inside today's society is the efficient use of natural resources[5]. Natural gas and oil are mainly based on saturated alkanes, which need to be activated in the first step, e.g. by oxidation. In particular, the direct selective activation of small alkanes to valuable oxygenates is quite challenging[6,7]. Oxygenates like methanol[8], acetic acid[9] or acetone[10] are produced via costly, multistep synthesis routes in the petrochemical industry or from valuable unsaturated hydrocarbons.

One of the rare examples for direct oxidation of alkanes to oxygenates is the selective oxidation of *n*-butane to maleic anhydride. This reaction is catalyzed by VPP[11], which is a transition metal phosphate catalyst. Metal oxides are the dominating catalysts in heterogeneous partial oxidations[12]. Due to the multi-

functionality of metal oxides, there is a great interest in the clarification of the kinetic, mechanistic and structural properties of these systems to enable a rational catalyst design. An interesting feature of metal oxide catalysts is the allocation of bulk oxygen. One of the possible reaction mechanisms was described first by P. Mars and D. W. van Krevelen[13]. In a first step the bulk oxygen reacts with the substrate. During the second step, bulk oxygen moves to the catalyst surface. In the final step, the catalyst is reoxidized. The mechanism is called Mars-van-Krevelen mechanism. They showed that bulk oxygen of vanadium oxide is used in the oxidation of benzene, toluene, naphthalene and anthracene.

This work reports a fundamental study over the state-of-the-art catalyst VPP as well as a novel mixed metal catalyst VWPO. Many compositions containing VPP phase have been successfully used as heterogeneous catalysts under conditions where the selectivity to maleic anhydride is in excess of 50 % at high conversions[14]. Although the productivity of this process could be steadily improved over the past decades, the yields are still below 65 %, which is mainly limited by selectivity[2,4,11,15–18]. Numerous studies were dedicated to analyzing the active sites and to understanding reaction kinetics, respectively. Due to its topotactic nature, the synthesis method strongly influences the formation of several vanadium-phosphorus oxide (VPO) by-phases on the VPP bulk leading to a rich number of catalysts with different catalytic performances[19–25]. The most successful synthesis leading to a high surface material providing high activity and selectivity is based on the organic route using alcohol, V_2O_5, and phosphoric acid[23].

The byproducts of *n*-butane oxidation are mainly carbon dioxide and carbon monoxide. These total oxidation pathways consume far more oxygen than the production of MAN. One of the key questions is the utilization of bulk oxygen and its role in selective and non-selective pathways. Further, the amount of bulk oxygen needs to be quantified in detail.

For a good understanding of this type of reaction, a precise kinetic model is needed as well as detailed understanding of the role of oxygen. Kinetics can be obtained by parameters field studies[26]. However, the parameter variation requires a long time-on-stream and catalysts need to be stable over a long period. A good way to accelerate data acquisition is parallel testing with high throughput setups. The principle of high throughput testing is the parallel testing of reaction parameters, which is different from traditional testing, where reaction conditions are tested

sequentially[27]. Although the number of measurements over a defined time is identical, parallel testing enables the acquisition of more reaction conditions with a lower time resolution.

The role of oxygen is hard to understand only from steady state kinetic studies. Therefore, isotope labeling is a good way to reveal new insights, e.g. steady-state isotopic-transient kinetic analysis (SSITKA)[28–31]. SSITKA has been used in a number of studies to determine *in situ* kinetic information about the reaction mechanism and the catalyst-surface reaction intermediates.

1.3 State of the Literature of Vanadyl Pyrophosphate

The literature on the selective oxidation of *n*-butane to maleic anhydride is rich. A detailed review was published by Centi et al. in the 90s[2]. The reaction is interesting for industry and academia as it is an extensive oxidation, with the cleaving of eight C–H bonds and the introduction of three oxygen atoms, yet it still manages to occur selectively. The process is a fourteen - electron oxidation, in comparison to other selective oxidation processes, which only require a maximum of four electrons. Due to this highly complex nature, many aspects of the reaction and the active site are still under debate. However, the following statements are accepted by a wide part of the community:

1. The most active and selective catalyst is based on $(VO)_2P_2O_7$ (VPP)[2].
2. VPP is the main phase of the catalyst[32].
3. Under lean reaction conditions, the oxidation state of the bulk catalyst is close to 4+[33].
4. Phosphorus is enriched on the surface[34].
5. Vanadium with the oxidation state 5 plays an important role[35].
6. The rate determining step is the *n*-butane activation by hydrogen abstraction[18].

Several factors have been identified as crucial for the active catalyst. The P/V ratio of the precursors is important and should be in the favor of phosphorus[36]. Thermal treatment time and activation temperature as well as the gas phase composition affect catalyst composition. Variation of these parameters results in a variety of crystalline phases. X-ray diffraction studies of the activated catalyst showed that VPP is dominantly present[37]. However, by-phases like α_{II}-$VOPO_4$ were identified (Figure 3). Derived from this finding it is assumed that VPP plays an important role in the

oxidation of *n*-butane to maleic anhydride. Inumaru et al. investigated different crystal faces of VPP[38]. VPP was deactivated by the surface deposition of SiO_2. The crystallites were fractured to expose the side facets like the (021) and (001) facets, which were found to be non-selective for maleic anhydride formation. Concluded from this result and other publications, most hypothesis assume the (100) face of VPP as the selective one, but it can also be a combination of phases responsible for the reaction[39–46]. First high resolution transmission electron microscopy (HRTEM) studies supported this hypothesis[47]. However, the sensitivity of VPP to electron beams should be considered. TEM studies conducted by Schlögl and coworkers show that equilibrated VPP catalysts have a visible, amorphous surface layer, which is not stable under the TEM conditions[6].

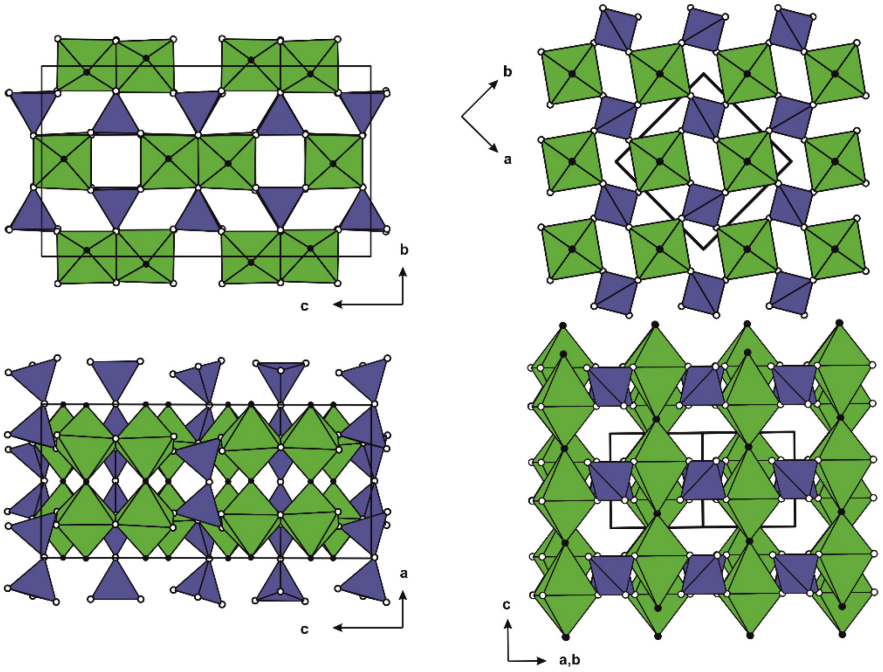

Figure 3 – Crystal structure of VPP (left) and α_{II}-$VOPO_4$ (right) with VO_6 units (green) and PO_4 units (blue). Oxygen atoms from phosphate groups are given as ○, vanadyl oxygen atoms as ●.

Another important aspect is the oxidation state of the vanadium. Most studies support that the final oxidation state is between +4.00 and +4.40[18,33,48–50]. The oxidation states of vanadium are correlated with different phases of vanadium, V^{5+} and V^{3+} phases might be important.

Guilants et al. prepared a series of vanadium phosphate catalysts containing different $VOPO_4$ phases beside VPP[51]. The experimental result showed that the $VOPO_4$ phases are detrimental to the performance of catalyst, supporting that VPP is the selective active phase. This result was supported by Cavani and Trifirò who

suggested that over oxidation of maleic anhydride to carbon oxides is catalyzed over V^{5+} sites[52].

A decent amount of publications does not support the single-phase theory. An in-situ formation of V^{5+} phases under reaction conditions as a result of a redox mechanism is suggested[53–55]. It is stated that oxygen associated with V^{4+} activates *n*-butane while oxygen associated with V^{5+} is later incorporated in the oxygen groups of MAN later. V^{4+} phases are highly active, but have a poor selectivity, while V^{5+} phases yield high selectivity, but low activity. Evidence for this mechanism was found by XPS studies of Culston et al.[56], TAP studes by Rodemerck et al.[57–59] and Lorence et al. [60]. In the absence of V^{5+} sites, the main reaction product was furan. In the presence of V^{5+} sites MAN was produced. Hutchings et al. proposed a V^{4+}/V^{5+} redox couple as the active site[61]. The active phase consists of a dispersed micro-crystalline $VOPO_4$ on a VPP matrix. Centi et al proposed that V^{5+}/V^{4+} couple is required for the final conversion of *n*-butane to MAN. However, V^{4+}/V^{3+} couple is needed for the activation of *n*-butane[62–64]. Recent studies by Eichelbaum et al. showed that the bulk electronic conductivity can be correlated with the selectivity for MAN by using microwave cavity perturbation technique. Additional in situ XPS studies showed that the reversible oxidation state change of the V^{4+}/V^{5+} redox couple is restricted to the topmost surface layers[49].

The phase, which contains the V^{5+}, is heavily debated[35,52]. Many possible vanadium phosphorus oxide phases have been found in VPP based catalysts and correlated with selectivity for MAN. The most commonly found phases in VPP are α_{II}-$VOPO_4$, γ-$VOPO_4$ and δ-$VOPO_4$[65,66]. Recently, ω-$VOPO_4$ has been identified inside the surface layer of VPP, which are activated in slightly reducing conditions[67]. Other modifications like β-$VOPO_4$ were not found. The crystal structures of β-$VOPO_4$, γ-$VOPO_4$, δ-$VOPO_4$ and ω-$VOPO_4$ are shown in Figure 4.

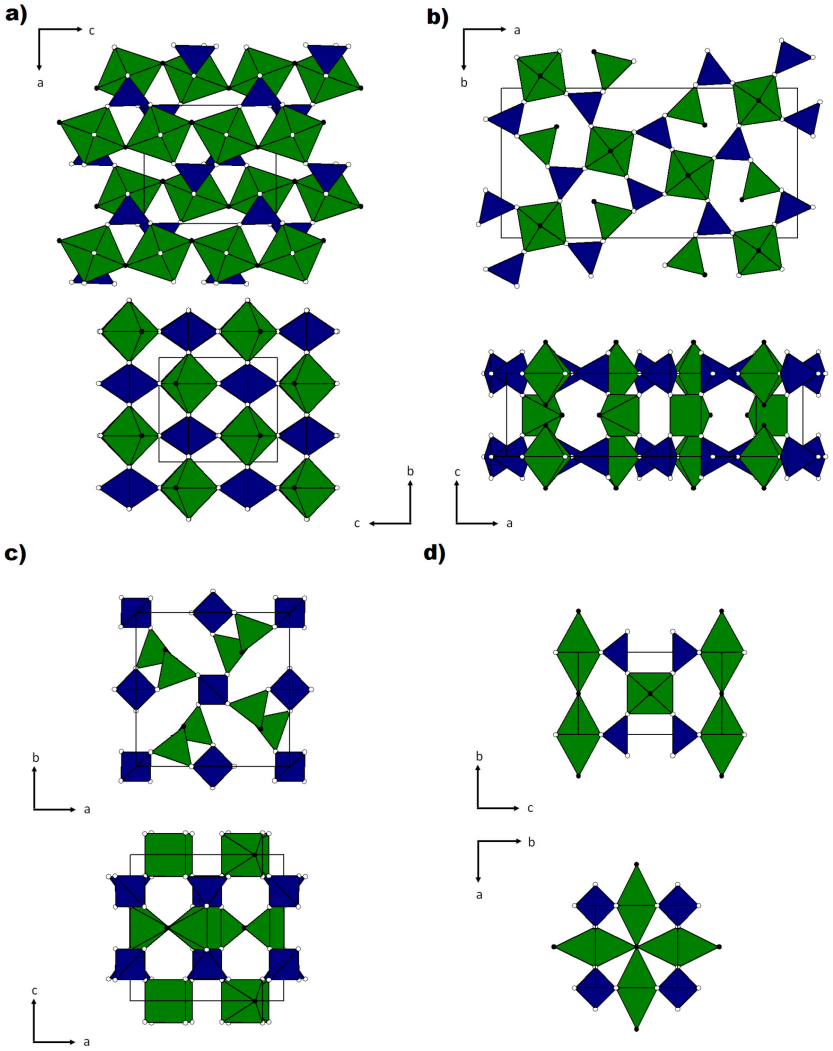

Figure 4 – Crystal structure of β-$VOPO_4$ (a), γ-$VOPO_4$ (b), δ-$VOPO_4$ (c) and ω-$VOPO_4$ (d) with VO_6 units (green) and PO_4 units (blue). Oxygen atoms from phosphate groups are given as ○, vanadyl oxygen atoms as ●.

Beside the crystalline phases, different discussion focusses on the role of amorphous materials, which are commonly found in vanadium phosphate catalysts. The activation of industrial catalysts takes more than 1000 h before the catalyst reaches a steady state[53]. During the activation process, the crystallinity of the catalyst increases leading to the hypothesis that the crystallinity improves the performance. A study by Guilants and coworkers showed that an amorphous layer can be found on fresh catalyst, which disappears under reaction conditions[68]. Nevertheless, other researches consider the active site within an amorphous layer on a supported VPP matrix. Due to the simultaneous presence of amorphous and crystalline phases, it cannot be stated with certainty, which phase is active. However, there are several publications, which support this finding. Ruiz et al. studied high and low P/V ratio catalysts[34]. Since the ratio for VPP is fixed with V/P=1:1 and other by-phases could

not be detected, it led to the hypothesis that active catalyst is based on VPP and an amorphous layer, with a high oxidation state near +5. Morishige et al. suggested that the amorphous layer is enriched with phosphorus[25]. Selective extraction of the amorphous phase supported this theory. Further, catalytic testing yielded the same activity and selectivity as VPP, suggesting that the amorphous phase is catalytically active. The amorphous phase is described as enriched with phosphorus, which explains the high P/V ratios found experimentally[34,52,69–71].

The influence of phosphorus on the selective of *n*-butane oxidation was also shown in recent studies by Strempel et al. Vanadium pentoxide is used as starting material for VPP based catalysts. It shows low selectivity for MAN. Modification of the surface with phosphorus introduced by ALD techniques leads to a significant increase in selectivity[72–75].

Studies with in situ Raman showed that precursors, prepared in aqueous solution, show structural disordering at 370°C during activation[66]. Under this condition the active catalyst is formed and could be correlated with the formation of MAN. This disordering was also found at lower temperatures around 300°C, when MAN was added to the reaction mixture. This study demonstrates nicely the influence of substrates on the structural transformation. It also shows that disordered structure might be important for selective *n*-butane oxidation. Hutching et al. studied cobalt doped catalysts[61]. Cobalt is used as a promotor and increase the performance of VPP. Sajip et al. found that cobalt-promoted catalysts are more disordered compared to undoped ones[76]. Interestingly, cobalt cannot be found in the bulk, but highly dispersed in the amorphous phase. The effect of the cobalt promotor might be the stabilization of the disordered phase as well as the V^{5+} phases. Hutching et al also prepared vanadium phosphate catalysts via supercritical precipitation methods[77–79]. XRD and electro diffraction analysis showed that the materials were amorphous. However, the performance was comparable to crystalline reference catalysts. This study supports the hypothesis that active phase might be located inside the amorphous layer. Schimoda and coworkers as well as other scientists have studied amorphous V^{4+} phases, which are less selective compared to crystalline VPP catalysts[80].

Several studies were dedicated the correlation between disordered planes and catalytic performance. Cavani et al. could show the precursors prepared in aqueous medium have greater crystallinity compared to precursors prepared in organic

solvents[32]. The organically prepared catalysts were more active in the *n*-butane oxidation, which was explained by some disorder in the (100) plane.

The reason for the disorder was explained by intercalation of organic compounds between the vanadium phosphate layers[19]. The disorder might come from structural modifications of the catalyst precursor. The kind of disorder might have unique effects on the catalytic performance. Cornaglia et al could show that selectivity for MAN correlates with the decrease of disorder in the (100) plane[81].

At this point it should also be mentioned that acid-base properties of the catalyst might be important for the catalyst performance. Infrared studies showed that Lewis and Brønsted sites are present on the catalyst surface[52,81–84]. Further, a correlation between strong Lewis acid sites and selectivity for MAN was found. Centi et al suggested that the Brønsted sites play an important role, since the surface is enriched with phosphorus, which result in the presence of P-OH groups[85]. These groups might be important in the stabilization of reaction intermediates. However, chemisorption studies with acetonitrile and pyridine by Cornaglia and coworkers showed no correlation between catalyst performance and either Lewis/Brønsted site ratio or the Lewis acid site concentration[81].

Besides the excellent performance of VPP for the selective oxidation of *n*-butane to maleic anhydride, VPP was found to be an efficient catalyst for the oxyfunctionalization of light paraffins in general like the oxidation of ethane to acetic acid[37], the oxidation of propylene to acrylic acid[86] as well as the oxidation of *n*-pentane to maleic and phthalic anhydrides[50,87–93].

1.4 Mechanism of *n*-Butane Oxidation

In total 14 electrons are transferred during the partial oxidation of *n*-butane to MAN. Although the active phase is still under debate, most mechanisms are based on (100) plane of vanadyl pyrophosphate. The most supported mechanism in the literature is a consecutive alkenyl mechanism[41–46,84]. At first *n*-butane is adsorbed onto the vanadium phosphate surface, where it is transformed via adsorbed alkenyl intermediates into maleic anhydride (Scheme 1).

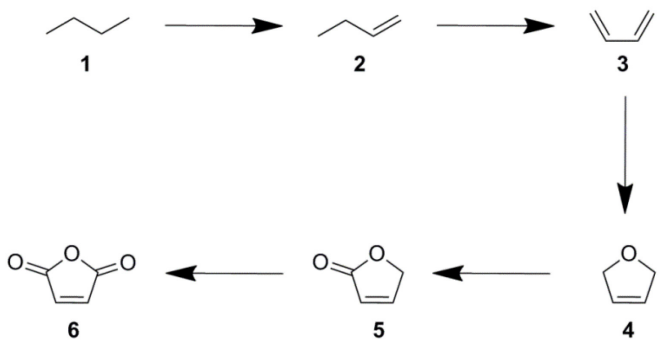

Scheme 1 – Consecutive alkenyl mechanism

The first step is the hydrogen abstraction from *n*-butane(**1**), yielding 1-butene(**2**), followed by further hydrogen abstraction to form 1,3-butadiene(**3**). An electrophilic oxygen atom on the catalyst surface is inserted producing dihydrofuran(**4**). Partial oxidation of dihydrofuran leads to the asymmetric lactone(**5**). The final oxidation of the remaining methylene group yields maleic anhydride(**6**).

Most evidence for this type of mechanism comes from TAP experiments. Gleaves and Centi detected all non-oxygenates under fuel-rich conditions in the same order proposed the reaction mechanism[43]. These experimental results are supported by Schiott and Jorgensen et al, who suggested that oxygen is adsorbed in an η^2-peroxo coordination mode[41,42]. Furan is formed by oxygen insertion into adsorbed 1,3-butadiene. They found evidence in the favorable overlap of the sigma-C-H-bond and the antibonding sigma-O-O bond. However, it should be kept in mind that the experimental results are measured under vacuum conditions, which are far away from industrial relevant ones.

The active oxygen species were investigated by Abon et al., using isotopic labeling experiments[40]. Under initial reaction conditions, the products contained only lattice ^{16}O. In the course of the reaction, the isotopic labeling occurs and more ^{18}O atoms are incorporated into the products. From these results, it was concluded that lattice oxygen was the active oxygen species, which is replenished by gas-phase oxygen.

Recent theoretical studies by Goddard et al. introduce a novel reaction model, *i.e.*, a reduction-coupled oxo activation (ROA) mechanism responsible for the catalytic selective activation and functionalization of *n*-butane to MAN over P-based active site[94,95].

1.5 Alternative Catalysts for *n*-Butane Oxidation

The literature only focuses on vanadium phosphorus catalysts[2]. The simultaneous presence of all elements (V, P, O) seems to be indispensable.

Many well characterized, crystalline vanadium phosphate phases have been identified, whose structure and catalytic properties have been intensively discussed in the literature. The most detailed studied systems are the V^{5+} vanadyl orthophosphates (*α*- , *β*- ,*γ*- , *δ*-, *ε*- and *ω*-$VOPO_4$, and $VOPO_4 \cdot 2H_2O$), and the V^{4+} vanadyl hydrogen phosphates ($VOHPO_4 \cdot 4H_2O$, $VOHPO_4 \cdot ½H_2O$, $VO(H_2PO_4)_2$), vanadyl pyrophosphate ($(VO)_2P_2O_7$) and vanadyl metaphosphate ($VO(PO_3)_2$)[37,51,80,96,97]. Within these compounds, $VOHPO_4 \cdot ½H_2O$ (vanadyl hydrogen phosphate hemihydrate) is of particular interest as a catalyst precursor, which after activation gives a catalyst mainly composed of $(VO)_2P_2O_7$ (vanadyl pyrophosphate, hereafter VPP).

Catalysts, which are not based on VPP are rarely described. A detailed study was dedicated to find thermodynamically stable catalysts with similar structure motifs to VPP or other vanadium phosphate phases[98]. In total 29 hitherto unknown vanadayl(IV)-, vanadyl(V)- and vanadate(V) phosphates were synthesized, characterized and catalytically tested. None of the tested materials were found to be an interesting catalyst for *n*-butane oxidation. In a recent patent, tungsten phosphates with a ReO_3 structure type were found to be an interesting class of materials for *n*-butane oxidation. Some of the materials are comparable to VPP based catalysts regarding selectivity of MAN. However, they show quite low activity. Nevertheless, this class of material might be promising in future studies.

1.6 Steady State Transient Kinetic Analysis

Steady-state isotopic-transient kinetic analysis (SSITKA) is a powerful tool for the kinetic study of heterogeneous catalytic reactions. The SSITKA technique was initially developed by Happel[99], Bennett[29], and Biloen[100]. It has been used in several studies to determine *in situ* kinetic information about the reaction mechanism and the catalyst-surface reaction intermediates. It is based upon the detection of

isotopic labels in the reactor effluent species versus time following a switch (step change) in the isotopic labeling of one of the reactant species in the reactor feed. To maintain steady state conditions, isothermal and isobaric reaction conditions, the reactant and product concentrations and flow rates must remain undisturbed during the step change. This is realized by adaption of the pressure and flow of the isotopically labeled line to the non-labeled one, which is basically the pressure of the reaction and the pressure drop of the packed reactor. Furthermore, kinetic isotope effects must be avoided[101], which is important for labeling with deuterium. In case of ^{18}O atoms, the effect is negligible. The reaction intermediates present on the catalyst surface do not change, and unlike for other transient techniques, analysis of the steady-state kinetic behavior of the catalyst surface is possible. The SSITKA techniques gives access to the concentration of different types of adsorbed reaction intermediates, coverages, surface residence times, site heterogeneity, activity distributions, and certain aspects of possible mechanisms. A typical response of a SSITKA experiment inside a plug flow reactor (PFR) can be found in Figure 5.

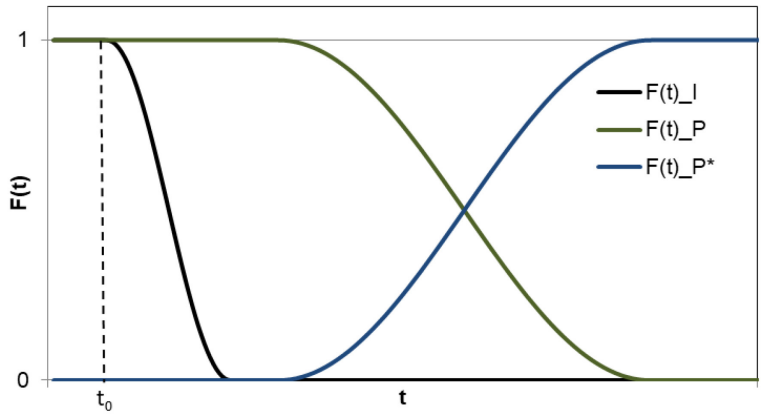

Figure 5 – Normalized transient response (F). Product (P) is replaced by its isotopically labelled equivalent (P*). An inert tracer (I) is used for correction of the gas-phase hold-up[28].

The isotope labeling is introduced by a step-change of the feed, which subsequently appears in the products. An inert tracer is used in SSITKA for determination of the gas-phase holdup for the reactor system. It is often added in small concentration of inert in either of the isotopic-tracer feed streams during the step change.

Inside a typical heterogeneous reaction, reactants are introduced over the gas-phase, adsorb and react to intermediates, which are desorbed in the gas-phase again. Under steady state conditions, the concentration of all species remain constant. The catalyst surface can be visualized as different interconnected pools of species, which are statistically labelled in the course of isotope exchange. The

isotopes are exchanged subsequently in each pool until all products are labelled. Integration of the reaction rate or normalized transient response yield the number of surface intermediates or the overall mean surface-residence time. Both number are corrected by the area of the inert.

The kind of the decay curve provides information about parallel and consecutive reactions as well as the surface coverage. Therefore, the kinetics need to be understand in detail and the active site needs to be quantified. At this point, it should be mentioned that diffusion and adsoprtion effects of the reactant and products needs to be considered. SSITKA can also be used for CSTRs.

Shannon und Goodwin et al. summerized in a detailed review all reaction, which are used for SSITKA so far. The studies mainly focused on CO hydrogenation with supported metal catalysts. Metal oxides are rarely researched. The most interesting studies here were done by Vogel et al. on the selective oxidation of propylene to acrylic acid[31,102].

1.7 Maleic Anhydride in the Industrial Value Chain

MAN production was one of the first industrial processes, which started in 1933 based on benzene[103]. Until the 1960s, benzene was the only raw material available for industrial production of MAN. Supported V_2O_5-MoO_3 catalysts were used in the industrial process. Compared to the *n*-butane route, the benzene oxidation has always carbon dioxide as a by-product. In the late 1970s, when pollution laws that restricted benzene emissions came into effect and prices for benzene increased, industry began to use the *n*-butane route[104]. Although the first plant based on *n*-butane was put into operation in the US in 1974 by Monsanto[105], the feed stock change took decades. In 1991, 36 % of the world capacity for MAN production was based on benzene[1]. Beside *n*-butane, 1-butene and butadiene can also be used as a feedstock[106]. The catalysts are based on vanadium phosphorus oxides doped with promotors like Nb, Cu or Li[107]. Compared to *n*-butane oxidation the exothermicity was lower, which lead to better control of the process. However, the cost of *n*-butane is significant lower. MAN is also produced as a by-product in the selective oxidation of *o*-xylene to phthalic anhydride[108]. Based on the phthalic anhydride capacity around 5 wt% of MAN can be recovered with high purity of 99.5 %[109]. The total capacity for MAN production was roughly 1 million metric tons in 2006[1]. An overview of all reaction is shown in Scheme 2.

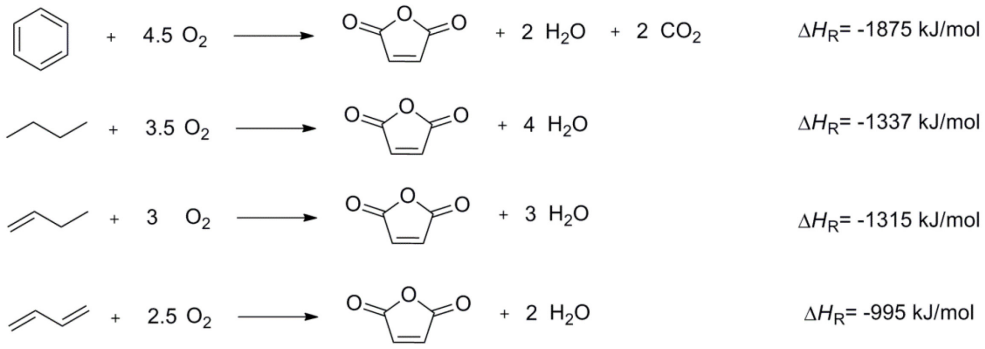

Scheme 2 – Different feedstock for MAN production

MAN is primarily used as a co-monomer for unsaturated polyester resins, which are important plywood manufacture and reinforced plastics. Further, it is used for agricultural chemicals, dye intermediates or pharmaceuticals. Fumaric and tartaric acid are also important chemical intermediates, which are based on MAN.

In a first step MAN is hydrogenated to 1,4-butanediol, which is used for production of polyurethanes. MAN can also be hydrogenated to THF, which can be further polymerized to poly-THF. Further, it can be easily hydrated to maleic acid or isomerized to fumaric acid[5].

In the chemical value chain MAN production from *n*-butane competes with Reppe chemistry. Acetylene and formaldehyde react over copper catalysts to 2-butyne-1,4-dioldiol, which is hydrogenated to 1,4-butanediol[1]. Acid catalyzed dehydration leads to THF[110]. Depending on the raw material prices, both processes are relevant for industrial production of MAN.

1.8 Improvement of Yield of MAN over the Past Decades

The industrial production of MAN over VPP has some limitation, which will be addressed in this chapter. The first patent was claimed in 1966 by Princeton Research. The selectivity was not reported, but the yield of MAN was quite low with 33 %[111]. The temperature was around 500-600 °C. The catalyst was prepared by an aqueous synthesis route, which is known for low specific surface areas of the catalyst[19,24]. As a result, high temperatures were needed for sufficient activity, which decreases the selectivity of MAN. Therefore, other important parameters as P:V ratio of 1.1 and cofeed of water were identified as crucial.

Monsanto developed improved synthesis protocols for VPP by the aqueous route[105]. The synthesis was quite similar to the first patent, but temperature treatment of the catalyst precursor was improved. The treatment is important as the equilibration of

the optimal V^{4+}/V^{5+} ratio of the active phase and by-phases under controlled atmosphere will influence the performance of the catalyst. The reaction temperature could be decreased from 500 °C to 350 °C. Due to this major improvement, the first plant was built. One of the main challenges is the heat removal. Therefore, a multi tubular reactor with salt bath for heating was chosen due to its good heat transfer properties[111,112].

The last major step forward was the switch from the aqueous to organic routes. Halide acids like hydrochloride were found to be good and mild reduction agents for the reduction of V^{5+} to V^{4+}[23]. The main innovation was substitution of corrosive HCl with iso-butanol, which lead to significant increase in MAN yield. The Standard Oil Company reported VPP based on the organic route, which gave 54.2 % yield of MAN at 380 °C, while in the reduction with HCl the yield obtained was 43 %[113].

The last improvements were achieved by introduction of promotors[114,115]. A variety of metals are known to increase the yield of MAN. The most relevant ones are Fe[3], Nb[116], Co[117], Sm[118] and Sb/Si[119]. BASF patented VPP with iron as dopant[3]. Comparison between doped and undoped catalyst showed that the yield of MAN was increased by 2.2 % from 57.3 % to 59.5 % at X(*n*-butane)=85 %. It is estimated that a new catalyst with a 1 % improved maleic anhydride yield pays off for itself within 1 year of operation[14]. Since the maximum yields are between 60 to 65 %, there is room for greater improvement.

1.9 Reactor Concepts for MAN Production

The industrial production of MAN over VPP produces a lot of heat. The state of the art reactor is a fixed bed reactor. For a sufficient heat, transport multitubular reactors are used[112]. There are two types of fixed bed reactors in commercial use: a) 3 m long reaction tubes, or b) 6.5 m reaction tubes. The inner diameter ranges from 21 to 25 mm. The number of tubes per reactor ranges between 10.000 and 20.000, which are placed inside a salt bath. Although the heat transfer is good, the conversion of *n*-butane is limited [14]. Above conversion of 85 %, thermal runaway will occur, which will significantly decrease the selectivity of MAN. There are several ways to increase the productivity of MAN. The last chapter focused on the correlation of synthesis methods catalyst performance. Another way would be the increase in *n*-butane concentration. The explosive limits of *n*-butane in air is at 1.9 Vol-%[120]. By applying enhanced safety technology, the industrial processes can operate at 2 Vol-% of *n*-butane[121]. This limitation can only be overcome by other reactor technologies. The

most expensive way would be the application of microreactors[122]. Due to the excellent heat transfer and small volumes, the reaction can also be handeled in the explosive regime. However, microreactor technology is rarely applied in industries and quite expensive. Another way would be the decoupling of oxidation and reduction reactions. By applying riser[123] or membrane reactors[121], *n*-butane and oxygen can be fed separately. Mallada et al.[121] could show that inside a membrane reactor *n*-butane concentrations can be increased up to 10 Vol-%. Commercial VPP catalysts from DuPont and Haldor Topsor were used. The maximum yield was 17.7 % at 5 Vol-% of *n*-butane and 20 Vol-% of oxygen. Compared to the state of the art, the yields are quite poor. However, the industrial catalsts are optimized for oxygen rich conditions. Nevertheless, new membranes might be able to enhance the technology and their application in industry.

Contractor et al. could show that the selectivity of MAN can be increased inside a riser reactor[123,124]. The highest selectivity of MAN was above 90 %. The setup consists of two reactors. In the first one the catalyst is reduced in the reaction with *n*-butane. In the second reactor the catalyst is oxidized. The main challenge is the attrition resistance of VPP. VPP extrudates in commercial processes are stabilized by addition of malonic acid, which also has a positive influence on the pores[14]. However, the particles are too soft for a riser application. Contractor et al. tried to use supported VPP on silica, which showed the same attrition properties. Nevertheless, the technology is promising and might be important in the future. Therefore, new catalysts must be found. One possible alternative might be core shell catalysts . The shell provides the stability, where the active material is inside the shell.

2 Experimental Section

2.1 Test Setups

2.1.1 Commercial Parallel Test Setup

Catalytic tests within the project are measured in a high-throughput setup from hte GmbH, Heidelberg (Figure 6). The setup consists of a gas dosing unit, a reactor unit, and an analytic unit (Figure 7). The setup is fully automated and includes several personal computers for data processing and management. The gas dosing unit allows mixing of feeds containing nitrogen, oxygen, *n*-butane, argon (as internal standard) and steam. The typical range of gas hourly space velocities (GHSV) is 500 to 5000 h^{-1}, and higher space velocities can be achieved easily by reducing the catalyst volume or modification of the MFCs. The volume concentration range for oxygen is 1 to 25 Vol-%, for alkanes 1 to 10 Vol-%, and for steam 1 to 60 Vol-%. Additional gases (e.g. butene or CO) may be added with low concentrations (< 5 %) for deeper

Figure 6 – Commercial parallel test setup from the GmbH

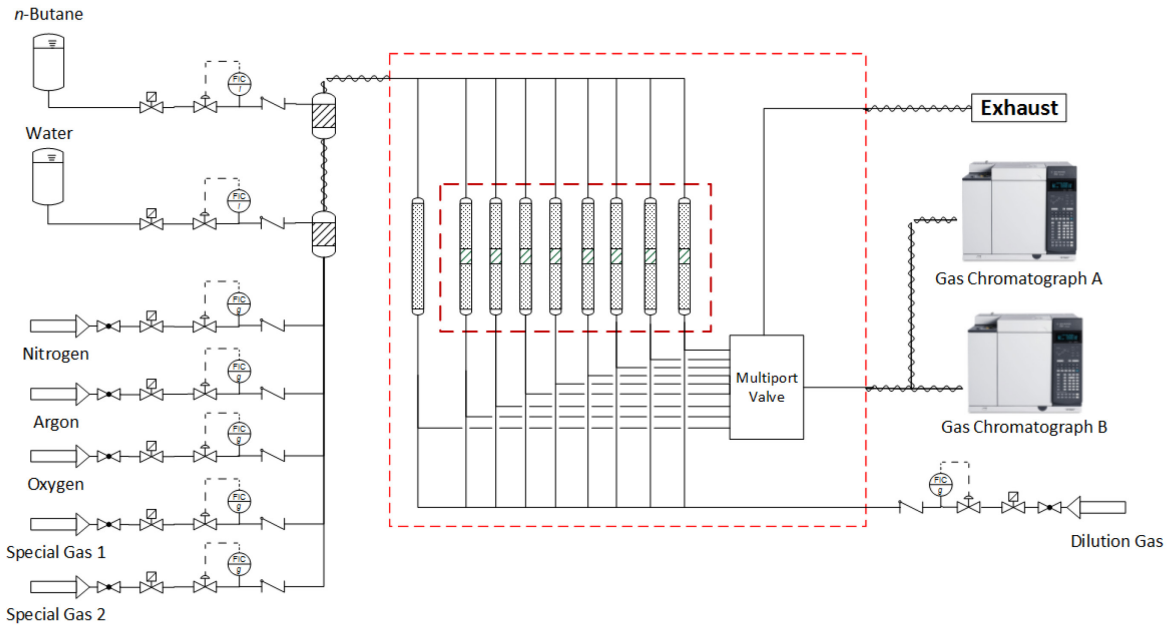

Figure 7 – Simplified process flow scheme of the parallel test setup

investigations of the reaction network. The reactor unit consists of 8 reactors for catalyst samples and one blank reactor filled with inert material. The reactors consist of stainless steel tubes with an outer diameter of 18 mm and an inner diameter of 10 mm. Thermal wells in the reactors consist of stainless steel tubes with an outer diameter of 1/8” and an inner diameter of 2 mm. The thermal wells are closed on one end and can be used to introduce temperature sensors with three thermocouples along the catalytic beds. The reactor temperature can be individually controlled for each reactor in the range of 250 to 550 °C. The effluent gas of each reactor can be analyzed by two gas chromatographs. In addition, the effluent gas of the blank reactor which equals the inlet gas of all reactors can also be analyzed by the gas chromatographs (GCs). Prior to GC analysis all effluent gas streams are diluted by inert gas streams to avoid any condensation of organic products or steam. The GCs are optimized to analyze the reaction products and by-products of the oxidation of butane to maleic anhydride. Samples of the effluent gases are taken online via sample loops and injection valves. The loops and all transfer lines between reactors and gas chromatographs are completely heated (200 °C) without any cold spot.

In a typical test run, the catalytic beds in each reactor consist of 1 ml of pressed, crushed and sieved catalyst samples (sieve fraction 100 – 200 µm). A laboratory press applied usually in spectroscopy labs is used to compact the fine powder of the original catalyst samples to pellets (for 2.5 min applying a pressure equivalent to a weight of 2 t on a 12 mm die). Afterwards pellets are crushed in an agate mortar and sieved using analytical sieves made of stainless steel. The catalytic beds are kept in their place in the reactors by beds of inert material below and above (calcined steatite, sieve fraction of 800 – 1000 µm, CeramTec). The reactors are brought into the oven at room temperature. The GHSV is set to 2000 h^{-1}. The catalysts are heated in a lean air mix of 5 % oxygen in nitrogen to 250 °C. After reaching 250 °C the feed gas composition is changed to 2 % *n*-butane, 3 % steam, 3 % argon (as internal standard) and 20 % oxygen in nitrogen. The reactor temperature is increased to 375 °C. After equilibrium time of 30 min the catalytic measurement is started. A total of 5 GC runs per reactor are recorded. Then the temperature is increased by 25 °C, and again 5 GC runs per reactor are recorded. Following this procedure, the reactor temperature is increased from 375 to 450 °C and then decreased again to 375 °C in steps of 25°C, respectively. Thus, information on activity, selectivity, thermal stability, and possibly deactivation of the catalysts is gathered. The total test run takes

typically 7 days. Finally, catalysts are cooled down to room temperature in a lean air mix of 5 % oxygen in nitrogen. The catalytic beds are then retrieved from the reactors and separated from residual inert material (steatite) by sieving.

2.1.2 Self Constructed Transient Kinetic Test Setup

The measurements were carried out on a self-constructed apparatus (Figure 8), which allows automatic changes in the temperature and concentration during reactions. The reactor consists of glassed line tubing (inner diameter 4 mm), which is encased by a copper case providing an excellent heat distribution. The catalyst is retained by spherical particles of steatite. At the beginning and in the middle of the catalyst bed the temperature is measured by thermocouples inside a stainless-steel tube (outer diameter 1 mm, wall thickness 150 µm). The reactor is placed inside an electric furnace, which has computer aided temperature and time controls in the range of 250-500 °C. Depending on selectivity/conversion performance of the investigated reaction system the mass of the catalyst varies between 50 and 600 mg at total flow rates of 10 and 50 mL min^{-1}. Educts (*n*-butane, O_2) and inert gas (He, N_2, Ar, Kr) are introduced to the reactor by mass flow controllers (Bronkhorst). Two identical saturators allow the introduction of liquid compounds such as H_2O or organic intermediates to the reactor. One saturator is directly connected to the feed line, the other one is connected to the pulse valves. Temperature of the saturators is controlled by thermostats with Pt100 temperature sensor measuring the gas phase temperature. Online gas analysis is carried out by gas chromatography (GC, Agilent) and mass spectrometry (MS, Pfeiffer Vacuum). For steady state measurements the gas chromatograph is used, whereas the mass spectrometer is used for transient and isotope measurements.

Figure 8 – Transient kinetic test setup

The gas stream is transferred to the MS at the exit of the reactor. A T-piece is connected to the 1/8” Swagelok tube. Inside the T-piece a 1/16” capillary is placed in the middle of the gas stream. A continuous stream of 3 mL/min is transferred to the

prepump of the MS via the heated capillary (200°C), where a small fraction of the stream is transferred to the ionization source. This setup is needed for fast response times of transient experiments. The time-resolution of the mass spectrometer, depending on scanned masses, ranges between 1 and 10 Hz. A crossbeam ion source with tungsten wires was used for ionization. A quadrupole analyzer is used for separation of the masses. The signal of the detected ions is enhanced by a 90°-off-axis secondary electron multiplier (SEM). Data evaluation of the MS is done with Vacuum Pfeiffer Software Quadera. The challenge that single peaks may origin from different gas compounds has been extensively discussed by Müller-Erlwein[125]. To compensate this effect a correction matrix based on calibration measurements, which take all possible reaction products, educts and inert gases into account, was used. The intensity of MS signals is transformed online into volume fractions with the aid of the correction matrix. Kr and N_2 are introduced as internal standards for MS and respectively GC. Ar is used as tracer for step change experiments.

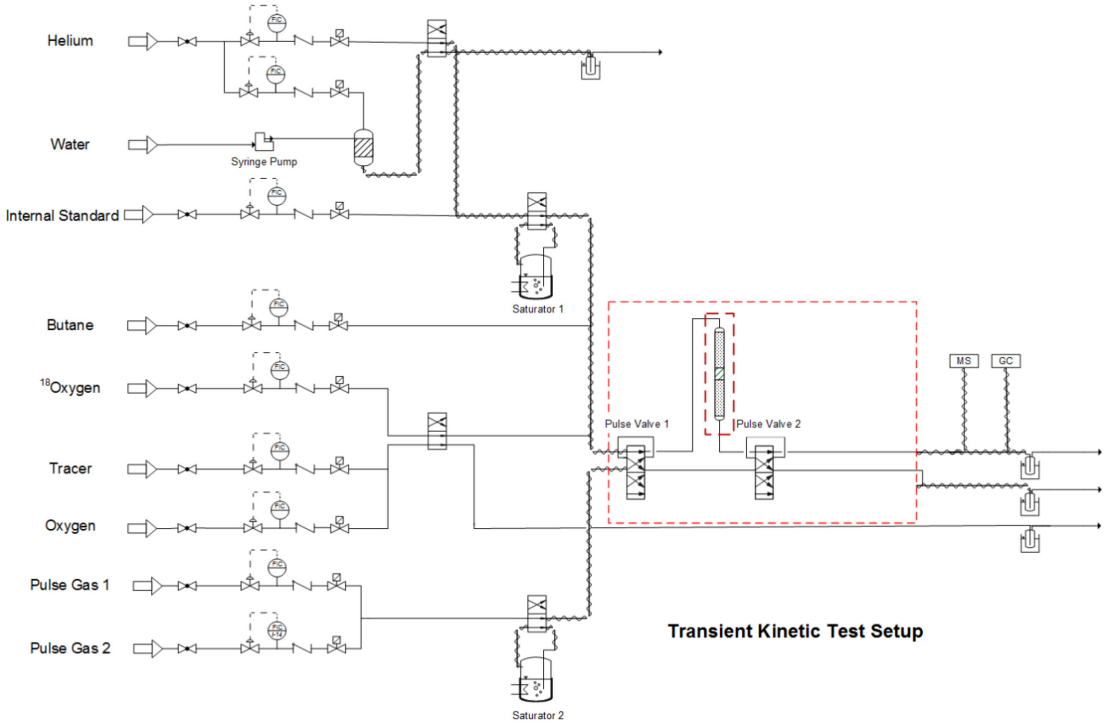

Figure 9 – Simplified flow process diagram of the transient kinetic test setup

The gas chromatograph is equipped with one FID and one TCD. Each detector is connected to its own separation column. On the FID line hydrocarbons are separated over a Plot-Q column and oxygenate are separated by a Rtx Wax column. Permanent gases are analyzed by TCD, first carbon dioxide is separated by a Plot-Q column. Oxygen, krypton, nitrogen and carbon monoxide are separated by a

molecular sieve. Higher hydrocarbons are excluded by a backflush column. One sampling run takes 17 min. Six-way-valves and four-way-valves that are common in chromatography are available to perform pulse- and step change experiments. Both valves are close to the entrance of the reactor. Pneumatic valves are controlled by an electronic valve system accessible via Ethernet connection. The amount of pulse gases is defined by different sample loops with total volumes of 50, 100, 250 and 500 µL. To get reference pulses during experiments a second valve is placed directly behind the reactor. Crucial for step change and pulse experiments are the avoidance of pressure gaps between feed and pulse/step change gas. Therefore, needle valves are installed in each line. In order to perform almost ideal pulse or jump experiments the dead volume and the use of 1/8”-supply tubes and fittings had to be minimized wherever possible. From inside the reactor a partial flow of the reaction gas is drawn off employing a 1/16”- tube, conveying the flow directly into the recipient of the mass spectrometer. A small part of the product stream is passed to the sampling valves of the GC through a Tee connecter. A bubbler at the end of the exhaust line provides a constant over pressure resulting in a constant flushing of the sample loops. All supply and exhaustion tubes are heated electrically (>200 °C) in order to avoid condensation. Tailing and memory effects are suppressed to the greatest possible extent. Data acquisition and automatic control of the setup is run by computers and appropriate interface devices.

2.2 Catalytic Testing

2.2.1 Parameters Field Study and Catalyst Screening

To exclude disturbing macro kinetic factors, thus ensuring a high quality of kinetic data, a pretest for mass and heat transport limitations was performed. To address the influence of mass transport (pore diffusion), four different particle size fractions from 50-100 µm up to 1-1.4 mm were tested. In addition, different degrees of dilution of the VPP catalyst with quartz in the same particle size are expected to reveal the influence of heat transport, which possibly lead to the formation of a hot spot in the catalyst bed. A detailed overview over this pretest is shown in Table 2. The same mass of active material (VPP) was filled into each reactor (0.72 g). The equally distributed gas flow is adjusted to provide a space-time velocity of 2775 ml g^{-1} h^{-1} over each reactor (33.3 ml min^{-1}). The feed contains 2 % *n*-butane, 20 % O_2,

3 % H_2O, 2 % Ar, and balance N_2. Activities and product selectivity for the 7 channels were compared at 420, 400, 380, and 360 °C with a holding time of 15 h at each temperature step.

Table 2 – Plate design for heat and mass transport limitation study

Liner	Catalyst	d_p / µm	Catalyst:Quartz Ratio
1	VPP	50–100	1:0
2	VPP	100–200	1:0
3	VPP	200–500	1:0
4	VPP	1000–1400	1:0
5	VPP/Quartz	100–200	1:1
6	VPP/Quartz	100–200	1:2
7	Steatite	-	-

Using the parallel testing setup the variation of space-time velocities was realized by loading the channels with different amounts of VPP catalyst (Table 3). According to the results of the mass and heat transfer analyses, a particle size fraction of 100-200 µm was chosen. Steatite was used to fix the undiluted bed of catalyst particles in the isothermal zone of the reactors. To continuously control the actual feed concentrations, a blank reactor filled with inert steatite completed the set of channels to be tested. The standard gas flow of 33.3 ml min^{-1} per reactor, which was kept constant throughout the study, results in GHSVs in between 2.000 and 16.000 h^{-1} to bring up both differential and integral rate data at almost each point of the parameters field study.

Table 3 – Plate design for parameters field study

Liner	Catalyst	m_{Cat} / g	V_{Cat} / mL	GHSV / h^{-1}
1	VPP	1.02	1	2.000
2	VPP	0.49	0.5	4.000
3	VPP	0.25	0.25	8.000
4	VPP	0.12	0.125	16.000
5	VWPO	5.77	4	500
6	VWPO	2.82	2	1.000
7	VWPO	1.39	1	2.000
8	VWPO	0.64	0. 5	4.000
9	Steatite	-	-	-

The sequence of catalytic testing comprises a 3×3 matrix of *n*-butane (2, 1, and 0.5 %) and O_2 (20, 15, and 10 %) feed concentrations with excess of O_2 in each point. Previous experiments showed that a full conversion of O_2 can lead to successive formation of coke, which irreversibly deactivates the catalyst. Partial pressures of *n*-butane beyond 2% are not accessible without entering the explosive range. The total gas pressure was kept constant at 1 bar(a) throughout the entire run. Matching industrially relevant feed conditions, H_2O was typically co-fed at a concentration of 3%. The reaction temperatures (420, 400, 380, and 360°C) were investigated in decreasing order. Each point was measured 5 times to check the time scale of equilibration required for stable catalytic performance. To monitor catalyst aging effects on activity and product selectivity, a reference point was frequently measured (420°C, 2 % *n*-butane, 20 % O_2). Details of the procedure are listed in the appendix. A co-feed of a gaseous P source, *e.g.*, triethyl phosphate (TEP), to compensate the loss of volatile phosphorus was avoided in this study as this compound significantly affects the catalyst performance by structural and/or electronic modification of active sites.

2.2.2 Pulse Studies

The catalyst was kept inside a single tube reactor in steady state at 2000 h^{-1} and 420 °C in a feed comprising 2 % *n*-butane, 20 % O_2, and 3 % H_2O in inert gas (He, Kr) for an initial equilibration period of 1 week. Pulsing of reactive compounds (carried by an Ar stream) was realized by a pulse valve in the H_2O/He line of the set-up, *i.e.*, the concentrations of *n*-butane and O_2 remained unchanged during the transient experiment. The amount of the reactive compound pulsed over the catalyst was adjusted to its carbon number in a way that 1 substrate carbon atom comes upon approx. 20 surface vanadium atoms to avoid severe and irreversible damage to the catalyst. This estimation is rather a rule of thumb and based on the specific surface area of the catalyst and the ideal crystal structure of VPP[126] although it is known that the surface layer of VPP under reaction conditions is rather amorphous[127] and dynamically responds to changes in the reaction conditions[49,128] Repeated performance tests (GC) before and after each pulse series (3 per compound) proved the pronounced stability and reproducibility of the system. The pulse itself was monitored by MS with a full scan (m/z 1-100) and a time-resolution of 2 s. The components pulsed over the catalyst were: furan, 2,5-dihydrofuran, 1-butene, acetaldehyde, acrolein, ethylene, acetylene, acetic acid, and acrylic acid.

2.2.3 Cofeed Studies

Cofeed experiments were performed in the same setup where the transient experiments were performed. Catalyst volumes were 0.1 mL and 0.2 mL for VPP and VWPO, respectively. The starting procedure and equilibration for the catalyst was identical to parameters field study. MAN was added to the reference gas stream by a saturator. Reference measurements were done prior and after cofeed experiments to exclude change in the active phase. Co-feed studies of CO, ethylene and water were performed at the end of the parameters field study as high water partial pressures will irreversibly change the catalyst. Minimizing the effect of additional reactants, cofeed compounds were matched to concentrations found under reference conditions. Ethylene, CO and water were added to the reference feed. The testing procedure includes 5 GC analyses per reactor. Before and after cofeed experiments, reference measurements under standard conditions were run to exclude changes in the active phase. Finally, the reactors were cooled down to ambient temperature in 5 % O_2 in N_2.

2.2.4 Steady State Isotope Transient Kinetic Analysis

The catalyst was equilibrated under reference conditions with and without H_2O, respectively. Kr was used as internal standard. Subsequently, the SSITKA experiments were performed, in which a stepwise change of the oxygen isotope – $^{16}O_2$ to $^{18}O_2$ (> 97 % ^{18}O, Campro Scientifc) – was completed at the reactor inlet by means of a four-way valve. After 8 h of isotope labeling the oxygen isotopes were stepwise changed back from $^{18}O_2$ to $^{16}O_2$. The SSITKA experiments were also conducted at ambient pressure and a total flow of 20 mL min^{-1}. In a different experiment the time between isotope switches was reduced to 30 s/15 s in a repeated manner.

2.2.5 TPO

TPO with $^{18}O_2$: The catalyst was heated under lean oxygen (5% O_2 in He) from room temperature to 200 °C. Oxygen feed was changed from $^{16}O_2$ to $^{18}O_2$ (> 97 % ^{18}O, Campro Scientific). The temperature ramp was programmed from 200 to 450 °C at 1 K min^{-1} and ambient pressure with a total flow of 20 mL min^{-1}.

2.3 Catalysts

2.3.1 Overview of Tested Materials

An overview of the tested materials can be found in Table 4. The catalysts were synthesized during cooperation with the group of Prof. Glaum from the University of Bonn. VPP without dopant was used as a reference.

Table 4 – Catalysts of screening study

Catalyst	$S_{BET,fresh}$ (m^2/g)	Structure Type[a]	Space Group	Scherrer Diameter (nm)
$VOPO_4$	3.5	β	*Pnma*	>200
$V_{0.99}W_{0.01}OPO_4$	1.3	β	*Pnma*	103
$V_{0.94}W_{0.06}OPO_4$	2.4	α_{II}	*P4/n*	>200
$V_{0.9}W_{0.1}OPO_4$	4.9	α_{II}	*P4/n*	165
$V_{0.8}W_{0.2}OPO_4$	3.4	α_{II}	*P4/n*	84
$WOPO_4$	3.9	$WOPO_4$	$P2_1/m$	78
$V_{0.8}Mo_{0.2}OPO_4$	0.8	β	*Pnma*	52
$V_{0.8}Mo_{0.2}OPO_4$	1.1	γ	*Pbam*	192
$W_{0.67}Fe_{0.33}OPO_4$	6.2	$WOPO_4$	$P2_1/m$	68
VPO_4-m1	1.9	VPO_4	C2/c	53
$(VO)_2P_2O_7$[b]	26	VPP	$Pca2_1$	31
$(VO)_2P_2O_7$[c]	2.1	VPP	$Pca2_1$	>200
$(V_{0.95}Mo_{0.05}O)_2P_2O_7$	1.5	VPP	$Pca2_1$	>200
$Fe(WO_2)_2(P_2O_7)(PO_4)$	1.1	VPO_4	C2/c	>200
V_2O_3	6.2	V_2O_3	*Pnma*	78
VO_2	1.1	VO_2	*P4/n*	87
V_2O_5	6.4	V_2O_5	*P4/n*	133

2.3.2 Catalyst Synthesis

Single phase solid solutions $(V_{1-x}W_x)OPO_4$ (α_{II}- and β-$VOPO_4$-type), $(V_{1-x}Mo_x)OPO_4$ (β- and γ-$VOPO_4$-type), $W_{0.67}Fe_{0.33}OPO_4$ ($WOPO_4$-type), $Fe(WO_2)_2(P_2O_7)(PO_4)$, and "$(V_{0.95}Mo_{0.05})_2P_2O_7$" were obtained by solid state synthesis or the solution combustion technique[129–131]. Single phase VPP was obtained by reducing β-$VOPO_4$ in argon ($p(O_2) = 10^{-5}$ mbar) at 750 °C for 2 days. Polycrystalline $WOPO_4$ was synthesized from $W_2P_2O_{10}$, WO_3, and P_4 in sealed silica tubes at 1000 °C for 7 days[132]. The reference catalyst VPO was synthesized according to patent via the organic synthesis route using an alcohol[133]. V_2O_5 (Merck, ≥99.6 %) was used as received.

V_2O_3 was obtained by the reduction of V_2O_5 in H_2 at 600 °C for 1 d. Reduction of V_2O_5 in H_2, which was moisturized inside a bubbler at room temperature (p_{sat} (H_2O) = 0.023 bar), at 315 °C for 3 d yields VO_2. All vanadium oxides were single-phase according to powder X-ray diffraction (XRPD; IP Guinier technique) analysis. Finally, the reduction of β–$VOPO_4$ in H_2, which was saturated by water inside a bubbler at room temperature (p_{sat} (H_2O) = 0.023 bar), at 500 °C for 1 day yields the literature unknown, thermodynamic metastable phase VPO_4-m1, which is structurally related to β–$VOPO_4$[131].

The fine powders of the original catalyst samples were pelletized in a lab press (2.5 min, pressure equivalent to a weight of 2 t on a 12 mm tablet), respectively. Afterwards the pellets were crushed in an agate mortar and a 100-200 μm particle size fraction was obtained using analytical sieves made of stainless steel.

2.3.3 Catalyst Stability

All materials were thermally treated prior to testing in *n*-butane oxidation to minimize phase transition under reaction conditions. Stability tests are crucial for evaluation of catalyst performance. Therefore, a first screening test was run for at least one week. The structural stability was verified by XRD measurements of the tested material, which were compared to the XRD spectra of freshly synthesized ones. Most catalyst were stable as demonstrated in Figure 10 for single phase solid solutions $(V_{1-x}W_x)OPO_4$.

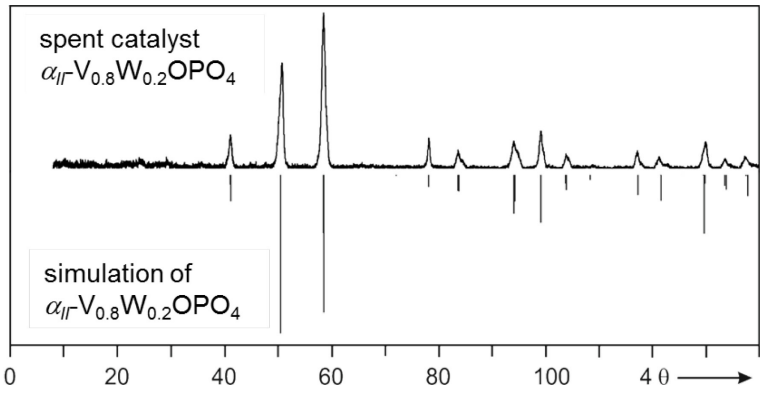

Figure 10 – Guinier photographs of single phase $V_{0.8}W_{0.2}OPO_4$ after catalytic testing and simulated XRPD pattern of $V_{0.8}W_{0.2}OPO_4$.[131]

However, VPO_4-m1, $W_{0.67}Fe_{0.33}OPO_4$ as well as $WOPO_4$ formed by-phases, which were analyzed. XRD analysis of VPO_4-m1 reveals several by-phases under reaction conditions (Figure 11). The most dominant by-phases are VPP and β-$VOPO_4$.

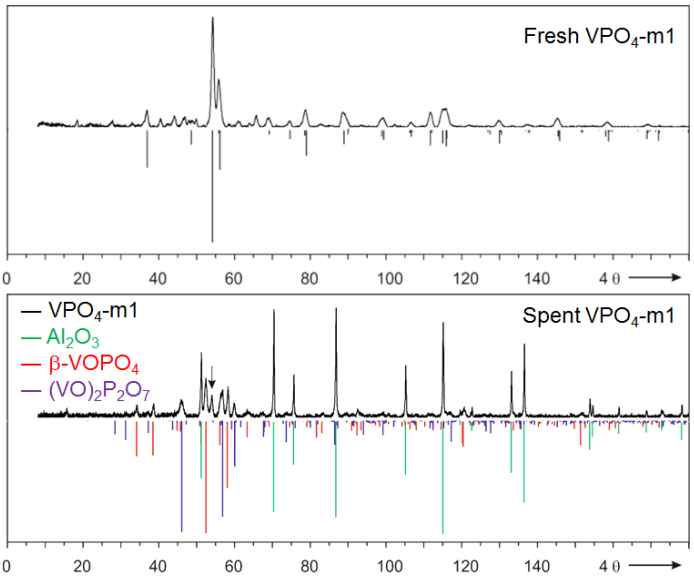

Figure 11 – Guinier photographs of VPO_4-m1 before (top) and after catalytic testing (bottom). Reflections of Al_2O_3 assigned to corundum, which was used as inert material and couldn't be separated from the catalyst.

2.4 Technical challenges

This section is dedicated to challenges, which were faced during this work. Since most challenges were faced in the initial phase and were mostly of technical nature, they were not mentioned in the publications. However, they were crucial for this study and a brief explanation is included in this thesis.

2.4.1 Liquid Dosing of *n*-Butane via Liquid MFC

Data quality is important for kinetic studies. Small errors in the experimental data will have a manifold higher impact on the error of the kinetic model[134]. Therefore, the dosing of all compounds needs to be stable. The state of the art technology for dosing of gases and liquids in lab-scale is done via thermal conductivity mass flow controllers[135]. Therefore, the fluid is supplied with a certain pressure to the MFC, which is equipped with a flow measurement unit and a magnetic valve. Depending on the measured flow, the magnetic valve is adjusted resulting in a steady flow. There are currently different types for flow measurements. The most common one, which was used in this work, is a thermal conductivity detector (Figure 12). A small part of the flow is bypassed. A heating wire is placed in the middle and surrounded by two thermocouples. The temperature increase correlates linear with the mass flow. This kind of detector can be used for most permanent gases. However, the different thermal conductivities will influence the flow range. Further, the fluid resistance of the sealings needs to be considered, which might be the case for liquid carbon dioxide.

Figure 12 – Bronkhorst liquid MFC

In the parallel test setup, *n*-butane is dosed by a thermal conductivity MFC. The flow distribution is provided by a capillary system, which increases the inlet pressure up to 8 bar(g). Therefore, *n*-butane is in liquid phase. During the initial phase, measurements of the inert liner (liner filled with inert material) showed high deviation in the *n*-butane concentration. As all MFCs are connected with each other, each MFC was checked and no general error could be identified. From the point of process engineering everything was fine. A detailed analysis of the MFC revealed that the magnetic valve was quite hot. The outside temperature was around 45 °C, which is in the range for gas-phase transition for *n*-butane at 8 bar(g). A first technical solution was the installation of a fan close to the magnetic valve. The air cooling increased the

results immediately. Later, a customized cooler was constructed and built from aluminia, which was in direct contact with the magnetic valve. A Peltier element was used for cooling.

2.4.2 Minimizing Pressure Differences Inside a GC Sample Loop

Online gas-phase analysis was done by an Agilent GC 7890A. The reaction mixture flows through a sample loop with a volume of 250 µL. Hence, the inner diameter is quite small, there is a pressure depending of the flow and gas composition. The reaction was done at atmospheric pressure. Different volume flows would change the reactor pressure. This challenge was mainly in the one-fold setup for isotope studies. The parallel setup has an automated pressure control system.

The reactor flow was splitted with a standard T-piece. One path leads to the GC sample loop and the other was connected directly to the exhaust. The main part of the flow in the range of 10-30 mL/min was sent to the exhaust via a washing bottle. The tube was placed 5 cm under the water surface inside the bottle. Consequently, there was a pressure drop of around 5mbar. A small portion of around 4 mL/min was sent to the GC. The advantage of the solution is the constant flow through the sample loop, which depends on the height of the water inside the washing bottle. Therefore, the water level needed to be checked before and in between each experiment. Another advantage of the washing bottle is the extraction of MAN, acetic and acrylic acid from the product stream.

3 Novel Catalysts for the Selective Oxidation of *n*-Butane to Maleic Anhydride

This study is dedicated to a better understanding of the selective oxidation of *n*-butane to maleic anhydride over vanadyl pyrophosphate. Due to the complexity of the reaction, key aspects of the reaction mechanism as well as the active site are still under debate. In the literature the number of materials selectively converting *n*-butane to MAN is limited to vanadium phosphorus oxides (VPO). Therefore, new catalysts were investigated. The most promising catalyst was kinetically investigated and compared to vanadyl pyrophosphate. From the findings, isotope labelling studies were done, which lead to new understanding of the active site.

Reprinted with permission from Elsevier. C. Schulz, S. C. Roy, K. Wittich, R. Naumann d'Alnoncourt, S. Linke, V. Strempel, B. Frank, R. Glaum, F. Rosowski, "α_{II}-$(V_{1-x}W_x)OPO_4$ Catalysts for the Selective Oxidation of *n*-Butane to Maleic Anhydride" Catalysis Today 333 (**2019**) 113-119, https://doi.org/10.1016/j.cattod.2018.05.040.

3.1 Abstract

The vanadyl pyrophosphate (VPP) based catalyst is unique in converting *n*-butane selectively (60–70 %) into maleic anhydride (MAN), whereas a MAN selectivity of 20 % may be regarded as high for structurally different catalyst systems. We present novel vanadium phosphorus oxides and mixed metal phosphate solid solutions tested for *n*-butane oxidation to MAN with a selectivity of >30 %. The majority of the catalysts were prepared by solution combustion synthesis. $(V_{1-x}W_x)OPO_4$ with α_{II} structure was found to be more active and selective in the oxidation of *n*-butane compared to β-$VOPO_4$. By adjusting the tungsten content the oxidation state of vanadium in $(V_{1-x}W_x)OPO_4$ can be tuned between 4.74 and 4.99, which is regarded as a key factor for MAN production. All catalysts were structurally stable, but the specific surface area increased during the reaction, as detected by X-ray diffraction and N_2 physisorption, respectively. $(V_{1-x}Mo_x)OPO_4$ was also stable, but the MAN selectivity was lower compared to β-$VOPO_4$. Low conversions result from the low surface area of the screening samples, however, could be overcome by advanced synthesis protocols.

3.2 Introduction

The catalytic oxidation of *n*-butane to maleic anhydride (MAN) is the first and so far only industrial process of selective alkane oxidation and has an annual world capacity of more than 1 million tons[1a]. Although the molar yield of the industrial process has been steadily improved over the past decades, the yields are still below 65 %, which is mainly limited by product selectivity[1a–9a]. The industrial state of the art catalyst is based on crystalline $(V^{IV}O)_2P_2O_7$ (vanadyl(IV) pyrophosphate, VPP). Due to several vanadium(V) orthophosphate by-phases, which are formed under reaction conditions, the catalyst is often referred to as vanadium phosphorus oxide (VPO). Significant improvements in activity and (by-)product selectivity with this catalyst system were achieved by increasing the specific surface area and by adding promotors like Nb[10a], Co[11a], Fe[12a], and Sm[13a]. Extensive research on VPP-based systems missed a significant breakthrough within the past decades. Thus, a new perspective on this reaction is expected from the search for new materials rather than improving the existing VPO system. The scientific literature on materials selectively converting *n*-butane to MAN is dominated by VPO[14a–21a]. The reports can be subdivided into a) vanadyl(IV) pyrophosphate and b) vanadyl(V) orthophosphate with different structure types as α_I-$VOPO_4$, α_{II}-$VOPO_4$, β-$VOPO_4$, γ-$VOPO_4$, and δ-$VOPO_4$[22a]. All of them are well discussed with regard to their catalytic performance in *n*-butane oxidation as a by-phase in VPO[23a–27a]. Less effort was put into the synthesis and catalytic testing of single phase bulk $VOPO_4$ catalysts. First results published by Shimoda et al. showed that single phase α_{II}-$VOPO_4$ and β-$VOPO_4$ can produce MAN from *n*-butane. Starting from $(NH_4)_2((VO)_2C_2O_4(HPO_4)_2)\cdot 5H_2O$ or NH_4HVPO_6 single phase α_{II}-$VOPO_4$ and β-$VOPO_4$ were synthesized. MAN selectivities ranged from 14 % to 20 %[23a]. Under reaction conditions most phases are stable and no indication for by-phases were found by in situ Raman studies[27a]. In our project novel materials with structural motifs similar to those of $VOPO_4$ and VPP were searched. The crystal structure of VPP consists of a chain-ladder-motif of edge- and corner-sharing VO_6-octahedra, which are connected to pyrophosphate anions. Similar motifs are present in α_{II}-$VOPO_4$. Here, the vanadium oxygen polyhedra are only connected by vertices. Pyrophosphate groups are replaced by orthophosphate anions (Figure 13).

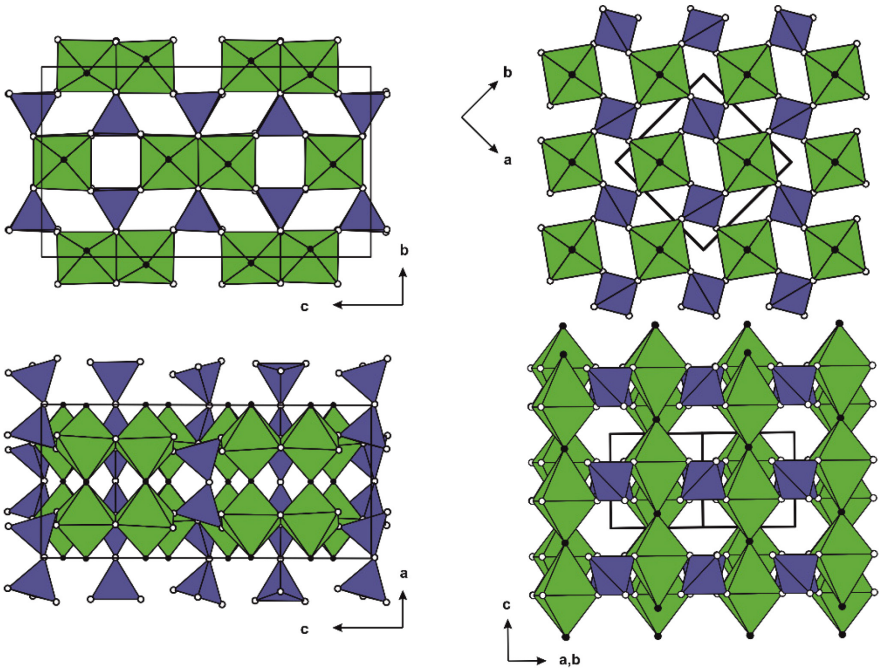

Figure 13 – Crystal structure of VPP (left) and α_{II}-type $VOPO_4$ (right) with VO_6 units (green) and PO_4 units (blue)[28,29]. Oxygen atoms from phosphate groups are given as ○, vanadyl oxygen atoms as ●.

Recently, Roy et al. reported a new class of V^{IV}/V^{V} containing mixed metal vanadium tungsten phosphate solid solutions. Solution combustion synthesis[30a,31a] starting from vanadium and tungsten precursors in nitric acid yields solid solutions $V_{1-x}W_xOPO_4$ ($0.04 \leq x \leq 0.26$), which crystallize with α_{II}-$VOPO_4$ and β-$VOPO_4$ structure ($0 \leq x \leq 0.01$), respectively[29a]. XPS studies showed that the substitution of V^{V} by V^{IV}/W^{VI} in the α_{II}-$VOPO_4$ lattice sensitively affects the average oxidation state of V, which can be finely adjusted between nominal values of 4.74–4.96 (α_{II}-$VOPO_4$-type) and 4.99–5.00 (β- $VOPO_4$ type). NAP XPS showed that V^{IV} and V^{V} are present with an average oxidation state of 4.3 on the surface of VPO[32a]. The presence of V^{V} on the surface is crucial as it can be correlated with MAN production[33a]. Therefore, the introduction of bulk catalysts with a tunable vanadium oxidation state is a promising approach. In the present study, triggered by this finding, further mixed metal (V, W, Mo, Fe) oxide phosphates in various oxidation states were synthesized and tested for their performance in the selective oxidation of *n*-butane. In particular, the substitution of V by Mo is of interest as Mo is a frequent constituent of many catalysts for hydrocarbon (amm)oxidation[34a,35a].

3.3 Experimental

3.3.1 Catalyst Preparation

Single phase solid solutions $(V_{1-x}W_x)OPO_4$ (α_{II}- and β-$VOPO_4$-type), $(V_{1-x}Mo_x)OPO_4$(β- and γ-$VOPO_4$-type), $W_{0.67}Fe_{0.33}OPO_4$ ($WOPO_4$-type),

$Fe(WO_2)_2(P_2O_7)(PO_4)$, and "$(V_{0.95}Mo_{0.05})_2P_2O_7$" were obtained by solid state synthesis or the solution combustion technique[29a,36a,37a]. Single phase VPP was obtained by reducing *β*-$VOPO_4$ in Ar ($p(O_2)$=10−5 mbar) at 750 °C for 2 days. Polycrystalline $WOPO_4$ was synthesized from $W_2P_2O_{10}$, WO_3, and P_4 in sealed silica tubes at 1000 °C for 7 days[38a]. The reference catalyst VPO was synthesized according to patent literature[12a] via the organic synthesis route using *iso*-butanol. Finally, the reduction of *β*-$VOPO_4$ in H_2, which was saturated with H_2O in a bubbler at ambient temperature ($p_{sat}(H_2O)$=0.023 bar), at 500 °C for 1 day yields the thermodynamically metastable phase VPO_4-m1, which is structurally related to *β*-$VOPO_4$[37a].

The fine powders of the original catalyst samples were pelletized in a lab press (2.5 min, pressure equivalent to a weight of 2 t on a 12 mm tablet), respectively. Afterwards the pellets were crushed in an agate mortar and a 100–200 µm particle size fraction was obtained using analytical sieves made of stainless steel. The estimation of the Weisz-Prater criterion as well as previous pre-tests with more active catalysts indicate that this sieve fraction is appropriate to exclude mass and heat transfer limitations under the reaction conditions chosen.

3.3.2 Catalyst Characterization

Routine XRPD analyses (IP-Guinier technique[39a]) were performed for phase identification and purity control. The patterns were recorded at ambient temperature using an image plate Guinier camera (HUBER G670, Cu-$K_{\alpha 1}$ radiation, λ=154.059 pm) with integrated read-out system[40a]. The finely ground powder samples were spread on Mylar foil (Fluxana GmbH & Co. KG, type TF-160). Powder patterns were recorded for 15 min in the range of $4° \leq 2\theta \leq 100°$. The cell parameters were determined with the software SOS[41a], α-SiO_2 (p. A., Merck) was used as an internal standard. Scherrer diameters (D) were calculated according to Eq. 1 with a Scherrer constant (K) of 0.94 for ω (FWHM) of spherical crystals with cubic symmetry. ω was corrected for instrumental broadening with Y_2O_3 standard.

$$D = \frac{K\lambda}{\omega \cos\theta} \qquad \text{(Eq. 1)}$$

BET measurements were carried out in a volumetric N_2 physisorption setup (Autosorb-6-B, Quantachrome) at the temperature of liquid N_2. The sample was degassed in a dynamic vacuum at 423 K for 2 h prior to physisorption. Full adsorption-desorption isotherms were recorded. The specific surface area according to the BET method was calculated from the linear range of the adsorption isotherm

(p/p_0=0.05-0.3). All catalysts were characterized before and after catalytic testing (Table 5).

Table 5 - Catalyst characterization by XRPD and BET measurements and surface before catalytic testing

Catalyst	$S_{BET,fresh}$ (m^2/g)	Structure Type[a]	Space Group	Scherrer Diameter (nm)
$VOPO_4$	3.5	β	*Pnma*	>200
$V_{0.99}W_{0.01}OPO_4$	1.3	β	*Pnma*	103
$V_{0.94}W_{0.06}OPO_4$	2.4	α_{II}	*P4/n*	>200
$V_{0.9}W_{0.1}OPO_4$	4.9	α_{II}	*P4/n*	165
$V_{0.8}W_{0.2}OPO_4$	3.4	α_{II}	*P4/n*	84
$WOPO_4$	3.9	$WOPO_4$	$P2_1/m$	78
$V_{0.8}Mo_{0.2}OPO_4$	0.8	β	*Pnma*	52
$V_{0.8}Mo_{0.2}OPO_4$	1.1	γ	*Pbam*	192
$W_{0.67}Fe_{0.33}OPO_4$	6.2	$WOPO_4$	$P2_1/m$	68
VPO_4-m1	1.9	VPO_4	*C2/c*	53
$(VO)_2P_2O_7$[b]	26	VPP	$Pca2_1$	31
$(VO)_2P_2O_7$[c]	2.1	VPP	$Pca2_1$	>200
$(V_{0.95}Mo_{0.05}O)_2P_2O_7$	1.5	VPP	$Pca2_1$	>200
$Fe(WO_2)_2(P_2O_7)(PO_4)$	1.1	VPO_4	*C2/c*	>200

[a] Greek letters refer to the various polymorphs of $VOPO_4$; [b] from organic synthesis route; [c] from SCS

3.3.3 Catalyst Test Setup

Catalytic tests were performed in a fully automated, commercial 8-channel parallel testing setup (hte GmbH, Figure 14). It consists of a gas dosing unit, a reactor unit, an analytical unit as well as several personal computers for data processing and management. The gas dosing unit provides mixed feeds comprising N_2, O_2 (0-25 %), *n*-butane (0-10 %), Ar (as an internal standard) and H_2O (0-60 %). The typical range of gas hourly space velocities (GHSV) is 500-5000 h^{-1}. The test unit consists of 8 reactors for catalyst samples and one blank reactor filled with inert material (calcined corundum, 400-700 µm, CeramTec). Catalyst volumes of 1 mL were placed inside stainless steel reactors with inner diameter of 10 mm. Stainless steel thermowells (OD=1/8”) are placed in the center of all reactors, which are used to guide thermocouples into the catalyst beds. The reactor temperature can be individually controlled in the range of 250-550 °C. The product gases are analyzed by two gas chromatographs (GC 7890A, Agilent). The effluent gas of the blank reactor, which

corresponds to the inlet gas of all reactors, is also analyzed. Prior to the GC analysis, all effluent gas streams are diluted with hot inert gas to avoid the condensation of organic products or steam. Transfer lines between reactors and gas chromatographs are completely heated (200 °C). The GCs are optimized for the analysis of the product spectrum of the oxidation of *n*-butane to MAN.

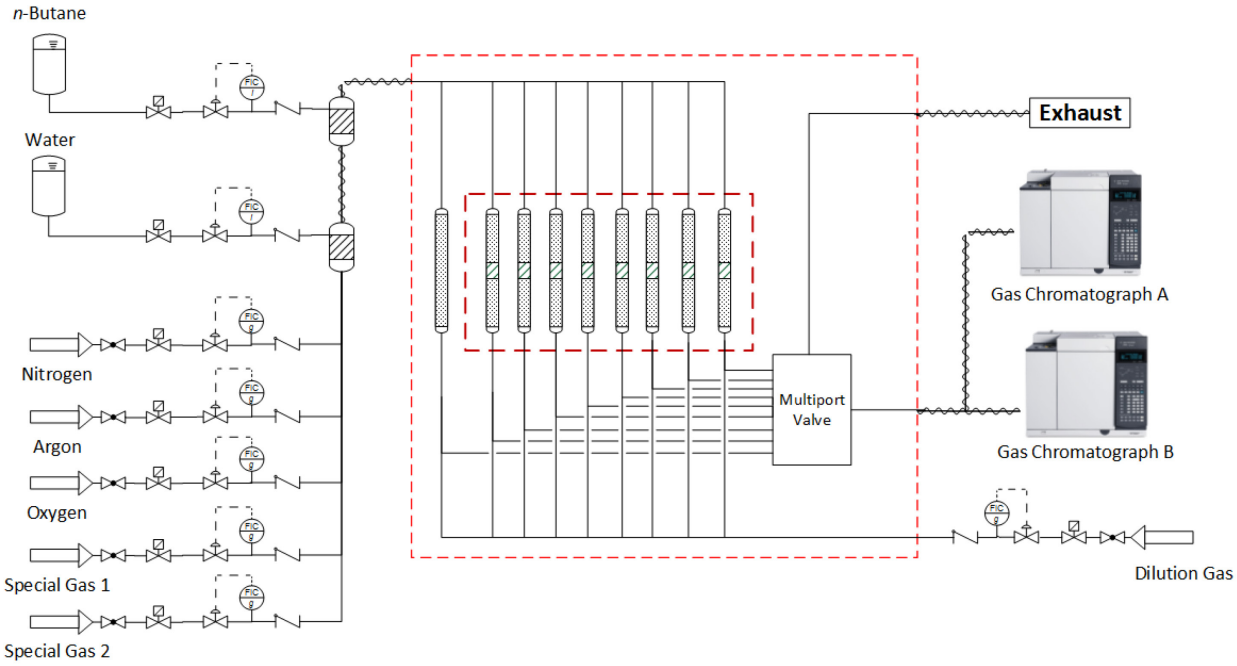

Figure 14 – Flow scheme of the laboratory scale test setup (hte GmbH) with 8 parallel fixed-bed reactors and 1 blank reactor, gas and liquid dosing unit and on-line gas chromatograph for product analysis.

The conversion (*X*) of *n*-butane (Eqs. 2 and 4) and the selectivities (*S*) of the respective products are calculated from the concentrations measured with reference to the internal standard Ar (Eqs. 3 and 5). The latter are averaged over 5 runs measured at each temperature step, respectively. The selectivities of the (by)products (Eq. 5) were normalized to the number of carbon atoms (N_c) in the (by)products and *n*-butane, respectively. Possible byproducts include butenes, acrylic acid, propionic acid, acetic acid, acrolein, acetaldehyde, propane, propene, acetylene, ethylene, ethane, carbon monoxide, and carbon dioxide. There are no unidentified peaks in the gas chromatograms. At low levels of *n*-butane conversion, the product-based analysis of selectivities and conversions (Eqs. 5 and 4) is preferred.

$$X = 1 - \frac{c_{n\text{-butane}}}{c_{n\text{-butane},0}} \times \frac{c_{Ar,0}}{c_{Ar}} \qquad \text{(Eq. 2)}$$

$$S_i = \frac{c_i \times c_{Ar,0}}{c_{n\text{-butane},0} \times c_{Ar} - c_{n\text{-butane}} \times c_{Ar,0}} \times \frac{N_{c,i}}{4} \qquad \text{(Eq. 3)}$$

$$X = 1 - \frac{c_{n\text{-butane}}}{\sum(c_{n\text{-butane}} + c_{products})} \times \frac{c_{Ar,0}}{c_{Ar}} \qquad \text{(Eq. 4)}$$

$$S_i = \frac{c_i \times c_{Ar,0}}{\sum(c_{n\text{-butane}} + c_{products}) \times c_{Ar} - c_{n\text{-butane}} \times c_{Ar,0}} \times \frac{N_{c,i}}{4} \qquad \text{(Eq. 5)}$$

3.3.4 Catalytic Testing

All catalysts were tested in groups of 8 samples following the same testing protocol. Catalyst volumes of 1 mL were kept in their position in the reactor tubes by two layers of inert corundum particles, respectively. The GHSV was fixed at 2000 h^{-1}. The catalysts were ramped at 2 K min^{-1} in a lean air mix of 5 % O_2/N_2 to 250 °C. At 250°C the feed gas was changed to 2 % *n*-butane, 20 % O_2, 3 % H_2O, 3 % Ar with N_2 balance and subsequently the reactor temperature was further increased to 375°C. After an initial equilibration period of 30 min the catalytic measurements were started. The standard testing procedure includes 5 GC analyses per reactor and temperature with the reactor temperature ramping up in 25 K steps up to a maximum temperature of 450 °C, followed by ramping down to 400°C. Finally, the reactors were cooled down to ambient temperature in 5 % O_2/N_2. Thus, information on activity, selectivity and thermal stability/deactivation of the catalysts is obtained. One testing cycle takes 8 days including the (dis)charging and cleaning of the reactors.

3.4 Results and Discussions

According to crystal structure and chemical composition of the catalysts, the results of characterization and catalytic testing are collected in two categories:

3.4.1 Vanadium Phosphorus Oxides

The group of vanadium phosphorus oxides investigated in our study comprises vanadium(III) orthophosphate VPO_4-m1 and vanadyl(IV) pyrophosphate $(VO)_2P_2O_7$. VPO_4-m1 is a new polymorph of VPO_4 and a promising model catalyst with V in the low oxidation state +III and absence of vanadyl oxygen atoms. The latter, however, are often discussed as crucial functional groups for the activation of *n*-butane[3a,42a]. XRPD analysis of the as-prepared sample clearly identifies “single phase” VPO_4-m1 (Figure 15).

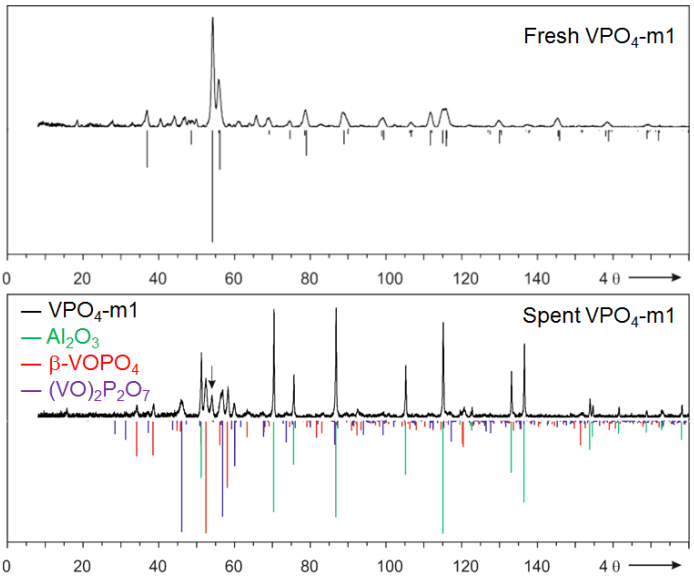

Figure 15 – Guinier photographs of VPO_4-m1 before (top) and after catalytic testing (bottom). Reflections of Al_2O_3 assigned to corundum, which was used as inert material and couldn't be separated from the catalyst.

VPO_4-m1 and its structure are part of ongoing investigations and not clarified to its full extend. Therefore, it is unclear if the additional reflections in the XRPD pattern indicate a superstructure or an adphase. The main reflections of its XRPD pattern are assigned on the basis of the β-$VOPO_4$ structure (*Pnma*, with z = 4, lattice parameters a = 7.7863(5) Å, b = 6.1329(3) Å, c = 6.9673(5) Å). Under reaction conditions VPO_4-m1 is oxidized to $(VO)_2P_2O_7$, β-$VOPO_4$. This oxidation is accompanied by a more than two-fold increase of the specific surface area (Table 6). In parallel, the conversion of *n*-butane as well as the selectivity for MAN steadily increases during the reaction. Likely the significant boost of activity can be correlated to both the increased surface area and the formation of highly active $(VO)_2P_2O_7$ and β-$VOPO_4$, respectively. This is confirmed by the final performance matching the reference VPO from solution combustion synthesis with regard to the selectivity for MAN (Table 7).

Table 7 – Catalyst performance data, stability, specific surface before and after catalytic testing.

Catalyst	X(*n*-butane)[f] (%)	S(MAN)[f] (%)	S(CO_x) (%)	$S_{BET,fresh}$ (m^2/g)	$S_{BET,used}$ (m^2/g)	Structure Stability
VPO_4-m1 [a]	6	21	72	1.9	-	-
VPO_4-m1 [b]	14	49	54	-	4.7	No[c]
$(VO)_2P_2O_7$[d]	80	70	29	26	26	Yes
$(VO)_2P_2O_7$[e]	14	43	45	2.1	1.8	Yes
$(V_{0.95}Mo_{0.05}O)_2P_2O_7$	15	30	34	1.5	1.3	Yes
$Fe(WO_2)_2(P_2O_7)(PO_4)$	3	0	68	1.1	0.8	Yes

[a]TOS = 254 h; [b]TOS = 480 h; [c] Formation of $(VO)_2P_2O_7$ and β-$VOPO_4$; [d] from organic synthesis route; [e] material from SCS; [f] temperature for catalytic testing at 400 °C

In principle $(VO)_2P_2O_7$ can be synthesized *via* two different routes[43a-49a]. In the aqueous route V_2O_5 is reduced by NH_2OH in the presence of H_3PO_4 yielding highly crystalline $(VO)_2P_2O_7$ after calcination of the $VOHPO_4 \cdot 0.5H_2O$ precursor[44a,48a-52a]. Instead, the organic route uses *iso*-butanol as the reducing agent[44a,53a,54a]. Here, V_2O_5, H_3PO_4, and *iso*-butanol are refluxed for several hours and converted to $VOHPO_4 \cdot 0.5H_2O$, which similarly forms $(VO)_2P_2O_7$ in the calcination process. However, the crystallinity of the "organic" material is significantly lower as shown by XRPD measurements, and typically leads to a higher surface area enhancing catalyst performance[44a]. Single-phase $(VO)_2P_2O_7$ with a high crystallinity can also be synthesized by the reduction of β-$VOPO_4$ in Ar at 750 °C, as done in the present study. The selectivity for MAN obtained over this material is lower compared to the industrial reference system VPO from the organic route (Table 6). However, it is in the same range as VPO catalysts synthesized via the water route with a P:V ratio of 1:1[55a].

For $(VO)_2P_2O_7$ the effect of Mo doping was tested. The sample with 5 % of V substituted by Mo $(V_{0.95}Mo_{0.05}O)_2P_2O_7$ was prepared by solution combustion synthesis (SCS). The influence on crystallinity and specific surface area is negligible (Table 2). However, in terms of catalyst performance the surface area-corrected conversion of *n*-butane normalized is similar as compared to the undoped material, whereas the selectivity for MAN is reduced to 30 %. Selectivity loss is mainly contributed to formation of acrylic (S(acrylic acid)=17 %) and acetic acid (S(acetic acid)=10 %). The formation of CO_x is also reduced, which indicates on the one hand inhibition of total oxidation of *n*-butane or MAN by Mo. On the other hand Mo enhances C-C cleavage of reaction intermediates. Since the amount of Mo is

small and the results match the undoped material quiet well it cannot be ruled out that Mo is not incorporated at all.

3.4.2 Mixed Metal Phosphate Solutions

The most extensively investigated sub-category within this class is based on the substitution of V by W according to the formula $(V_{1-x}W_xOPO_4)$[29a]. XRPD patterns of these materials indicate single phases (β for $x \leq 0.01$, α_{II} for $0.04 \leq x \leq 0.26$) with a mean crystallite size in the range of 37 (x = 0.2) to 54 nm (x = 0.06). These phases are stable and neither phase transformation nor formation of an adphase was observed after the catalytic testing (Figure 16).

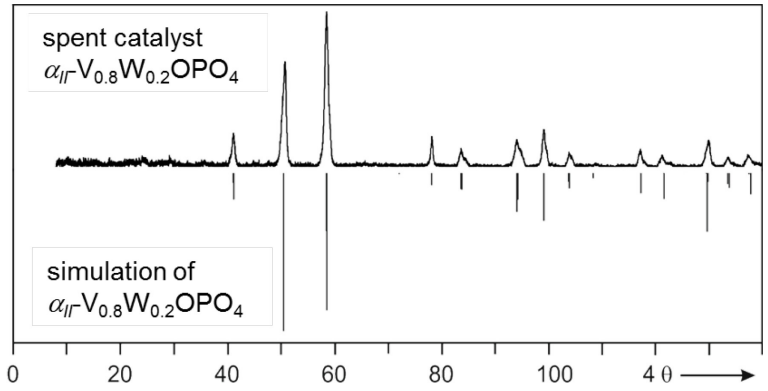

Figure 16 – Guinier photographs of single phase $V_{0.8}W_{0.2}OPO_4$ after catalytic testing and simulated XRPD pattern of $V_{0.8}W_{0.2}OPO_4$.[131]

The BET surface area of the as-prepared samples, which are generally very low in the range of 1–4 $m^2\ g^{-1}$, occasionally changed during the catalytic process (Table 8). An almost doubled specific surface area as well as activation is observed for the tungsten-rich $V_{0.8}W_{0.2}OPO_4$. On the one hand our results could indicate a dramatic reconstruction of the morphologies of particle and surface during the catalytic process. On the other hand, pores might be blocked by residual organic compounds from synthesis. Calcination of all samples at higher temperatures compared to reaction temperatures should be sufficient for carbon removal from synthesis. However, the effect on surface area is small. With decreasing W content within these solid solution-type catalysts the effect of reaction conditions on the specific surface area is reduced, which is almost absent on $V_{0.99}W_{0.01}OPO_4$ and even negative (reduction of S_{BET}) for the tungsten-free $VOPO_4$ catalyst. Instead, the industrial reference VPO, owing to elaborated synthesis protocols, has an approximately 10-fold higher and stable specific surface area of 26 $m^2\ g^{-1}$, which is retained after the catalytic test.

Table 8 – Catalyst stability, specific surface before and after catalytic testing, and activation energy

	Structure Type[a]	$S_{BET,fresh}$ (m^2/g)	$S_{BET,used}$ (m^2/g)	Structure Stability	E_a[b] (kJ mol^{-1})
$VOPO_4$	β	3.5	2.6	Yes	74
$V_{0.99}W_{0.01}OPO_4$	β	1.3	1.2	Yes	93
$V_{0.94}W_{0.06}OPO_4$	α_{II}	2.4	3.9	Yes	93
$V_{0.9}W_{0.1}OPO_4$	α_{II}	4.9	6.5	Yes	108
$V_{0.8}W_{0.2}OPO_4$	α_{II}	3.4	6.3	Yes	115
$WOPO_4$	$WOPO_4$	3.9	5.5	No[c]	24
$V_{0.8}Mo_{0.2}OPO_4$	β	0.8	0.5	Yes	98
$V_{0.8}Mo_{0.2}OPO_4$	γ	1.1	1.3	Yes	111
$W_{0.67}Fe_{0.33}OPO_4$	$WOPO_4$	6.2	6.1	No[d]	n.a.

[a]Greek letters refer to the various polymorphs of $VOPO_4$; [b]Activation energies derived from Arrhenius plots; [c]By-phase related to MPTB. [d]After catalytic testing one additional reflection occures

Catalytic tests of samples of compositions $V_{1-x}W_xOPO_4$ show a remarkably high selectivity for MAN in the range of 20-31 % (Figure 17). XPS studies showed that W^{5+} is oxidized to W^{6+} in $V_{1-x}W_xOPO_4$ reducing an equimolar amount of V^V to V^{IV} [29a]. The comparison of $V_{0.8}W_{0.2}OPO_4$ and $VOPO_4$ clearly shows an increased selectivity for MAN, which might be attributed to the reduced (average) oxidation state of vanadium[29a]. Activation energy can be correlated with tungsten content or the amount of V^{IV}. Isotope labeling studies of *n*-butane showed that C-H activation of methylene groups is the rate determining step and the activation is correlated with the presence of V^V [6a]. By substitution of vanadium by tungsten, the oxidation state of vanadium is reduced, which explains the higher activation energy. Nevertheless, a direct correlation between substituted V and selectivity for MAN is hardly possible. Our results indicate a maximum selectivity near 20 % substitution of V by W ($V_{1-x}W_xOPO_4$ with x = 0.2). On the other hand, vanadium-free $WOPO_4$ does not convert *n*-butane to maleic anhydride, which underlines that W plays not an active role in the catalytic cycle. The change in surface area on the course of the reaction, which is observed for several samples, is typically accompanied by a corresponding change in activity, whereas selectivity for MAN remains constant. Notably, the activity of most of these catalysts if referred to the specific surface area is comparable or even higher than for the reference VPO. For instance, the most selective $V_{0.8}W_{0.2}OPO_4$ provides a conversion and specific surface area (after reaction) of 42 % and 3.4 m^2 g^{-1}, however, 80 % of butane conversion over VPP can be considered mainly as a result

of the superior surface area (26 m^2 g^{-1})[12a]. Thus, a high potential for improvement of these catalysts is expected from the optimization of synthetic strategies.

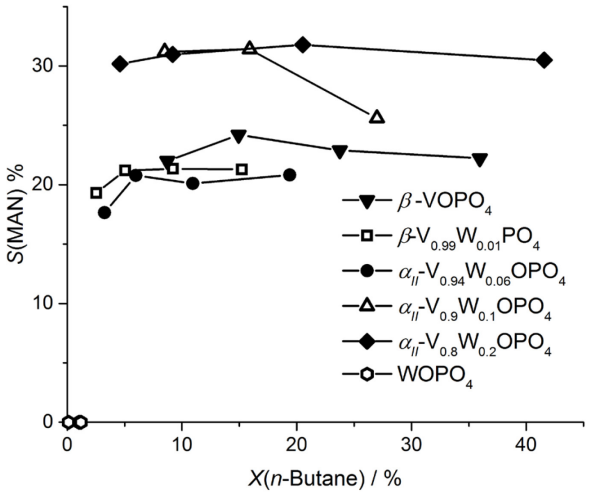

Figure 17 – Selectivity for MAN as a function of conversion of *n*-butane.

The main by-products are CO_x. The organic by-products of *n*-butane oxidation over $V_{1-x}W_xOPO_4$-type materials comprise acrylic and acetic acids (< 8 %), as well as traces of 1-butene, ethylene, furan, and propene (< 1 %).

Molybdenum is a common constituent of selective oxidation catalysts, such as MoVTeNb mixed oxides for ammoxidation of propane to acrylonitrile, oxidation of propane to acrylic acid, or oxidative dehydrogenation of ethane to ethylene[56a-60a]. Thus, Mo was in our focus for the substitution of V in $VOPO_4$. We tested the *γ*- and the *β*-phase with 20 % substitution ($V_{0.8}Mo_{0.2}OPO_4$), respectively (Figure 18)[61a].

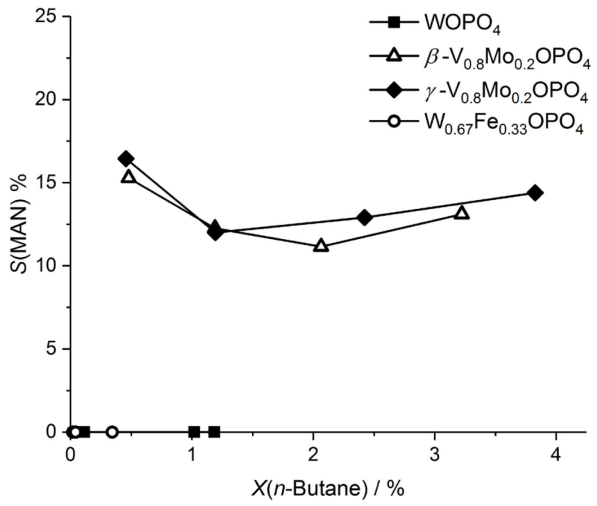

Figure 18 – Selectivity for MAN dependent on conversion of *n*-butane under GHSV = 2000 h^{-1} $c(C_4)/c(O_2)/c(H_2O)$=2 %/20 %/3 %.

Neither phase changes, decomposition nor significant changes in specific surface area were observed after exposure to reaction conditions (Table 2). However, the catalysts were nearly inactive, which might be explained by the very low surface areas and/or by a negative effect of Mo. Compared to the mixed-metal phosphates $V_{1-x}W_xOPO_4$, the selectivity for MAN drops significantly. Similar to $(V_{0.95}Mo_{0.05}O)_2P_2O_7$ selectivity for acetic and acrylic acid is enhanced whereas CO and CO_2 formation is reduced. The surface-corrected net activity is also much lower than for the W-substituted vanadyl phosphates. However, the level of selectivity for MAN of the mixed-metal phosphates $V_{1-x}W_xOPO_4$ and β-$VOPO_4$ is in good agreement with single phase α-$VOPO_4$ and β-$VOPO_4$ catalysts as shown by Shimoda[23a]. Finally, we tested the substitution of W^{5+} by $(Fe^{3+}_{1/3}W^{6+}_{2/3})$ in $WOPO_4$ ($W_{1-x}Fe_xOPO_4$ with x = 0.33). This sample, which was obtained by SCS, provides a relatively high specific surface area of 6.2 $m^2\,g^{-1}$ but is unstable under reaction conditions. This instability under the testing conditions is rather surprising since zero activity for *n*-butane activation indicates little interaction with the gas phase. Although Fe[62a] and W[63a] are known as efficient promotors for selective oxidation catalysts, this is further indication for the active role of V in the activation of *n*-butane as stated by Centi et al.[3a].

3.5 Conclusions

A variety of catalysts were synthesized and tested for selective oxidation of *n*-butane based on $(VO)_2P_2O_7$ and $VOPO_4$. Vanadium was substituted or replaced by other transition metals like tungsten, molybdenum or iron. Substitution of V by W leads to $V_{1-x}W_xOPO_4$ with α_{II} structure type, which is a new class of catalysts for *n*-butane. The amount of tungsten can be tuned in the range from $0.04 \leq x \leq 0.26$. All catalysts are phase stable under reaction conditions, although the specific surface area increases during the reaction, which needs to be studied in detail. Reducing the oxidation state of vanadium increase the activation energy for *n*-butane. Compared to β-$VOPO_4$, the selectivity for MAN could be increased from 20 % up to 31 %. Nevertheless, $V_{1-x}W_xOPO_4$ catalysts are less selective and active than VPO reference. However, it could be shown that the oxidation state of vanadium influences the selectivity for MAN. Substitution of V with Mo in $(VO)_2P_2O_7$ and $VOPO_4$ showed different results. In $VOPO_4$, V by Mo can be easily substituted leading to pure β- and γ-phases, which are more stable under reaction conditions compared to $V_{1-x}W_xOPO_4$. In case of $(V_{0.95}Mo_{0.05}O)_2P_2O_7$ there is no evidence in the XRPD that Mo is incorporated in the $(VO)_2P_2O_7$ crystal structure. In both cases, the effect on catalysis is comparable. Selectivity for MAN and CO_x is reduced compared to the non-substituted catalysts. Further, addition of Mo strongly influences the C-C cleavage leading to the formation products like acetic and acrylic acid. Additionally, we could show that vanadyl pyrophosphate synthesized by solution combustion synthesis is similar to VPO from aqueous routes. Differences in activity can be explained by low surface areas. The reduced selectivity for MAN might be correlated with a 1:1 ratio of P:V since an excess of phosphorus enhances the selectivity. VPO_4-m1 is a new polymorph of VPO, which was introduced by removing the vanadyl oxygen atoms of β-$VOPO_4$. Under reaction conditions it is oxidized to $(VO)_2P_2O_7$ and β-$VOPO_4$. The performance is comparable to VPO by SCS and stresses the importance of stable catalysts as well as the inflexibility of $(VO)_2P_2O_7$. Complete substitution of V in $(VO)_2P_2O_7$ and $VOPO_4$ with iron or tungsten yields phase-stable materials that are not active in the selective oxidation of *n*-butane. In general, the combination of vanadium in the oxidation state +4 and +5 and the ratio of vanadium and phosphate are crucial parameters for selective oxidation of *n*-butane to MAN. Although, VPO is the best catalyst known, it has limited options for optimization due to the inflexible crystal structure and limited effect of promotors[62a]. Therefore, mixed

transition metal $V_xM_{1-x}OPO_4$ might be a good starting point for novel catalysts with higher potential for improvement. It could be shown that solid state synthesis methods like solution combustion synthesis might be a good way to access mentioned new materials/structure motifs for catalysis. However, surface areas are quite low. Consequently, other synthesis methods like hydrothermal routes should be considered as well as supporting of the active catalyst. Transition metals should be selected based on their catalytic performance in oxidation catalysis or by their potential for reduction of vanadium since recent NAP XPS studies of VPO showed that under working conditions the average oxidation state of surface vanadium is +4.3[32a].

From a mechanistic point of view, kinetics and reaction networks of the newly found mixed-metal phosphates $V_{1-x}W_xOPO_4$ should be analyzed and compared to VPO as well as β-$VOPO_4$, which could be a crucial step towards understanding the active site. Especially, the surface composition and oxidation state under reaction conditions needs to be analyzed in detail.

3.6 Literature

[1a] N. Ballarini, F. Cavani, C. Cortelli, S. Ligi, F. Pierelli, F. Trifirò, C. Fumagalli, G. Mazzoni, T. Monti, Top. Catal. 38 (2006) 147–156.
[2a] F. Trifirò, R.K. Grasselli, Top. Catal. 57 (2014) 1188–1195.
[3a] G. Centi, Catal. Today 16 (1993) 5–26.
[4a] C.H. Bartholomew, R.J. Farrauto, Fundamentals of Industrial Catalytic Processes, John Wiley & Sons, Inc, Hoboken, NJ, USA, 2005.
[5a] J.-C. Volta, Comptes Rendus de l'Académie des Sciences - Series IIC - Chemistry 3, (2000), 717–723.
[6a] G. Centi, F. Trifiro, J.R. Ebner, V.M. Franchetti, Chem. Rev. 88 (1988) 55–80.
[7a] M.A. Pepera, J.L. Callahan, M.J. Desmond, E.C. Milberger, P.R. Blum, N.J. Bremer, J. Am. Chem. Soc. 107 (1985) 4883–4892.
[8a] R. Glaum, C. Welker-Nieuwoudt, C.-K. Dobner, M. Eichelbaum, F. Gruchow, C. Heine, A. Karpov, R. Kniep, F. Rosowski, R. Schlögl, S.A. Schunk, S. Titlbach, A. Trunschke, Chem. Ing. Tech. 84 (2012) 1766–1779.
[9a] M.-J. Cheng, W.A. Goddard, J. Am. Chem. Soc. 135 (2013) 4600–4603.
[10a] F. Ghelfi, G. Mazzoni, C. Fumagalli, F. Cavani, F. Pierelli, EP Patent (2004) EP1663482 (A1).
[11a] V.A. Zazhigalov, J. Haber, J. Stoch, A.I. Pyatnitzkaya, G.A. Komashko, V.M. Belousov, Appl. Catal. A: Gen. 96 (1993) 135–150.
[12a] C. Dobner, M. Duda, A. Raichle, H. Wilmer, F. Rosowski, M. Hölzle, Katalysator und Verfahren zur Herstellung von Maleinsäureanhydrid, Patent Application (2006),
EP1915210 (A1).
[13a] H.-Y. Wu, H.-B. Wang, X.-H. Liu, J.-H. Li, M.-H. Yang, C.-J. Huang, W.-Z. Weng, H.-L. Wan, Appl. Surf. Sci. 351 (2015) 243–249.
[14a] H.-Y. Wu, P. Jin, Y.-f. Sun, M.-H. Yang, C.-J. Huang, W.-Z. Weng, H.-L. Wan, J. Mol. Catal. A: Chem. 414 (2016) 1–8.
[15a] B. Jordan, C. Calvo, Can. J. Chem. 51 (1973) 2621–2625.
[16a] B.D. Jordan, C. Calvo, Acta Crystallogr. B Struct. Crystallogr. Cryst. Chem. 32
(1976) 2899–2900.

[17a] R. Gopal, C. Calvo, J. Solid State Chem. 5 (1972) 432–435.
[18a] D. Ballutaud, E. Bordes, P. Courtine, Mater. Res. Bull. 17 (1982) 519–526.
[19a] M. Tachez, F. Theobald, E. Bordes, J. Solid State Chem. 40 (1981) 280–283.
[20a] G. Ladwig, Z. Anorg. Allg. Chem. 338 (1965) 266–278.
[21a] R.N. Bhargava, R.A. Condrate, Appl. Spectrosc. 31 (1977) 230–236.
[22a] E. Bordes, Catal. Today 1 (1987) 499–526.
[23a] T. Shimoda, T. Okuhara, M. Misono, Bull. Chem. Soc. Jpn. 58 (1985) 2163–2171.
[24a] Z.-Y. Xue, G.L. Schrader, J. Phys. Chem. B 103 (1999) 9459–9467.
[25a] M. Abon, J. Catal. 156 (1995) 28–36.
[26a] V.V. Guliants, J.B. Benziger, S. Sundaresan, I.E. Wachs, J.-M. Jehng, J.E. Roberts, Catal. Today 28 (1996) 275–295.
[27a] F. Benabdelouahab, J. Catal. 134 (1992) 151–167.
[28a] S. Geupel, K. Pilz, S. van Smaalen, F. Büllesfeld, A. Prokofiev, W. Assmus, Acta Crystallogr. C Cryst. Struct. Commun. 58 (2002) i9–i13.
[29a] S.C. Roy, R. Glaum, D. Abdullin, O. Schiemann, N. Quang Bac, K.-H. Lii, Z. Anorg. Allg. Chem. 640 (2014) 1876–1885.
[30a] M.S. Hegde, G. Madras, K.C. Patil, Acc. Chem. Res. 42 (2009) 704–712.
[31a] A. Varma, A.S. Mukasyan, A.S. Rogachev, K.V. Manukyan, Chem. Rev. 116 (2016) 14493–14586.
[32a] C. Heine, M. Hävecker, E. Stotz, F. Rosowski, A. Knop-Gericke, A. Trunschke, M. Eichelbaum, R. Schlögl, J. Phys. Chem. C 118 (2014) 20405–20412.
[33a] G.W. Coulston, Science 275 (1997) 191–193.
[34a] E. Mannei, F. Ayari, C. Petitto, E. Asedegbega–Nieto, A.R. Guerrero–Ruiz, G. Delahay, M. Mhamdi, A. Ghorbel, Microporous Mesoporous Mater. 241 (2017) 246–257.
[35a] K. Amakawa, Y.V. Kolen'ko, A. Villa, M.E. Schuster, L.-I. Csepei, G. Weinberg, S. Wrabetz, R. Naumann d'Alnoncourt, F. Girgsdies, L. Prati, R. Schlögl, A. Trunschke, ACS Catal. 3 (2013) 1103–1113.
[36a] S.C. Roy, B. Raguž, W. Assenmacher, R. Glaum, Solid State Sci. 49 (2015) 18–28.
[37a] S.C. Roy, Thermodynamically Stable and Metastable Solids: New Approaches to the Synthesis of Anhydrous Phosphates Containing Vanadium, Molybdenum, and/or Tungsten. PhD Thesis, Bonn, (2015).
[38a] S.L. Wang, C.C. Wang, K.H. Lii, J. Solid State Chem. 82 (1989) 298–302.
[39a] S. Fischer, H. Fischer, S. Diele, G. Pelzl, K. Jankowski, R.R. Schmidt, V. Vill, Liq. Cryst. 17 (1994) 855–861.
[40a] I. Tanaka, M. Yao, M. Suzuki, K. Hikichi, T. Matsumoto, M. Kozasa, C. Katayama, J. Appl. Crystallogr. 23 (1990) 334–339.
[41a] G. Meyer, SOS. Staatsexamenarbeit, Gießen, (1980).
[42a] 11th International congress on catalysis - 40th anniversary, Proceedings of the 11th ICC, (1996) Elsevier.
[43a] J.W. Johnson, D.C. Johnston, A.J. Jacobson, J.F. Brody, J. Am. Chem. Soc. 106 (1984) 8123–8128.
[44a] G. Busca, J. Catal. 99 (1986) 400–414.
[45a] H.E. Bergna, Method of Making Maleic Anhydride, US Patent (1988), US 4769477.
[46a] E. Bordes, Catal. Today 16 (1993) 27–38.
[47a] H. Morishige, J. Tamaki, N. Miura, N. Yamazoe, Chem. Lett. 19 (1990) 1513–1516.
[48a] E.A. Lombardo, C.A. Sánchez, L.M. Cornaglia, Catal. Today 15 (1992) 407–418.
[49a] G. Poli, I. Resta, O. Ruggeri, F. Trifirò, Appl. Catal. 1 (1981) 395–404.
[50a] G.J. Hutchings, M.T. Sananes, S. Sajip, C.J. Kiely, A. Burrows, I.J. Ellison, J.C. Volta, Catal. Today 33 (1997) 161–171.
[51a] L.M. Cornaglia, C.A. Sánchez, E.A. Lombardo, Appl. Catal. A: Gen. 95 (1993) 117–130.
[52a] N. Batis, J. Catal. 128 (1991) 248–263.
[53a] F. Cavani, G. Centi, F. Trifiro, Appl. Catal. 9 (1984) 191–202.
[54a] M. O'Connor, F. Dason, B.K. Hodnett, Appl. Catal. 64 (1990) 161–171.

[55a] R.I. Bergman, N.W. Frisch, Production of maleic anhydride by oxidation of n-butane, US Patent (1966), US3293268A.
[56a] A. Celaya Sanfiz, T. Hansen, A. Sakthivel, A. Trunschke, R. Schlögl, A. Knoester, H. Brongersma, M. Looi, S. Hamid, J. Catal. 258 (2008) 35–43.
[57a] R. Naumann d'Alnoncourt, Y.V. Kolen'ko, R. Schlögl, A. Trunschke, Comb. Chem. High Throughput Screen. 15 (2012) 161–169.
[58a] A. Celaya Sanfiz, T.W. Hansen, D. Teschner, P. Schnörch, F. Girgsdies, A. Trunschke, R. Schlögl, M.H. Looi, S.B.A. Hamid, J. Phys. Chem. C 114 (2010) 1912–1921.
[59a] J.S. Valente, R. Quintana-Solórzano, H. Armendáriz-Herrera, G. Barragán-Rodríguez, J.M. López-Nieto, Ind. Eng. Chem. Res. 53 (2014) 1775–1786.
[60a] R.K. Grasselli, J.D. Burrington, D.J. Buttrey, P. DeSanto Jr, C.G. Lugmair, A.F. Volpe Jr, T. Weingand, Top. Catal. 23 (2003) 5–22.
[61a] A. Raminosona, E. Bordes, P. Courtine, J. Solid State Chem. 68 (1987) 1–10.
[62a] G.J. Hutchings, R. Higgins, J. Catal. 162 (1996) 153–168.
[63a] B.Y. Jo, S.S. Kum, S.H. Moon, Appl. Catal. A: Gen. 378 (2010) 76–82.

4 Kinetic Analysis of VWPO and VPP

Reprinted with permission from American Chemical Society. C. Schulz, F. Pohl, M. Driess, R. Glaum, F. Rosowski, B. Frank, “Selective Oxidation of *n*-Butane over Vanadium Phosphate Based Catalysts: Reaction Network and Kinetic Analysis”, Industrial & Engineering Chemistry Research **2019**, 58, 7, 2492-2502, https://doi.org/10.1021/acs.iecr.8b04328.

4.1 Abstract

The reaction network of *n*-butane selective oxidation was comparatively analyzed over a novel α_{II}-$V_{0.8}W_{0.2}OPO_4$ orthophosphate and a reference vanadyl pyrophosphate (VPP) based catalyst via parameters field studies (T = 360-420 °C, x(*n*-butane) = 0.5-2.0 %, $x(O_2)$ = 10-20 %) as well as co-feed and pulse experiments with presumed reaction intermediates. For VPP the selectivity to the target product maleic anhydride (MAN) is particularly sensitive to the reaction temperature, *n*-butane concentration, and the amount of co-fed H_2O, whereas the selectivity to MAN over the W-containing catalyst is almost independent of all reaction parameters. The roles of 1-butene, acetylene, furan, acetaldehyde, water, and 2,5-dihydrofuran are discussed. Pulsing of possible C4 intermediates indicates that their desorption from the catalyst surface is detrimental to MAN selectivity. Ethylene and acetylene may be formed from MAN. The consecutive reaction of acetylene with H_2O can lead to acetic acid, whereas all other by-products are predominantly formed directly from *n*-butane. The pronounced stability of both samples was confirmed by repeated catalyst performance test under reference conditions, XRD, and SEM. Mass and heat transport limitations were experimentally excluded. A formal kinetic model including *n*-butane, MAN, CO, CO_2, acetic acid, and acrylic acid was developed, in which the acids were found to be less relevant on the $V_{0.8}W_{0.2}OPO_4$ catalyst. However, the main reaction pathways were found to be similar over both catalysts, which differ mainly in product selectivities.

4.2 Introduction

Since the discovery of vanadyl pyrophosphate $(VO)_2P_2O_7$ (VPP) based catalysts in the 1970s[1b], major efforts were put in the understanding of the reaction mechanism of the selective oxidation of *n*-butane to maleic anhydride (MAN), which is one of the few industrial examples of oxidative activation of alkanes with molecular oxygen[2b--

[13b]. A significant improvement of the yield could be realized by advanced synthesis protocols leading to high specific surface areas and defect densities, respectively, as well as by the addition of promotors[10b,14b-19b]. The selectivity of MAN, however, appears to be limited to 70 % at an industrially relevant conversion of 80-85 % and no further breakthrough could be obtained within the past 30 years[20b]. The origin of this observation and especially the nature of the active sites as well as the reaction mechanism of this highly complex reaction are still under debate. A Mars-van Krevelen mechanism as proven by the participation of bulk oxygen in the reaction led to the concept of a riser reactor, which can further increase the yield of MAN, however, on the cost of complex engineering and attrition or friction issues to be solved[21b]. Recent theoretical studies by Goddard et al. introduce a novel reaction model, *i.e.*, a reduction-coupled oxo activation (ROA) mechanism responsible for the catalytic selective activation and functionalization of *n*-butane to MAN over P-based active site[22b-24b].

Several kinetic studies under steady state conditions have been performed to derive kinetic expressions of the reaction sequence[25b]. All of them, however, focus on the main reaction products MAN and CO_x. In a highly cited report Buchanan and Sundaresan[26b] published kinetic data for VPP with different V/P ratios (1.0 and 1.1), however, fitted only for MAN, CO, and CO_2, although by-products like acetic acid (AceA), acrylic acid (AcrA), and ethylene were also detected. Noteworthy, a kinetic inhibition of the redox process by MAN and H_2O was found. In a recent study Mestl *et al.* distinguish between the intrinsic kinetics and P and/or H_2O induced dynamics of the activity[27b]. In their study experimental data were measured in a bench-scale fixed bed reactor using an industrial vanadium phosphorus oxide (VPO) catalyst. However, the data quality possibly suffered from mass and heat transport limitation, and the formation of acrylic and acetic acid was neglected.

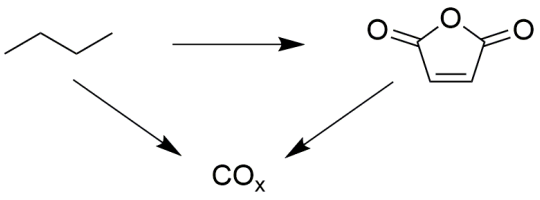

Scheme 3 – Simplified reaction network over VPP for *n*-butane oxidation.

Regarding the reaction network over VPP the main products are MAN, CO, and CO_2. By-products like acetic and acrylic acids are formed in selectivity ranges below 3 %[25b,26b]. Furthermore, a variety of alkenes and oxygenates are found. The sum of

all by-products (w/o acids) is typically below 1 % selectivity. Since the CO/CO_2 ratio in the product gas is almost constant, *i.e.*, VPP is not active for CO oxidation, most kinetic expressions are based on a triangular reaction scheme including the main products (Scheme 1).

The low concentration or even absence of (possible) reaction intermediates hinder the disclosure of the reaction sequence *via* kinetic analyses. A deuteration study by Pepera et al. clearly show that the C-H activation in a methyl group is the rate determining step of n-butane oxidation[9b]. The most accepted reaction pathway for MAN formation follows dehydrogenation of *n*-butane over 1-butene to butadiene. Oxygen insertion and ring closure leads to a 2,5-dihydrofuran intermediate, which is converted to MAN (Scheme 2). However, although all possible C_4 intermediates can be converted to MAN[12b], it remains unclear if the selective conversion of *n*-butane to MAN necessarily requires desorption and readsorption steps or if the entire 14 electron transfer is realized on a single active site.

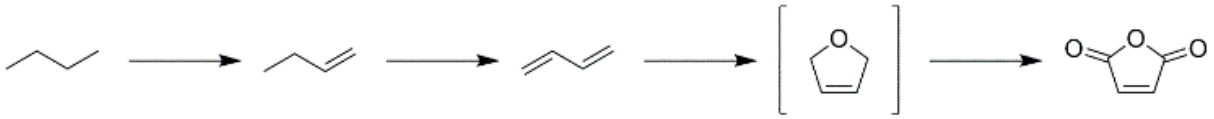

Scheme 2. Postulated pathway of the selective oxidation of *n*-butane to MAN via gas-phase and surface intermediates[7b,28b].

To overcome the limitations of VPP based catalysts, which could not be substantially improved in the past decades[2b,6b,20b], a systematic search for other active and selective phases was performed. In a recent study[29b] we identified the W-substituted α_{II}-$VOPO_4$ as one of the very few alternatives to produce MAN from *n*-butane at all. Although the selectivity of 30 % is relatively low as compared to the industrial standard, this performance belongs to one of the best ever found for VPP-free systems. V^V has been identified as an important constituent of the selective catalyst[4b,30b]. The substitution of 20 % V^V by W^{VI} introduces an equimolar fraction of V^{IV} [31b] to approach the average near-surface oxidation state of VPP, which was found to be 4.1-4.3 under reaction conditions[11b]. Therefore, the catalyst can be seen as an interesting complement to VPP. Hence, we subjected this interesting material to a deeper analysis.

Herein we present a detailed parameters field study of the selective oxidation of *n*-butane over $V_{0.8}W_{0.2}OPO_4$ (in the following denoted as VWPO) and a reference

VPP catalyst, including the derivation of a formal kinetic model including MAN, CO, CO_2, H_2O, acetic acid, and acrylic acid. The loss of phosphorus of VPP, which is discussed as an important issue in long term application, is not considered in this study. However, the decrease in selectivity of MAN was found to be negligible within a total time on stream (TOS) of ≤ 50 d. An optimized parallel testing unit facilitates the acquisition of dense and consistent catalytic performance data, which allows a detailed analysis of aging issues. The general catalyst performance in terms of activity and selectivity to MAN is similar to previously described industrial VPO[27b]. However, we believe that the quality of the manuscript benefits from the detailed comparison with previously published data. The ability to reproduce state-of-the-art knowledge from literature will enhances the credibility of novel aspects.

4.3 Experimental Section

Single-phase microcrystalline VWPO was prepared by solution combustion synthesis (SCS) using $(NH_4)_6W_{12}O_{39}$ *x* H_2O, NH_4VO_3, and $(NH_4)_2HPO_4$ as the precursors. Briefly, the components were mixed together with glycine as the fuel and HNO_3 as the oxidizer, ignited in a muffle furnace at 500 °C, and calcined at 700 °C for 4 d in air. Details of the preparation and characterization of VWPO are described elsewhere[29b,31b]. The VPP catalyst was prepared according to patent literature *via* an organic route[19b]. Briefly, V_2O_5 was dissolved in H_3PO_4 and reduced with isopropanol. The VPP precursor was obtained by filtration, dried, and pre-activated at 300 °C in air. The pelletized powder was used in kinetic studies after activation and equilibration under reference reaction conditions. Different particle size fractions in the range of 50 – 1400 µm were separated using analytical sieves made of stainless steel.

BET measurements were carried out in a volumetric N_2 physisorption setup (Autosorb-6-B, Quantachrome) at the temperature of liquid N_2. The sample was degassed in a dynamic vacuum at 423 K for 2 h prior to physisorption. Full adsorption-desorption isotherms were recorded. The specific surface area according to the BET method was calculated from the linear range of the adsorption isotherm (p/p_0 = 0.05-0.3). The catalyst was characterized before and after catalytic testing.

XRD measurements were performed in Bragg-Brentano reflection geometry on a theta/theta diffractometer (D8 Advance, Bruker AXS) equipped with a secondary graphite monochromator (Cu $K_{\alpha 1+2}$ radiation) and scintillation detector. Sample powder was filled into the recess of a cupshaped sample holder, the surface of the

powder bed being flushed with the sample holder edge. Data analysis was performed using the software package Topas (v 2.1, Bruker AXS). Crystallite size values are based on the double-Voigt approach and reported as $L_{Vol\text{-}IB}$ values (volume weighted mean column length based on integral breadth) without further assumptions about crystallite shape or size distribution[32b].

SEM measurements were carried out using a Hitachi S-4800 microscope operating at 2 kV. The relative V, P, and O contents were determined by means of energy dispersive X-ray spectroscopy (EDX) using an EDAX Genesis spectrometer attached to the microscope, operated at 15 kV.

Catalytic tests were performed in a fully automated, commercial 8-channel parallel testing setup (hte GmbH). The stainless steel reactors (ID 10 mm) are equipped with thermowells (OD 1/8''). An additional reactor is filled with inert material (calcined corundum) to control the inlet concentrations. All effluent gas streams are diluted with hot inert gas to avoid product condensation. Permanent gases were detected via TCD whereas organic compounds were quantified over an FID. A detailed description of the setup can be found elsewhere[29b].

The conversion (X) of *n*-butane (Eqs. 6 and 8) and the selectivities (S) of the respective products are calculated from the concentrations measured with reference to the internal standard Ar (Eqs. 7 and 9). The latter are averaged over 5 runs measured at each temperature step, respectively. The selectivities of the (by)products (Eq. 7) were normalized by the number of carbon atoms (N_C), respectively. Possible by-products include butenes, acrylic acid, propionic acid, acetic acid, acrolein, acetaldehyde, propane, propene, acetylene, ethylene, ethane, carbon monoxide, and carbon dioxide. There are no unidentified peaks in the gas chromatograms. At low levels of *n*-butane conversion, the product-based analysis of selectivities and conversions (Eqs. 8 and 9) is preferred.

$$X = 1 - \frac{c_{n\text{-butane}}}{c_{n\text{-butane},0}} \times \frac{c_{Ar,0}}{c_{Ar}} \qquad \text{(Eq. 6)}$$

$$S_i = \frac{c_i \times c_{Ar,0}}{c_{n\text{-butane},0} \times c_{Ar} - c_{n\text{-butane}} \times c_{Ar,0}} \times \frac{N_{c,i}}{4} \qquad \text{(Eq. 7)}$$

$$X = 1 - \frac{c_{n\text{-butane}}}{\sum(c_{n\text{-butane}} + c_{products})} \times \frac{c_{Ar,0}}{c_{Ar}} \qquad \text{(Eq. 8)}$$

$$S_i = \frac{c_i \times c_{Ar,0}}{\sum(c_{n\text{-butane}} + c_{products}) \times c_{Ar} - c_{n\text{-butane}} \times c_{Ar,0}} \times \frac{N_{c,i}}{4} \qquad \text{(Eq. 9)}$$

To exclude disturbing macro kinetic factors, thus ensure a high quality of kinetic data, a pretest for mass and heat transport limitations was performed. To address the influence of mass transport (pore diffusion), four different particle size fractions from 50-100 µm up to 1-1.4 mm were tested. In addition, different degrees of dilution of the VPP catalyst with quartz in the same particle size are expected to reveal the influence of heat transport, which possibly lead to the formation of a hot spot in the catalyst bed. A detailed overview over this pretest is shown in Tab. 1. The same mass of active material (VPP) was filled into each reactor (0.72 g). The equally distributed gas flow is adjusted to provide a space-time velocity of 2775 ml g^{-1} h^{-1} over each reactor (33.3 ml min^{-1}). The feed contains 2 % *n*-butane, 20 % O_2, 3 % H_2O, 2 % Ar, and balance N_2. Activities and product selectivity for the 7 channels were compared at 420, 400, 380, and 360 °C with a holding time of 15 h at each temperature step.

Using the parallel testing setup the variation of space-time velocities was realized by loading the channels with different amounts of VPP catalyst (Tab. 2). According to the results of the mass and heat transfer analyses, a particle size fraction of 100-200 µm was chosen. Steatite was used to fix the undiluted bed of catalyst particles in the isothermal zone of the reactors. To continuously control the actual feed concentrations, a blank reactor filled with inert steatite completed the set of channels to be tested. The standard gas flow of 33.3 ml min^{-1} per reactor, which was kept constant throughout the study, results in GHSVs in between 2.000 and 16.000 h^{-1} to bring up both differential and integral rate data at almost each point of the parameters field study.

The sequence of catalytic testing comprises a 3×3 matrix of *n*-butane (2, 1, and 0.5 %) and O_2 (20, 15, and 10 %) feed concentrations with excess of O_2 in each point. Previous experiments showed that a full conversion of O_2 can lead to successive formation of coke, which irreversibly deactivates the catalyst. Partial pressures of *n*-butane beyond 2 % are not accessible without entering the explosive range. The total gas pressure was kept constant at 1 bar(a) throughout the entire run. Matching industrially relevant feed conditions, H_2O was typically co-fed at a concentration of 3 %. The reaction temperatures (420, 400, 380, and 360 °C) were investigated in decreasing order. Each point was measured 5 times to check the time scale of equilibration required for stable catalytic performance. To monitor catalyst aging effects on activity and product selectivity, a reference point was frequently

measured (420 °C, 2 % *n*-butane, 20 % O_2). Details of the procedure are listed in the appendix. A co-feed of a gaseous P source, *e.g.*, triethyl phosphate (TEP), to compensate the loss of volatile phosphorus was avoided in this study as this compound significantly affects the catalyst performance by structural and/or electronic modification of active sites.

Pulsing of reaction products and possible intermediates was performed in a self-constructed set-up described elsewhere[33b]. The catalyst was kept inside a single tube reactor in steady state at 2000 h^{-1} and 420 °C in a feed comprising 2 % *n*-butane, 20 % O_2, and 3 % H_2O in inert gas (He, Kr) for an initial equilibration period of 1 week. Pulsing of reactive compounds (carried by an Ar stream) was realized by a pulse valve in the H_2O/He line of the set-up, *i.e.*, the concentrations of *n*-butane and O_2 remained unchanged during the transient experiment. The amount of the reactive compound pulsed over the catalyst was adjusted to its carbon number in a way that 1 substrate carbon atom comes upon approx. 20 surface vanadium atoms to avoid severe and irreversible damage to the catalyst. This estimation is rather a rule of thumb and based on the specific surface area of the catalyst and the ideal crystal structure of VPP[34b], although it is known that the surface layer of VPP under reaction conditions is rather amorphous[35b] and dynamically responds to changes in the reaction conditions[11b,36b]. Repeated performance tests (GC) before and after each pulse series (3 per compound) proved the pronounced stability of the system. The pulse itself was monitored by MS with a full scan (m/z 1-100) and a time-resolution of 2 s. The components pulsed over the catalyst were: furan, 2,5-dihydrofuran, 1-butene, acetaldehyde, acrolein, ethylene, acetylene, acetic acid, and acrylic acid.

Cofeed experiments were performed in the same setup where the transient experiments were performed. Catalyst volumes were 0.1 mL and 0.2 mL for VPP and VWPO, respectively. The starting procedure and equilibration for the catalyst was identical to parameters field study. MAN was added to the reference gas stream by a saturator. Reference measurements were done prior and after cofeed experiments to exclude change in the active phase. Co-feed studies of CO, ethylene and water were performed during the parameters field study prior at the end of the parameters field study. Minimizing the effect of additional reactants, cofeed compounds were matched to found concentrations under reference conditions. Ethylene, CO and water were added to the reference feed. The testing procedure includes 5 GC analyses per reactor. Before and after cofeed experiments, reference measurements under

standard conditions were run to exclude changes in the active phase. Finally, the reactors were cooled down to ambient temperature in 5 % O_2 in N_2.

A simple power-law kinetics (Eq. 11) with Arrhenius-type expressions for the rate constants (Eq. 12) was found to be appropriate to describe the catalytic data.

$$r_i = k_i \, p_a^m \, p_b^n \quad \text{(Eq. 10)}$$

$$k_i = k_0 \exp(-E_{a,i}/R/T) \quad \text{(Eq. 11)}$$

Regarding the formation of CO and/or CO_2 from combustion pathways of hydrocarbons and oxygenates it was assumed that (i) carbon atoms in an oxidation state > +2 react to CO_2, whereas (ii) for all other carbon atoms a common factor φ was established to describe the ratio of CO in the sum of carbon oxides formed by the combustion of this fragment (Eq. 12). Exemplarily, the MAN molecule contains 2 carbon atoms located at the anhydride functionality (oxidation state +3), which are expected to form CO_2. Instead, the two vinylic C atoms (oxidation state -1) form 2 φ CO and 2 (1-φ) CO_2. The resulting stoichiometric equation for the combustion of MAN is shown in Eq. 13.

$$\varphi = CO/(CO+CO_2) \quad \text{(Eq. 12)}$$

$$C_4H_2O_3 + (3 - \varphi)\, O_2 \rightarrow 2\, \varphi\, CO + (4 - 2\, \varphi)\, CO_2 + H_2O \quad \text{(Eq. 13)}$$

The kinetic constants as well as φ were fitted to the entire dataset with the software Berkeley Madonna[37b], using a 4th order Runge Kutta algorithm and least square regression. The concentration profiles of main components (*n*-butane, O_2, MAN, CO, CO_2) were weighted equally (factor 1), whereas the trace components (AceA, AcrA, C_2H_2, C_2H_4) were weighted with a factor of 10. Values for rate orders and apparent activation energies obtained from graphical analyses *via* log-log and Arrhenius plots, respectively, were taken for the initialization of the numerical fitting procedure.

4.4 Results and Discussions

Figure 19 illustrates the pretest results for mass and heat transfer effects, which were only examined for the VPP sample due to its much higher activity. Here, the reference (abscissa) is the undiluted 100-200 µm fraction. The impact of pore diffusion on *n*-butane conversion is negligible and agrees with the absence of micro- and mesopores in the VPP catalyst. Even at the upper temperature limit of 420°C ($X \approx 80\%$) the conversion drops only by <5 % for the bigger particles as compared to the reference. Instead, the lower conversions observed for the smallest particle size fraction (50-100 µm) is likely explained by channeling effects. The dilution of the

catalyst bed with quartz has only a minor effect on the activity and also confirms the absence of a significant hot spot in the catalyst bed. Negligible deviations from the ideal parity line can likely be explained by unavoidable experimental errors such as slight deviations in reactor temperature, catalyst weight, or flow rate, respectively. In summary, the quality of catalytic performance data can be regarded as reliable and consistent.

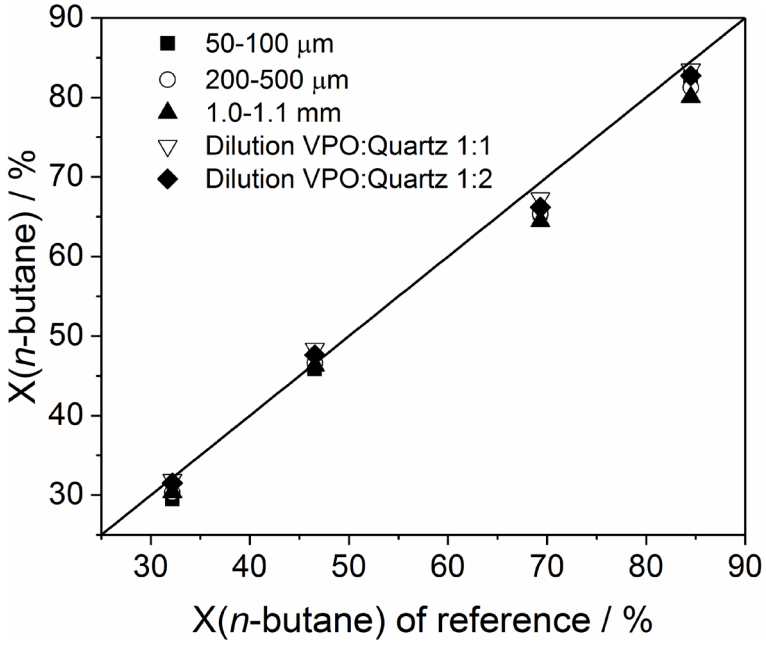

Figure 19 – Experimental analysis of mass and heat transfer limitations for VPP. 2 % *n*-butane, 20 % O_2, 3 % H_2O, balance N_2, 2775 ml g^{-1} h^{-1}, 360-420 °C.s

VPP and VWPO catalysts provide specific surface areas of 30 and 3 m^2 g^{-1}, respectively, which are well preserved after the parameters field study. As confirmed by the similarly stable N_2 physisorption isotherms the particles are free of considerable amounts of meso- or micropores. The structural stability is confirmed by SEM overview images in different magnifications. The EDX analysis averaged over 5 different locations reveal that the P/V and P(V+W) ratio of 1±0.1 remains constant, *i.e.*, a significant loss of P is not detected within the time-scale of the study. Accordingly, the XRD analysis confirmed a pronounced stability of both catalysts as well.

For both samples the average C balance is 100±3 % throughout the whole parameters field study, which lasted approx. 60 days. The absence of gas phase reactions as investigated in a separate reactor filled with inert steatite (Tab. 2) was confirmed by zero conversion of *n*-butane and O_2, respectively, at each point of the testing program.

For the kinetic analysis of a catalytic reaction the stability of the catalyst over the extended duration of the parameters field study is a critical factor. Frequently changing reaction conditions can induce additional stress to the structural integrity. However, only a consistent dataset will allow to create a meaningful kinetic and/or mechanistic model. To quantitatively follow the catalyst deactivation the catalytic performance under reference reaction conditions (2 % *n*-butane, 20 % O_2, 3 % H_2O, balance N_2, 420 °C) was frequently tested (Figure 21). Clearly, in terms of *n*-butane and O_2 consumption the systems are sufficiently stable up to a TOS of 1000 h VWPO: 600 h, see caption of Fig. 20), except for a short initial activation period of VPP. Due to the pronounced stability in *n*-butane conversion the product selectivities can be directly compared. Thus, the slight loss of MAN selectivity at the extended TOS can possibly be correlated with a marginal loss of (near-surface) P, which cannot be detected by EDX and is not replenished by a gaseous P source in this study. For both catalysts the selectivities for CO, CO_2, acetic acid, acrylic acid, and C_2H_2, which are the compounds considered in the kinetic model, remain stable as well. These results nicely confirm the absence of structural changes in the used catalyst samples as evidenced by the physico-chemical characterization.

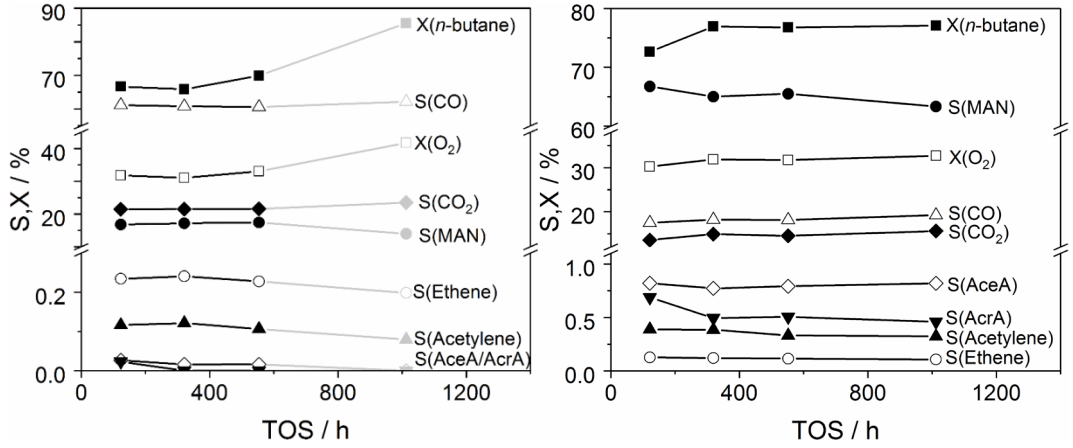

Figure 21 – Aging behavior of *n*-butane conversions and product selectivities during the testing sequence over VWPO (top) and VPP (bottom). 2 % *n*-butane, 20 % O_2, 3 % H_2O, balance N_2, VWPO: 500 h^{-1}, VPP: 4000 h^{-1}, 420 °C Note that a power shut-down at t = 600 h caused an activity increase of VWPO, whereas VPP returned to its previous activity, thus catalytic data measured at t > 600 h (grey) is not considered in the discussion for VWPO.

For both catalysts the main products of the reaction are MAN, CO, and CO_2, with the higher MAN selectivity for the VPP sample. The lower MAN selectivity of 20 % observed over VWPO as compared to our previous study[29b] (30 %) is the stable value after initial equilibration for two weeks. The formation of by-products is detected throughout the test in low quantities. Acetic and acrylic acids are the most important by-products over VPP and frequently discussed in literature. Their abundance,

however, is lower over VWPO. According to the detection limit of our GC, trace amounts of acetaldehyde, ethylene, acetylene, propene, furan, and acrolein are formed. The systematic variation of contact times allows for the comparison of product selectivities at different degrees of *n*-butane conversion under the same reaction conditions, respectively (Figure 22).

On the basis of *S*/*X* trajectories exemplarily shown in Figure 22 for the reference reaction conditions the reaction network can be discussed. As the MAN and CO_x trajectories cannot be extrapolated to an intercept of zero, all main products stem from primary reactions. The constant (VWPO) or slowly decreasing (VPP) selectivity of MAN shows the remarkably high stability of this molecule over both catalysts and suggests that the selectivity issue is related to a primary step of C-H activation rather than a secondary combustion of the activated product. However, beyond a conversion of *n*-butane of 80 % the combustion of MAN becomes increasingly relevant over VPP and the decreasing CO/CO_2 ratio indicates that the secondary combustion forms more CO_2 than the direct alkane combustion. Unfortunately, due to the low activity of VWPO a conversion higher than 70 % is hardly achieved, thus deeper information about MAN combustion cannot be extracted from this dataset. Similarly, all other oxygenates (acetic acid, acrylic acid, acetaldehyde, furan, acrolein) are formed in primary reactions from *n*-butane. These compounds, however, are much less stable than MAN and combust rapidly, with acetic acid being the most abundant oxygenate at high *n*-butane conversion. For most compounds a connection to MAN cannot be found. Regarding acetic acid, however, a pretest with VPP indicated that in the absence of *n*-butane and in a H_2O-rich feed MAN may react to acetic acid, whereas co-dosing of MAN to the regular feed yields exclusively CO and CO_2 in a ratio of almost 1:1 (Table 9).

Table 9 – Results of the co-feed experiments of reactive components over VWPO and VPP catalysts during butane oxidation.

Catalyst	Reaction conditions[b]	GHSV [h^{-1}]	*X*(*n*-butane) [%]	*S*(MAN) [%]	*S*(CO) [%]	*S*(CO_2) [%]	*S*(AceA) [%]	*S*(AcrA) [%]
VWPO	Ref.[a]	2,000	35.9	24.6	56.1	18.0	0.38	0.10
	0.4% MAN	2,000	35.8	15.3	60.8	22.4	0.44	0.14
	0.4% MAN, 400°C	2,000	27.7	15.6	59.8	22.6	0.94	0.19
	0.4% MAN, 10% O_2	2,000	31.8	20.4	56.5	21.5	0.60	0.23
	0.2% MAN	2,000	36.6	19.8	58.3	20.4	0.45	0.16

VPP	Ref.[a]	2,000	80.0	66.4	18.2	14.6	0.80	0.62
	0.5% MAN	2,000	78.6	58.6	20.7	18.3	1.05	0.98
	Ref.[a]	4,000	77.4	63.2	19.4	15.7	0.81	0.48
	1% CO	4,000	78.2	63.9	19.1	15.6	0.82	0.47
	Ref.[a]	4,000	77.9	63.3	19.4	15.6	0.81	0.48
	0.14% C_2H_4	4,000	76.8	63.1	19.5	15.6	0.88	0.49
	0% H_2O	4,000	80.7	61.2	20.9	16.4	0.54	0.34
	Ref.[a] (3% H_2O)	4,000	77.8	63.0	19.5	15.7	0.77	0.46
	10% H_2O	4,000	72.6	65.3	17.3	14.7	1.47	0.73

[a] 420°C, 2 % *n*-butane, 20 % O2, 3 % H2O; catalytic performance as measured before adding respective component [b] Reactive component added to or modified concentrations with respect to the reference conditions, respectively. MAN co-feed was measured in a different reactor set-up at a lower gas flow and optimized isothermicity, which may explain that measured conversions at the same GHSV slightly deviate from the data obtained in the 8-channel set-up (Fig. 2 and kinetic model).

In fact, an apparent stability of acetic acid could originate from its regeneration as a secondary product from MAN, which superimposes the direct formation and degradation pathways. In principle, furan may react to MAN, however, its concentration is far too low to represent a main pathway of the network. Traces of alkenes and alkynes are also present. 1-Butene is formed via oxidative dehydrogenation of *n*-butane and as for furan its low concentration questions its role as a significant intermediate in MAN formation, although a consecutive oxidation to MAN is likely. Indeed for some datasets the selectivity of MAN weakly increases in the range of 10-40 % of *n*-butane conversion (e.g. Figure 22d), which could be attributed to such selective side reactions. The partial oxidation of *n*-butane leads to <0.03 % propene which can further be oxidized to acetaldehyde, acetic acid, acrylic acid, or CO_x. With regard to the C_2 hydrocarbons ethylene and acetylene a significant difference appears. As for the oxygenates and other alkenes, ethylene is a primary product from the degradation of *n*-butane over both catalysts. For VWPO this is valid also for acetylene (Figure 22c). Instead, when plotting the acetylene selectivities vs. *n*-butane conversions for VPP over the entire parameters field (not shown) an intercept near 0% is visible. This is indicative for a consecutive product likely arising from the decomposition of MAN, although the co-feed of MAN predominantly yields CO and CO_2 (Figure 22f). Ethylene and acetylene formed in the reaction network are much more stable than propene and 1-butene. The resulting general reaction network for both catalysts is similar and shown in Scheme 4.

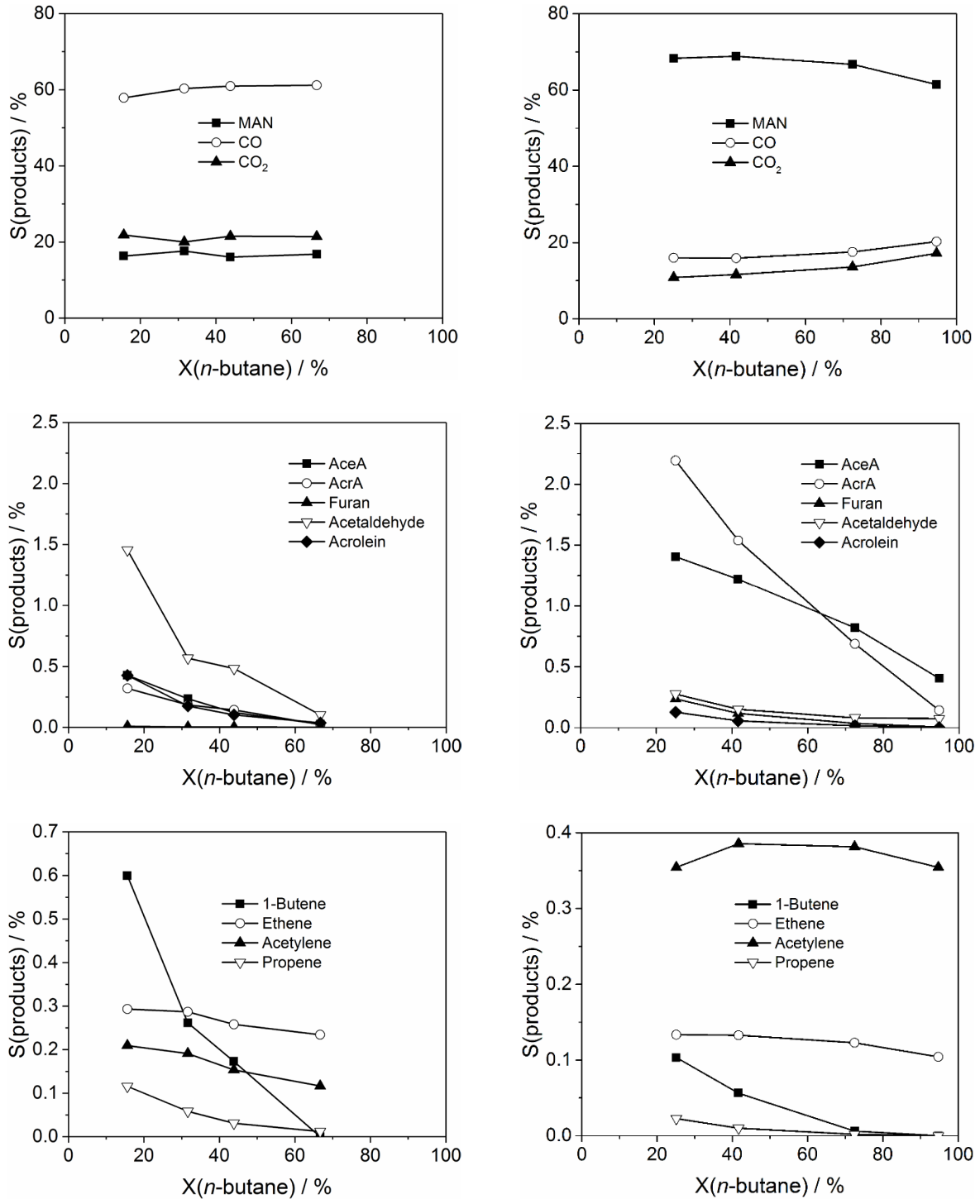

Figure 22 – S/X plots by GHSV variation (2 % *n*-butane, 20 % O2, 3 % H2O, balance N2, 420°C) as obtained for VWPO (a-c, 500-2,000 h^{-1}) and VPP catalysts (d-f, 2,000-16,000 h^{-1}). The product spectrum is subdivided into main products (a,d), oxygenates (b,e) and hydrocarbons (c,f).

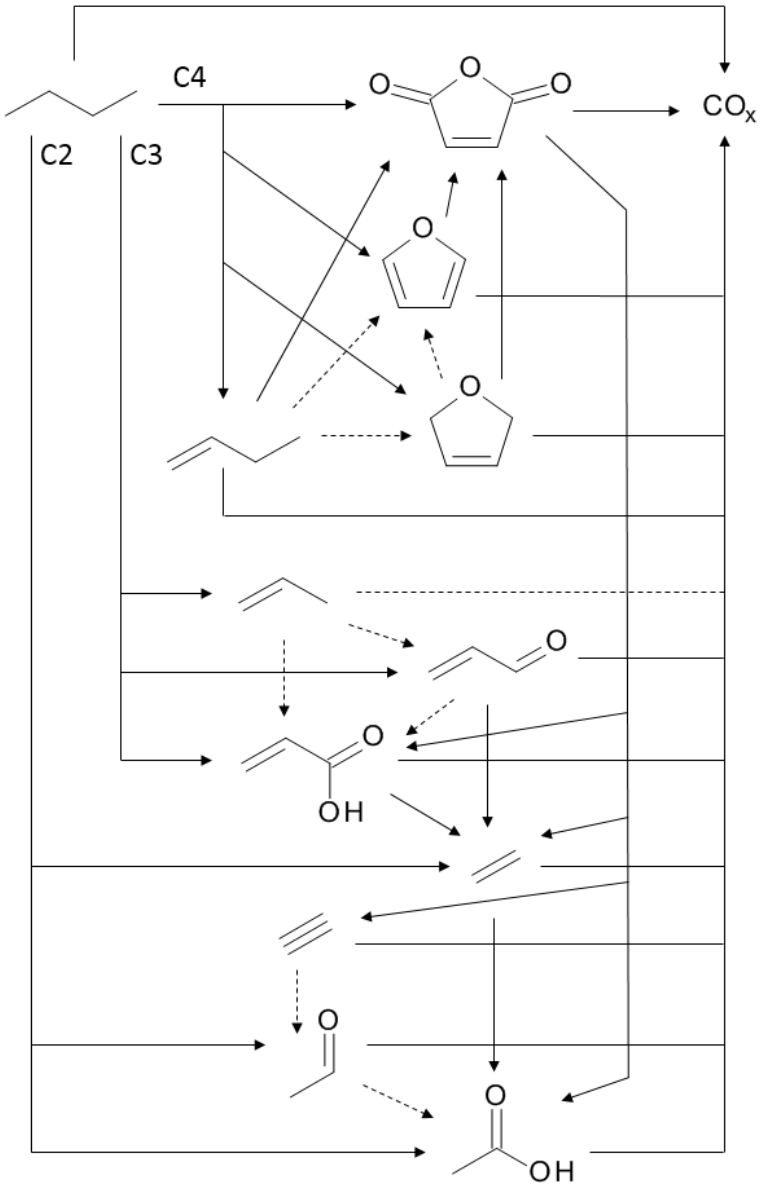

Scheme 4 – Speculative reaction network as discussed. Solid lines: suggested by experiments, dashed lines: assumed/based on literature.

As mentioned above for VWPO it turned out that the maximum conversion of *n*-butane obtained at 420 °C and 1 % *n*-butane/ 20 % O_2 is still too low to identify a significant degradation of MAN in the S/X plot. Consequently, kinetic parameters for MAN combustion as described later could not be obtained. To overcome this, a co-feed study was performed adding MAN at different concentrations (0.2 and 0.4 %), O_2 concentrations (10 and 20 %) and temperatures (400 and 420 °C), as listed in Tab. 8. With regard to the reaction network it is clearly seen that MAN mainly reacts to CO and CO_2 in a ratio of approx. 1:1, however, small amounts of acetic and acrylic acids are formed as well from MAN.

For VPP the reaction network was further investigated by co-feeding of selected reaction products in concentrations similar to their appearances in the product

stream, respectively (Table 10). As discussed above, the co-feed of MAN is predominantly converted to CO_x. Instead, CO and C_2H_4 are not oxidized and totally inert with respect to the *n*-butane conversion. A significant influence, however, is observed for H_2O, which increases the MAN selectivity, however, on the cost of activity. Notably, the formation of acetic and acrylic acids is much stronger promoted by H_2O. Furthermore, transient reactant pulsing was performed over the working VPP catalyst. Figure 23 exemplarily shows the characteristic MS traces (after correction for fragments of other species) for the furan pulse. Furan itself is fully converted during the pulse, thus no signal at m/z 68 is observed during the transient experiment. The products detected are MAN, CO, CO_2, and H_2O, however, with an unexpectedly low selectivity to MAN (Table 10). Clearly, when using the MS scan the limit of fragment deconvolution for minor by-products is much lower than the detection limit of regular GC analysis used in the parameters field test.

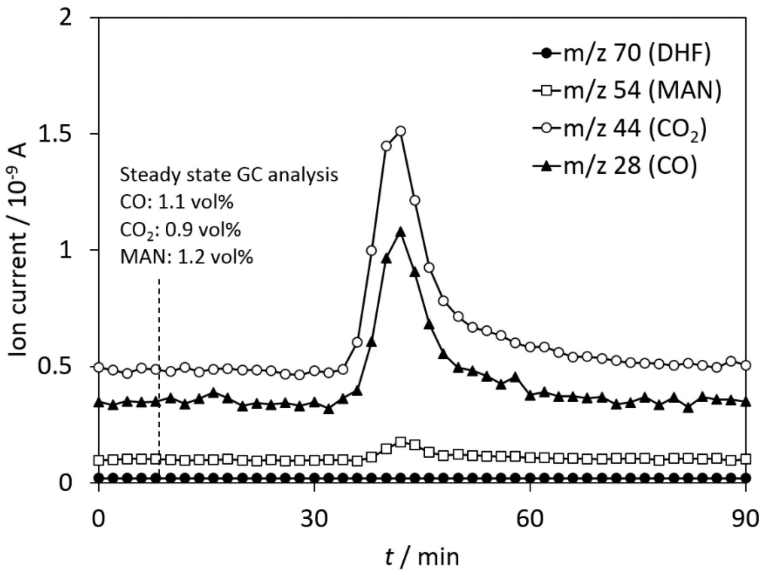

Figure 23 – Product traces after pulsing of furan over VPP under reaction conditions. DHF = 2,5 Dihydrofuran.

Table 10 – Results of the pulsing study of reactive components over VPP.

Substrate	*X* [%]	*S*(MAN) [%]	*S*(others) [%]	CO/CO_2
Furan	100	45	-	1.0
2,5-Dihydrofuran	100	40	-	0.9
1-Butene	100	18	-	0.9
Acrolein	100	-	<1 (Ethylene)	1.7
Acetaldehyde	99	-	-	3.3
AceA	100	-	-	1.6
Acetylene	55	-	<0.1 (AceA)	4.5
Ethylene	18	-	-	8.3
AcrA	100	-	<1 (Ethylene)	2.2

This finding is similar with other C_4 compounds, which are frequently discussed as the intermediates of the multistep conversion of *n*-butane to MAN, such as 1-butene or 2,5-dihydrofuran (Table 10). The MAN selectivity obtained with these substrates is lower than with *n*-butane. A possible interpretation of the experimental results is that the surface intermediates once desorbed into gas phase under certain reaction conditions cannot completely re-adsorb in a way to continue the original reaction sequence starting from *n*-butane. A possible explanation could be the parallel process of immediate reoxidation of vacant surface vanadia sites by gas phase O_2 or bulk-to-surface diffusion of mobile O species (Scheme 5), resulting in an oxidized state of the active site that might favor the total oxidation of activated hydrocarbons such as alkenes and oxygenates.

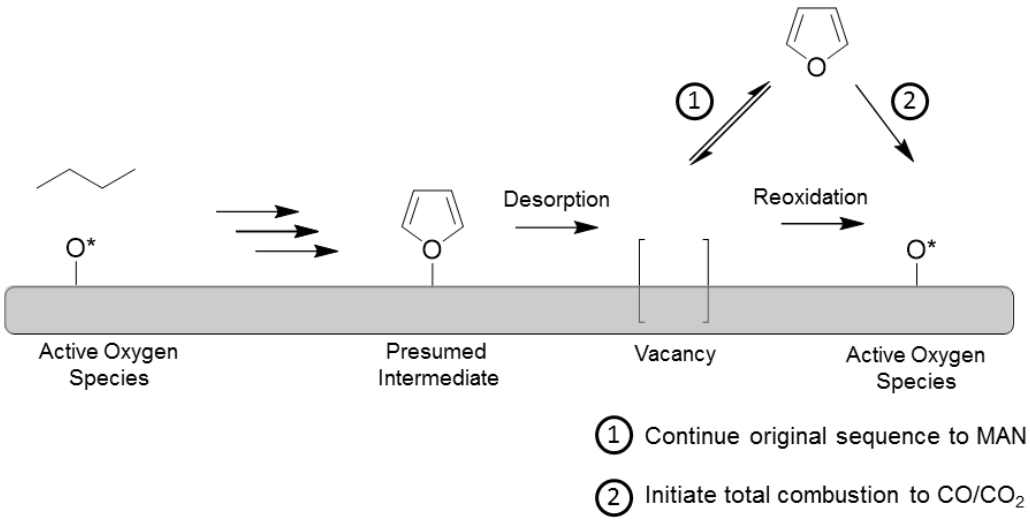

Scheme 5 – Suggested interaction of presumed reaction intermediates with surface V sites.

The results of the series of pulsing experiments are assembled in Tab. 9. For all substrates except ethylene and acetylene full conversion is observed, *i.e.*, these compounds react much faster with the catalyst than *n*-butane. The relative stability of ethylene and acetylene agrees well with their detection as by-products (S > 0.1 %) under typical reaction conditions, and particular with the plateau-like shape of their *S*-*X* curves (Figure 22e), whereas all other C_{2+} by-products approach zero selectivity at full *n*-butane conversion (Figure 22d and e). Notably, the expected transformations from acetaldehyde and acrolein to acetic acid and acrylic acid, respectively, could not be detected. Instead, acrolein forms traces of ethylene and traces of acetic acid are formed from acetylene, whereas all other C_2 and C_3 components exclusively react to CO and CO_2.

Under the selected reference conditions, acetic and acrylic acids are fully converted indicating primary formation from *n*-butane. However, acetylene is converted to acetic acid with low selectivities indicating a new pathway. At least for the route from butenes to acetic acid a reaction pathway via 2-butanol is proposed[38b], with the hydration step likely being catalyzed by acidic P-OH groups as present on VWPO and VPP catalysts. However, with regard to this route it should be noted that in our study neither 1-butene nor acetaldehyde and acrolein was converted to acetic acid. The compounds MAN, CO, C_2H_4, and H_2O were introduced in steady-state co-feed mode (420°C, 20 % O_2, 2 % *n*-butane) in a concentration range that covers the typical concentration of each compound, respectively, in the parameters field test. Tab. 8 shows the results of the co-feed study with the given concentrations of co-feed.

As discussed above MAN is predominantly formed in a primary reaction from *n*-butane as well as by a minor contribution from intermediary formed 1-butene and 2,5-dihydrofuran, respectively. The latter pathways likely occur also on VWPO. For VPP, MAN combustion becomes significant as the conversion of *n*-butane reaches 80–90 % as indicated by a sharp decline of MAN selectivity. In general, the S/X curve is relatively stable and within the entire parameters field the selectivity for MAN do no differ by more than 10 percentage points from the curve obtained under the reference conditions. Whereas for VWPO the MAN selectivity appears to be totally independent from reaction conditions (within the range covered by the parameters field test) some trends are observed for VPP: (i) The influence of temperature on selectivity of MAN is quite small. Temperatures were varied in the range of 360-420°C. A parallel shift of *S*/*X* trajectories is observed with the highest MAN selectivity at the lower end of reaction temperatures. (ii) The MAN selectivity also steadily increases with increasing *n*-butane 0.5-2 vol %) and also (iii) with increasing H_2O 0-10 vol %) feed concentrations, respectively, whereas (iv) the concentration of O_2 has no effect on the *S*/*X* trajectory.

Over both catalysts acetic and acrylic acids are formed with a selectivity below 3 %. Both acids are susceptible to combustion. Over VPP, however, acetic acid is apparently more stable than acrylic acid as indicated by the different signs of curvature, which are typically concave and convex for acrylic and acetic acid, respectively (Figure 22e). Convex shaping, however, could also be induced by secondary formation of acetic acid from MAN, e.g., according to a potential reaction sequence depicted in Scheme 5. This pathway is clearly identified for both catalysts (Tab. 8). The significance of hydrolysis pathways is suggested by the increased formation of acetic acid in the presence of H_2O in the feed as well as the pulse studies. Similarly, monodecarboxylation of hydrolyzed maleic acid, which is already known from patent literature[39b,40b], may serve as a secondary source for acrylic acid (Tab. 8). Taking such hydrolysis pathways of MAN into account it should be noted that in the presence of additional H_2O in the feed the selectivity to MAN is still higher than in the dry feed.

However, for both catalysts the main source for acetic and acrylic acids are the direct formation pathways from *n*-butane, as the trajectories have a positive intercept at zero *n*-butane conversion. Interestingly, for the variation of H_2O and *n*-butane, the trends of formation of organic acids are similar to MAN, *i.e.*, their selectivities

increase with the increasing content of H_2O and/or *n*-butane, respectively, in the feed. It should be noted that the higher hydrocarbon concentration inevitably leads to higher H_2O concentrations at similar degrees of conversion, thus the effect seen for the *n*-butane variation may be (in parts) linked to a surface modification by H_2O.

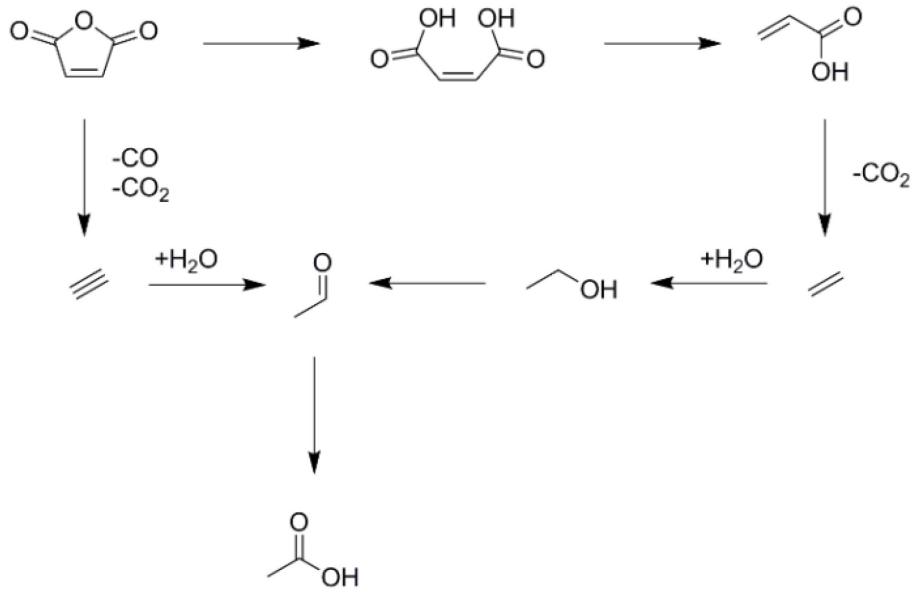

Scheme 6 – Speculative reaction routes from MAN to AceA.

The decrease in activity can be explained by competitive adsorption of H_2O and *n*-butane. The positive effect on selectivity is still under discussion[41b] and focus of our successive report[33b]. In our parameters field test the variation of water feed was done at the end of the study after TOS of 50 d. It should be mentioned that selectivity and conversion are slightly different from the first reference point due to small aging effects. Conversion of *n*-butane increases by 3 % whereas selectivity of MAN decreases by 3 %. During the long test period VWPO and VPP may suffer from the loss of surface phosphorus, which explains the found trends.

The differential and integral kinetic data of the parameters field studies were used to establish steady-state kinetic models for both catalysts, which enable the simulation of the concentration profiles of reactants and products within the reactor as a function of residence time. Besides reactor modeling it can also be used for extrapolation to indicate attractive reaction conditions, which have not been covered by the widespread parameters field study. The formal kinetic models include the main reaction products MAN, CO, CO_2. Acetic and acrylic acids are included only for VPP, whereas their traces over VWPO were found to be insufficiently consistent with regard to the reaction conditions. The latter is likely due to their lower overall concentrations and possibly a result of a lower time-on-stream stability for these by-

products. As discussed above, a factor φ was introduced to describe the ratio of CO/CO_x arising from the combustion of non-oxygenated carbon atoms in any combustible reaction product. Thus, the stoichiometric equations considered in the model are the following:

r_{0c}: $C_4H_{10} + (6.5 - 2\,\varphi)\,O_2 \rightarrow 4\,\varphi\,CO + (4 - 4\,\varphi)\,CO_2 + 5\,H_2O$ (Eq. 14)

r_{1f}: $C_4H_{10} + 3.5\,O_2 \rightarrow C_4H_2O_3 + 4\,H_2O$ (Eq. 15)

r_{1c}: $C_4H_2O_3 + (3 - \varphi)\,O_2 \rightarrow 2\,\varphi\,CO + (4 - 2\,\varphi)\,CO_2 + H_2O$ (Eq. 16)

r_{2f}: $C_4H_{10} + (3.5 - 0.5\,\varphi)\,O_2 \rightarrow C_3H_4O_2 + \varphi\,CO + (1 - \varphi)\,CO_2 + 3\,H_2O$ (Eq. 17)

r_{2c}: $C_3H_4O_2 + (3 - \varphi)\,O_2 \rightarrow 2\,\varphi\,CO + (3 - 2\,\varphi)\,CO_2 + 2\,H_2O$ (Eq. 18)

r_{3f}: $C_4H_{10} + 2.5\,O_2 \rightarrow 2\,C_2H_4O_2 + H_2O$ (Eq. 19)

r_{3c}: $C_2H_4O_2 + (2 - 0.5\,\varphi)\,O_2 \rightarrow \varphi\,CO + (2 - \varphi)\,CO_2 + 2\,H_2O$ (Eq. 20)

Here, the indices 0, 1, 2, 3, f, and c stand for *n*-butane, MAN, acrylic acid, acetic acid, formation, and combustion, respectively. The kinetic constants extracted from the simultaneous fit are listed in Tab. 1. As a representative example, experimental data at the reference conditions together with simulated concentration profiles are shown in Figure 24.

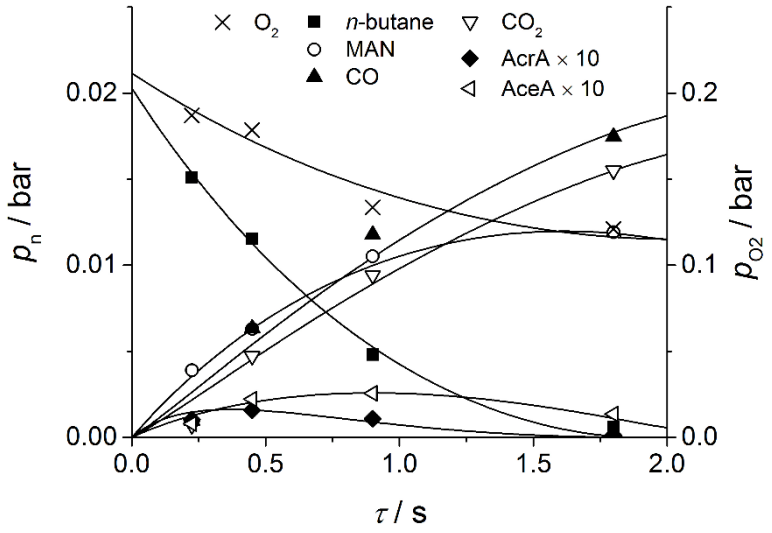

Figure 24 – Kinetic modelling of *n*-butane oxidation. Exemplarily shown for the reference conditions over VPP: 2 % *n*-butane, 20 % O_2, and 3 % H_2O at 420 °C, 2,000-16,000 h^{-1}. Symbols: experimental data, lines: kinetic model.

Table 11 – Kinetic parameters of *n*-butane oxidation as derived from formal kinetic analysis.

	r_{0c}	r_{1f}	r_{1c}	r_{2f}	r_{2c}	r_{3f}	r_{3c}
VWPO							
E_a / kJ mol^{-1}	85	67	72[b]	-	-	-	-
k_0 / mol kg^{-1}s^{-1}	1.14×10^{4}	3.22×10^{3}	1.65×10^{3} [b]	-	-	-	-
n_C[a]	0.90	0.93	0.99[b]	-	-	-	-
n_{O2}	0.13	0.00	0.49[b]	-	-	-	-
VPP							
E_a / kJ mol^{-1}	101	82	86	156	144	52	92
k_0 / mol kg^{-1}s^{-1}	4.34×10^{4}	1.46×10^{4}	4.36×10^{3}	1.84×10^{9}	1.70×10^{9}	2.21×10^{0}	8.52×10^{2}
n_C[a]	0.34	0.50	0.50	0.83	0.68	0.63	0.21
n_{O2}	0.37	0.42	0.24	0.53	0.33	0.17	0.11

[a] carbonaceous substrate; [b] estimated from co-feed study (Tab. 8)

4.5 Conclusion

The parameters field study inside a parallel test setup was found to be an advantageous method for acquiring steady state kinetic data in a short time scale. An important aspect is the absence of mass and heat transfer limitations. The repeated measurement of the catalyst performance under reference reaction conditions shows a low activation with minor decrease in MAN selectivity for VPP, whereas VWPO unintendedly activates in the middle of the parameters field test while keeping the selectivity pattern. The data unsuitable for kinetic fitting could be easily identified by control experiments. For both catalysts VWPO and VPP the stability of crystal structure and specific surface area were confirmed by XRD and SEM measurements. The product spectrum and reaction network of the selective oxidation of *n*-butane appeared similar over both catalyst systems and is coherent with the reports published in literature with the exception of acetylene which was not reported so far. Notably, MAN appears to be more stable over VWPO, however, on the cost of a much lower initial selectivity. The assignment of these findings to electronic or structural properties of the model catalysts might lead to further improvements. The appearances of ethylene and acetylene, as well as acetic and acrylic acids were found to correlate with selectivity of MAN, indicating them (partially) as by-products of MAN decomposition. New reaction pathways for acetic and acrylic acids were proposed based on parameters field, pulse, and cofeed studies. Acrylic acid can be

formed by hydrolysis of MAN, which is subsequently monodecarboxylated. Further, decarboxylation leads to ethylene. Ethylene is oxidized to acetic acid via ethanol and acetaldehyde. Another pathway of acetic acid formation is based on acetylene, which is formed from MAN. Hydrolysis of acetylene leads to acetaldehyde, which can be selectively oxidized to acetic acid. Furan, 2,5-dihydrofuran and 1-butene are discussed as crucial reaction intermediates in the literature. Pulse studies over equilibrated catalyst showed that MAN is formed from all assumed intermediates, but selectivites are lower than expected. The finding might be attributed to readsorption on the surface, which leads to non-selective pathways. Nevertheless, the results are in good agreement to the literature. Carbon monoxide is not readsorbed on the active site and cannot be oxidized to carbon dioxide. Temperature, water and *n*-butane partial pressure have a positive impact on *n*-butane concentration whereas oxygen partial pressure has none. We implemented a kinetic model which includes main reaction products MAN, CO, CO_2 as well as by-products like acetic acid and acrylic acid. Further, the role of oxygen activation is included and reflects experimental evidence.

As a very important result the success in kinetic modelling supports the reaction network proposed. The resulting model can now be used for further experiments, i.e., advanced modelling of profile reactors as already done by Horn et al.[42b], or extrapolation for the search of optimized reaction conditions. The straightforward discussion of kinetic parameters in terms of the reaction mechanism is not possible due to the formal character of the kinetic model. In general, the apparent activation energies for *n*-butane combustion (r0c) as well as formation and combustion of MAN (r1f, r1c) are by approx. 15 kJ/mol lower for VWPO than for VPP, which is possibly due to the higher average oxidation state of VWPO. Such a phenomenon has recently been reported for the oxidative dehydrogenation over carbon-based catalysts[43b]. In fact, the pre-exponential factors of VWPO are only by factor 3-4 smaller than those of VPP, although the specific surface area is by factor of 10 smaller, indicating that the net activity of VWPO could be substantially increased by increasing the specific surface area (3 m^2/g), e.g., by advanced synthesis protocols or by supporting the active phase. Notably, the apparent activation energies of acetic acid formation and combustion, respectively, are much higher than the values for the other reactions over VPP. As we discussed previously, acetic acid may also be formed in a secondary step from MAN. Thus, the exceptionally high apparent

energies could point at a more complex reaction network as the basis for kinetic modelling. To solve this issue, dedicated co-feed studies with MAN and acetic acid are required. The apparent rate orders for most reactions lie in between 0.1 and 0.9, with the rate order of the carbonaceous compound being always higher that the rate order of O_2. This can be tentatively interpreted as an indication that both steps, the catalyst oxidation and the hydrocarbon conversion, contribute equally to the overall rate with the catalyst being in a rather oxidized state. Mechanistic models to be developed and fitted to the dataset can possibly shed light on this aspect. MAN formation over VWPO (r1f) is an single example with an almost first order reaction with respect to *n*-butane and zero rate order with respect to O_2. Here, we can conclude that the surface active site for the rate determining step is fully oxidized and the overall rate is only limited by the activation of *n*-butane. However, for all other reactions the situation is more complex.

If the product pattern and kinetic aspects of a catalyst under certain reaction conditions can be regarded as a sensitive fingerprint for the nanostructure of the active site of a catalyst, then the apparent similarities between VWPO and VPP point at a similarly structured active domain. This aspect should be discussed in terms of the novel mechanistic reaction model suggested recently by Goddard et al.[22b-24b] The ROA mechanism is based on the redox-transformation of reduced $(VO)_2P_2O_7$ and oxidized X1-$VOPO_4$ phases. Such transformation cannot easily be transferred to the α_{II} phase of our VWPO catalyst, although the surface composition and structure of both VPP and VWPO systems are still under debate and unknown, respectively. We will address this apparent contradiction in future surface-sensitive studies.

Further development and validation of the kinetic model is crucial. Experiments including macro kinetics like heat and mass transport limitation are advisable based on this micro kinetic model. The reaction network is quite simple and should include all other by-products. Therefore, detailed reaction network studies are necessary. Reaction intermediates have to be introduced over equilibrated catalysts. The role of bulk oxygen is quite controversial, so isotope labelling studies should be taken into consideration. For VPP we identified the reaction temperature as the most important factor to realize changes in MAN selectivity. A lower reaction temperature, however, is accompanied by a significant loss of activity, thus future efforts should address structural factors like specific surface area, e.g., by supporting VPP, or developing templating techniques.

4.6 Literature

[1b] R.I. Bergman, N.W. Frisch (1964) US 3,293,268.
[2b] G. Centi, Catal. Today 16 (1993) 5–26.
[3b] G.J. Hutchings, J. Mater. Chem. 14 (2004) 3385.
[4b] G.W. Coulston, Science 275 (1997) 191–193.
[5b] J.-C. Volta, C.R. Acad. Sci., Ser. IIc: Chim. 3 (2000) 717–723.
[6b] N. Ballarini, F. Cavani, C. Cortelli, S. Ligi, F. Pierelli, F. Trifirò, C. Fumagalli, G. Mazzoni, T. Monti, Top. Catal. 38 (2006) 147–156.
[7b] C.H. Bartholomew, R.J. Farrauto, Fundamentals of industrial catalytic processes, John Wiley & Sons, Inc, Hoboken, NJ, USA, 2005.
[8b] B.K. Hodnett, Catal. Rev. 27 (2006) 373–424.
[9b] M.A. Pepera, J.L. Callahan, M.J. Desmond, E.C. Milberger, P.R. Blum, N.J. Bremer, J. Am. Chem. Soc. 107 (1985) 4883–4892.
[10b] V.V. Guliants, J.B. Benziger, S. Sundaresan, I.E. Wachs, J.-M. Jehng, J.E. Roberts, Catal. Today 28 (1996) 275–295.
[11b] M. Eichelbaum, M. Hävecker, C. Heine, A. Karpov, C.-K. Dobner, F. Rosowski, A. Trunschke, R. Schlögl, Angew. Chem. Int. Ed. 51 (2012) 6246–6250.
[12b] V.V. Guliants, J.B. Benziger, S. Sundaresan, Stud. Surf. Sci. Catal. 101 (1996) 991–1000.
[13b] S.S. Chadwick, Reference Services Review 16 (1988) 31–34.
[14b] V.A. Zazhigalov, J. Haber, J. Stoch, A.I. Pyatnitzkaya, G.A. Komashko, V.M. Belousov, Appl. Catal. A 96 (1993) 135–150.
[15b] G.J. Hutchings, R. Higgins, J. Catal. 162 (1996) 153–168.
[16b] G.J. Hutchings, M.T. Sananes, S. Sajip, C.J. Kiely, A. Burrows, I.J. Ellison, J.-C. Volta, Catal. Today 33 (1997) 161–171.
[17b] J.W. Johnson, D.C. Johnston, A.J. Jacobson, J.F. Brody, J. Am. Chem. Soc. 106 (1984) 8123–8128.
[18b] F. Ghelfi, G. Mazzoni, C. Fumagalli, F. Cavani, F. Pierelli (2004) US 7,638,457 (B2).
[19b] J. Weiguny, S. Storck, M. Duda, C. Dobner, EP Patent (2003) EP1487576 (A1).
[20b] F. Trifirò, R.K. Grasselli, Top. Catal. 57 (2014) 1188–1195.
[21b] R.M. Contractor, A.W. Sleight, Catal. Today 3 (1988) 175–184.
[22b] W.C. O'Leary, W.A. Goddard, M.-J. Cheng, J. Phys. Chem. C 121 (2017) 24069–24076.
[23b] M.-J. Cheng, W.A. Goddard, R. Fu, Top. Catal. 57 (2014) 1171–1187.
[24b] M.-J. Cheng, W.A. Goddard, J. Am. Chem. Soc. 135 (2013) 4600–4603.
[25b] G. Centi, F. Trifirò, J.R. Ebner, V.M. Franchetti, Chem. Rev. 88 (1988) 55–80.
[26b] J.S. Buchanan, S. Sundaresan, Appl. Catal. 26 (1986) 211–226.
[27b] G. Mestl, D. Lesser, T. Turek, Top. Catal. 59 (2016) 1533–1544.
[28b] B. Chen, E.J. Munson, J. Am. Chem. Soc. 121 (1999) 11024–11025.
[29b] C. Schulz, S.C. Roy, K. Wittich, R.N. d'Alnoncourt, S. Linke, V.E. Strempel, B. Frank, R. Glaum, F. Rosowski, Catal. Today (2018) 10.1016/j.cattod.2018.05.040.
[30b] K. Aït-Lachgar, M. Abon, J.C. Volta, J. Catal. 171 (1997) 383–390.
[31b] S.C. Roy, R. Glaum, D. Abdullin, O. Schiemann, N. Quang Bac, K.-H. Lii, Z. Anorg. Allg. Chem. 640 (2014) 1876–1885.
[32b] R.L. Snyder, J. Fiala, H.-J. Bunge, Defect and microstructure analysis by diffraction, Oxford University Press, Oxford, 1999.
[33b] C. Schulz, B. Frank, R. Krähnert, F. Rosowski (Submitted).
[34b] S. Geupel, K. Pilz, S. van Smaalen, F. Büllesfeld, A. Prokofiev, W. Assmus, Acta Crystallogr., Sect. C: Cryst. Struct. Commun. 58 (2002) i9-i13.
[35b] C. Heine, M. Hävecker, E. Stotz, F. Rosowski, A. Knop-Gericke, A. Trunschke, M. Eichelbaum, R. Schlögl, J. Phys. Chem. C 118 (2014) 20405–20412.
[36b] M. Abon, J. Catal. 156 (1995) 28–36.
[37b] R. Macey, G. Oster, Berkeley Madonna, 2009.
[38b] T. Yamashita, S. Ninagawa, T. Kato, Bull. Japan Petrol. Inst. 18 (1976) 167–177.
[39b] O.S. Fruchey, C.T. Reeves, W.C. Brooks, E.J. Yang, R.L. Roundy, EP Patent (2008) EP2786980 (A1).

[40b] A.P. Lloyd, US Patent (1966) US3476803 (A).
[41b] D. Lesser, G. Mestl, T. Turek, Appl. Catal. A 510 (2016) 1–10.
[42b] Y. Dong, M. Geske, O. Korup, N. Ellenfeld; F. Rosowski, C. Dobner, R. Horn, Chem. Eng. J. 350 (2018) 799.
[43b] O. V. Khavryuchenko, B. Frank, J. Phys. Chem. C 121 (2017) 3958.

5 Oxygen Activation and Dynamics over Vanadyl Pyrophosphate

Reproduced with permission from Wiley-VCH Verlag GmbH & Co. KGaA. C. Schulz, R. Krähnert, F. Rosowski, B. Frank: Selective Oxidation of *n*-Butane over Vanadium-Phosphorus Oxide: Oxygen Activation and Dynamics. ChemCatChem. 2018, 10, 5523-5532. https://doi.org/10.1002/cctc.201801177

5.1 Abstract

The complex microkinetics of the selective oxidation of *n*-butane to maleic anhydride (MAN) over vanadyl pyrophosphate (VPP) based catalysts has been widely investigated so far, however, is still under debate. We present novel results of kinetic analyses and isotope labeling to shed light on the activation of gas-phase oxygen and the dynamics of oxygen species on the catalyst surface and in the bulk. We suggest the existence of at least two catalytically relevant surface oxygen species responsible for selective and unselective activation of *n*-butane, which are formed by adsorption and consecutive dissociation of O_2 at the active site. The formation of selective [O] from unselective [O_2] is likely promoted by co-fed H_2O, which increases the MAN selectivity. Regarding the VPP bulk serving as a reservoir for active [O] species it is concluded that the dynamic exchange is limited to the amorphous surface layer forming under reaction conditions, whereas the crystalline bulk is not involved into the reaction. Labelling studies are heavily influenced by vital $^{16}O/^{18}O$ scrambling of MAN isotopes with the reaction product H_2O.

5.2 Introduction

The catalytic oxidation of *n*-butane to maleic anhydride (MAN) is one of the few industrial processes of a single-step selective alkane oxidation and has an annual world capacity of more than 1 million tons[1c]. Although the productivity of this process could be steadily improved over the past decades, the yields are still below 65 %, which is mainly limited by selectivity[1c-4c]. The industrial state of the art catalyst is based on crystalline $(V^{IV}O)_2P_2O_7$ (vanadyl pyrophosphate, VPP). Numerous studies were dedicated to analyzing the active sites and to understanding reaction kinetics, respectively. Due to its topotactic nature, the synthesis method strongly influences the formation of several vanadium phosphorus oxide (VPO) by-phases leading to a rich number of catalysts with different catalytic performances. The most successful synthesis leading to a defect-rich material providing high activity and selectivity is

based on the organic route using alcohol, V_2O_5, and phosphoric acid[5c]. Approaches for surface analysis of the working phase reveal several challenges, i.e., VPP is beam sensitive[6c] and vanadium oxides can be easily reduced under reduced pressure[7c]. Recently, near ambient pressure X-ray photoelectron spectroscopy (NAPXPS) studies revealed that under reaction conditions the average oxidation state of near-surface vanadium is 4.3[7c], which is significantly higher compared to other studies[8c]. Accordingly, the catalytically active redox pair is based on V^{4+} and V^{5+} ions as shown by XPS and total-reflection-angle X-ray spectroscopy (TRAXS) studies. There is an enrichment of P near the surface, which can be correlated with product selectivity. Several facets of VPP crystals have been proposed to be active, although the top layer of the surface termination is rather amorphous and dynamic with regard to its composition [7c] Furthermore, several orthophosphate by-phases were discussed to be involved into the reaction mechanism. The most recent proposal for a reaction mechanism involves the participation of P=O bonds[9c]. Several studies were dedicated to the nature of active oxygen species and their role in formation of MAN. Especially the role of nucleophilic and electrophilic oxygen atoms and their origin from surface and bulk dynamic processes are still under controversial discussion. Studies by Pepera[4c] et al., Abon[10c] et al., and Wang[11c] et al. claim that lattice oxygen ions (nucleophilic oxygen) in a few surface layers are involved in the formation of MAN and COx, whereas Trifiro[12c] et al. proposed adsorbed oxygen to be involved in oxygen insertion steps from butadiene to MAN. Zazhigalov[13c] et al. concluded from pulse flow reactor studies, that MAN formation is mainly due to gas-phase oxygen. Contractor et al. transferred VPO catalysts from fixed bed reactor to riser reactors. Separation of oxidation and reduction steps increased the selectivity to MAN, which could even be improved by stripping of the freshly oxidized catalysts[14c] The contribution of electrophilic short-lived oxygen species, which are formed during the reoxidation sequence before they are incorporated into the catalyst lattice, to the undesired formation of COx, is proposed as the explanation of this finding.

Water as an omnipresent by-product, was found to reduce reaction rates[15c] and to increase the selectivity by adsorption on surface sites as well as facilitate re-oxidation of the catalyst[16c]. Further, there is a correlation between H_2O and the mobility of P on the surface. Cavani[17c] et al. could show that excess H_2O depletes phosphorus. Isotope labelling studies with ^{18}O inside a TAP reactor indicated an incorporation of

oxygen from water into the reaction products by hydrolysis of V-O-P and P-O-P bonds. A further beneficial effect of water might be the prevention of large amounts of carbonaceous surface species, which may restrain the reoxidation of the catalyst. This study is focused on analysis of the active phase of VPO catalyst under industrially relevant conditions. Steady state isotope transient kinetic analysis (SSITKA) including $^{18}O_2$ was used to further clarify the role of bulk oxygen, which must be subdivided with regard to its location in the crystalline bulk oxygen (VPP) or in the few nm thick amorphous surface layer. The role of water was revisited in more detail as well as considered for oxygen exchange with MAN.

5.3 Experimental

5.3.1 Catalyst Preparation and Characterization

The VPO reference catalyst was synthesized according to patent[5c] via the organic synthesis route using iso-butanol. The catalyst was used in a previous study[18c]. Briefly, the material is phase-pure VPP with a specific surface area of 30 m^2 g^{-1}. Details of the characterization (XRD, SEM, N_2-physisorption) can be found elsewhere[18c]. P/SBA-15 was produced by impregnation of SBA-15 with phosphoric acid.

5.3.2 Set-up for Catalytic Testing

The measurements were carried out on a self-constructed apparatus (Fig. 20), which allows automatic changes in the temperature and concentration during reactions. The reactor consists of glassed line tubing (inner diameter 4 mm), which is encased by a copper shroud providing an excellent heat distribution. The catalyst is retained by spherical particles of Steatite. At the beginning and in the middle of the catalyst bed temperature is measured by thermocouples inside a stainless steel tube (outer diameter 1 mm, wall thickness 150 µm). The reactor is placed inside an electric furnace, which has computer aided temperature and time controls in the range of 250-500 °C. Depending on selectivity/conversion-behavior of the investigated reaction system the mass of the catalyst varies between 50 and 600 mg at total flow rates of 10 and 50 mL min-1. Educts (*n*-butane, O_2) and inert gas (He, N_2, Ar, Kr) are introduced to the reactor by mass flow controllers (Bronkhorst). Two identical saturators allow the introduction of liquid compounds such as H_2O or organic intermediates to the reactor. One saturator is directly connected to the feed line, the other one is connected to the pulse valves. Temperature of the saturators is controlled by thermostats with Pt100 thermocouple measuring the gas phase

temperature. Online gas analysis is carried out by gas chromatography (GC, Agilent) and mass spectrometry (MS, Pfeiffer Vacuum). For steady state measurements the gas chromatograph is used, whereas the mass spectrometer is used for transient and isotope measurements. The time-resolution of the mass spectrometer, depending on scanned masses, ranges between 1 and 10 Hz. The challenge that single peaks may origin from different gas compounds has been extensively discussed by Müller-Erlwein. To compensate this effect a correction matrix based on calibration measurements, which take all possible reaction products, educts and inert gases into account, was used. The intensity of MS signals is transformed online into volume fractions with the aid of the correction matrix. Kr and N_2 are introduced as internal standards for MS and respectively GC. Ar is used as tracer for step change experiments.

The gas chromatograph is equipped with one FID and one TCD. Each detector is connected to its own separation column. On the FID line hydrocarbons are separated over a Plot-Q column and oxygenate are separated by a Rtx Wax column. Permanent gases are analyzed by TCD, first carbon di-oxide is separated by a Plot-Q column. Oxygen, krypton, nitrogen and carbon monoxide are separated by a molecular sieve. Higher hydrocarbons are restricted by a backflush column. One sampling run takes 17 min. Six-way-valves and four-way-valves that are common in chromatography are available to perform pulse- and step change experiments. Both valves are close to the entrance of the reactor. Pneumatic valves are controlled by an electronic valve system accessible via Ethernet. The amount of pulse gases is defined by different sample loops with total volumes of 50, 100, 250 and 500 µL. To get reference pulses during experiments a second valve is placed directly behind the reactor. Crucial for step change and pulse experiments are the avoidance of pressure gaps between feed and pulse/step change gas. Therefore, needle valves are installed in each line. In order to perform almost ideal pulse or jump experiments the dead volume and the use of 1/8”-supply tubes and fittings had to be minimized wherever possible. From inside the reactor a partial flow of the reaction gas is drawn off employing a 1/16”-tube, conveying the flow directly into the recipient of the mass spectrometer. A small part of the product stream is passed to the sampling valves of the GC through a Tee connecter. A bubbler at the end of the exhaust line provides a constant over pressure resulting in a constant flushing of the sample loops. All supply and exhaustion tubes are heated electrically (>200 °C) in order to avoid

condensation. Tailing and memory effects are suppressed to the greatest possible extent. Data acquisition and automatic control of the setup is run by computers and appropriate interface devices.

The conversion (X) of *n*-butane (Eqs. 21 and 23) and the selectivities (S) of the respective products (Eqs. 22 and 24) are typically calculated from the concentrations measured with reference to the internal standard Ar (Eqs. 21 and 22). The latter are averaged over 5 runs measured at each temperature step, respectively. The selectivities of the (by)products were normalized to the number of carbon atoms (Nc) in the (by)products and *n*-butane, respectively. Possible byproducts include butenes, acrylic acid, propionic acid, acetic acid, acrolein, acetaldehyde, propane, propene, acetylene, ethylene, ethane, carbon monoxide, and carbon dioxide. There are no unidentified peaks in the gas chromatograms. At low levels of *n*-butane conversion, the product-based analysis of selectivities and conversions (Eqs. 23 and 24) is preferred.

$$X = 1 - \frac{c_{n\text{-butane}}}{c_{n\text{-butane},0}} \times \frac{c_{Ar,0}}{c_{Ar}} \quad \text{(Eq. 21)}$$

$$S_i = \frac{c_i \times c_{Ar,0}}{c_{n\text{-butane},0} \times c_{Ar} - c_{n\text{-butane}} \times c_{Ar,0}} \times \frac{N_{c,i}}{4} \quad \text{(Eq. 22)}$$

$$X = 1 - \frac{c_{n\text{-butane}}}{\sum(c_{n\text{-butane}} + c_{products})} \times \frac{c_{Ar,0}}{c_{Ar}} \quad \text{(Eq. 23)}$$

$$S_i = \frac{c_i \times c_{Ar,0}}{\sum(c_{n\text{-butane}} + c_{products}) \times c_{Ar} - c_{n\text{-butane}} \times c_{Ar,0}} \times \frac{N_{c,i}}{4} \quad \text{(Eq. 24)}$$

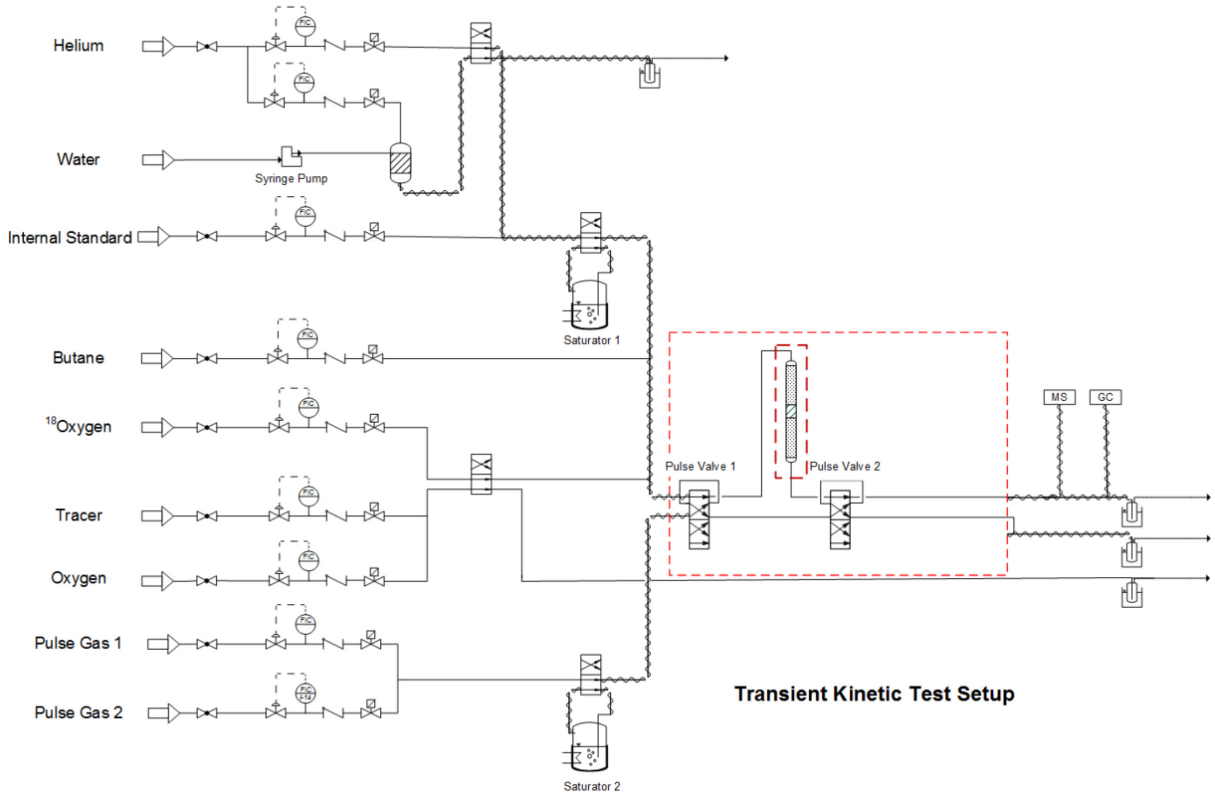

Figure 25 – Flow chart of transient kinetic test setup.

5.3.3 Catalytic Testing

TPO with $^{18}O_2$: The catalyst was heated under lean oxygen from room temperature to 200°C. Oxygen feed was changed from $^{16}O_2$ to $^{18}O_2$ (> 97 %,Campro Scientific). The temperature ramp was programed from 200 to 450°C at 1 K min^{-1} and ambient pressure with a total flow of 20 mL min^{-1}. MAN$^{16}O_3$/$H_2{}^{18}O$ Labeling Experiments: The catalyst was equilibrated under reference conditions at 420°C. MAN was added in concentration of 0.5 % to the reference gas stream by saturator. Further, $H_2{}^{16}O$ (3 %) was replaced by $H_2{}^{18}O$ (3 %). Catalyst was equilibrated for 5 h. Afterwards, GHSV was increased from 2000 h^{-1} to 4000 h^{-1}. After 5 h the temperature was decreased to 380°C at 1 K min^{-1} and held for additional 5 h. SSITKA Experiments: The catalyst was equilibrated under reference conditions with and without H_2O, respectively. Kr

was used as internal standard. Subsequently, the SSITKA experiments were performed, in which a stepwise change of the oxygen isotope – $^{16}O_2$ to $^{18}O_2$ (> 97 %, Campro Scientifc) – was completed at the reactor inlet by means of a fourway valve. After 8 h of isotope labeling the oxygen isotopes were stepwise changed back from $^{18}O_2$ to $^{16}O_2$. The SSITKA experiments were also conducted at ambient pressure and a total flow of 20 mL min^{-1}. In a different experiment the time between isotope switches was reduced to 30 s/15 s in a repeated manner.

5.4 Results and Discussions

5.4.1 Kinetic Considerations

A key observation in our previous parameters field test with the identical VPP catalyst[18c] is the fact that – at iso conversion – the MAN selectivity increases with increasing *n*-butane concentration in the feed gas, which points at a complex mode of O_2 activation and active site assembly for selective and unselective reaction pathways. To exclude non-relevant aspects of the reaction network we compared a selection of four possible schemes (Scheme 7) and their general abilities to reflect this behavior.

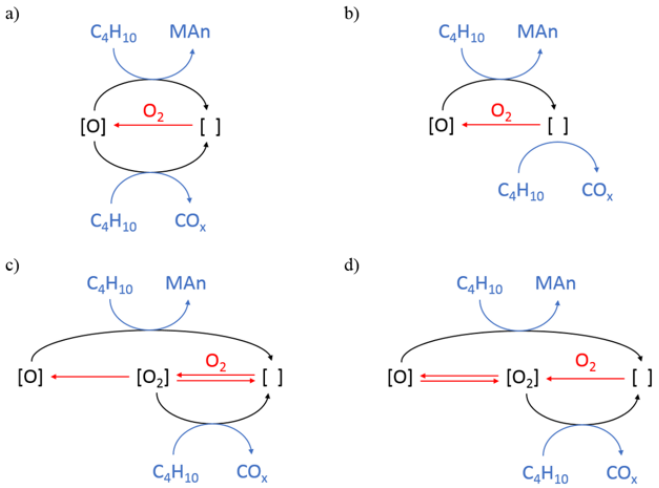

Scheme 7 – Possible reaction schemes for oxygen activation as well as selective and unselective reaction pathways for *n*-butane oxidation.

Here, model (a) is the typical redox scheme often applied in semi-mechanistic kinetic studies[19c]. The active site [O] is generated by fast dissociative adsorption of O_2 on surface vacancies and the model considers only one kind of active site, which is responsible for both selective and unselective reactions. Additional oxygen species required for stoichiometric conversion of the hydrocarbon can be delivered from bulk-to-surface diffusion of bulk [O] or from gas phase O_2. The hydrocarbon conversion finally leaves vacant sites to re-start the catalytic cycle. The kinetic analysis of this

model, however, predicts a rigid MAN selectivity (*S*/*X* profile) independent from the *n*-butane inlet concentration, thus cannot be applied to this system. The origin of the constant selectivity pattern is the fact that the system contains only one type of active site present for both selective and unselective pathways. Thus, MAN selectivity depends only on the rate constants of the reaction network, which are independent from the reactants' partial pressures. Model (b) considers the fact that the catalyst is not inevitably fully oxidized under steady state conditions, thus reduced V sites may also be accessible for hydrocarbon molecules and their adsorption presumably leads to C-C cleavage and CO_x formation[20c]. Clearly, an increased hydrocarbon-to-oxygen ratio leads to an increased fraction of active sites in a reduced state, which is due to the enhanced consumption rate of oxidized active sites. This might be the origin of a positive rate order (+0.42) with respect to O_2 partial pressure[18c]. However, as a consequence, model (b) predicts the inverse trend of MAN selectivity, *i.e.*, a decreased MAN selectivity with increasing *n*-butane partial pressures. As these findings are in contrast with the experiment, we can exclude simple models (a) and (b) for our system.

To account for the desired model flexibility a second type of active site must be introduced and for this purpose we chose an intermediate of O_2 activation. It is generally accepted that the activation of gas phase O_2 over oxidation catalysts are multi-step processes comprising adsorption, electron transfer, and dissociation[21c]. For vanadia-based catalysts capable for selective alkane activation, the sequence may look as follows:

$$O_{2,g} \rightarrow O_{2,ads} \rightarrow [O_2] \rightarrow [O_2^-] \rightarrow [O_2^{2-}] \rightarrow 2\,[O^-] \rightarrow [2\,O^{2-}] \qquad \text{(Eq. 25)}$$

The resulting $[O^{2-}]$ could be assigned, *e.g.*, to vanadyl oxygen, which in the case of bulk catalysts can diffuse into the volume and back to the surface (Mars-van Krevelen mechanism)[22c]. $[O^{2-}]$ is typically regarded as a "selective" oxygen species due to its high nucleophilicity, whereas the intermediates of O_2 activation such as $[O_2^-]$ are highly electrophilic and preferably attack the carbon chain of substrate molecules resulting in unselective CO_x formation. Notably, the assignment of monoatomic nucleophilic and binuclear electrophilic oxygen species to selective and unselective C H activation, respectively, is a well-known traditional approach to explain selectivity patterns[16c]. However, convincing experimental evidence is seldom

reported, which is due to the fact that short-lived intermediates of O_2 activation are spectroscopically challenging against the background of oxide-based catalysts. Thus, isotope studies are a method of choice to get further insight into this aspect of the reaction. As a surface sensitive spectroscopic analysis of active oxygen species is not part of this study, the sequence of O_2 activation for kinetic modeling is simplified to:

$$O_{2,g} \rightarrow [O_2] \rightarrow 2\,[O] \qquad \text{(Eq. 26)}$$

Recently, Yan *et al.* reported on the H_2O assisted dissociation of adsorbed $[O_2]$ species on metal surfaces[23c]. The adsorption of H_2O facilitates the electron transfer from the metal surface to vacuum, which explains why the adsorbed O_2 in the presence of water carries more negative charges than that without water. Furthermore, the dissociation is promoted by hydrogen bonding interaction[23c]. This is an interesting, however speculative, approach to explain the improved MAN selectivity in *n*-butane oxidation in the presence of significant amounts of co-fed H_2O[18c]. The resulting reaction schemes (c) and (d) consider the mononuclear [O] as the selective active site, whereas the intermediary formed $[O_2]$ is regarded as the initiator of unselective processes, *i.e.*, combustion of *n*-butane and MAN, respectively. However, these two models differ in the location of equilibrium steps. In model (c) the adsorption of O_2 is considered as a fast equilibrium, whereas the subsequent dissociation is regarded as irreversible. Instead, model (d) implies the adsorption as irreversible step, which is supported by TPO experiments described below, and dissociation of adsorbed $[O_2]$ as an equilibrium. It should be noted that in the kinetic models [O] and $[O_2]$ characterize only the initial interaction of *n*-butane with the respective active site responsible for the reaction path taken. As mentioned above, additional oxygen species required for stoichiometric conversion of the hydrocarbon can be delivered from bulk-to-surface diffusion of bulk [O] or from gas phase O_2 meaning that CO_2 may also comprise former “bulk” oxygen atoms.

For model (c) the increased *n*-butane concentration increases the ratio $[O_2]/[O]$. The reaction with *n*-butane consumes both types of surface species, however, $[O_2]$ is rapidly regenerated by equilibrium adsorption of $O_{2,gas}$, whereas the regeneration of [O] is kinetically limited. Thus, model (c) predicts a lower MAN selectivity at high *n*-butane partial pressures, in contrast to the experimental finding. Finally, it turned

out that from the selection of above models (Scheme 7) only case (d) is generally capable for predicting an increasing MAN selectivity with increasing *n*-butane concentration. By choosing an appropriate pattern of rate constants, an increasing MAN selectivity with increasing *n*-butane partial pressure can be predicted by the mathematical model. Thus, our previous experiments (co-feed of *n*-butane and O_2)[18c] point at a reversible dissociation of surface [O_2] species.

Furthermore, the increased catalytic performance of VPO in a riser reactor points at the irreversibility of this step. Contractor *et al.* showed that a short quenching period with inert gas after catalyst reoxidation can significantly increase the MAN selectivity[14c], which does not support an equilibrium of O_2 dissociation/recombination. The reaction scheme without equilibria (Scheme 8) is much more complex from a mathematical point of view (thus was not considered in the first selection), however, is capable to describe the trend of MAN selectivity as well.

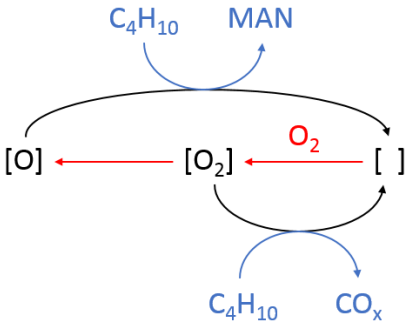

Scheme 8 – Reaction scheme for *n*-butane oxidation discriminated from experimental studies[14c,18c].

Obviously, this purely mathematical approach cannot distinguish between physico-chemical properties of the active site such as, e.g., molecular structure or oxidation states, which have to be discussed with regard to the "real" active surface under reaction conditions. However, a stimulating approach to understand *n*-butane oxidation to MAN on a molecular level was introduced by Grasselli[24c] et al., who showed that alternative oxidants like N_2O do not selectively oxidize *n*-butane to MAN at all. The authors concluded that a peroxo- or ozonide-like structure is responsible for the selective pathway, which is in apparent contrast to our results. In fact, zero conversion of *n*-butane/N_2O over VPP[24c] could also be interpreted in a way that VPP in general is not capable for activating N_2O. In any case, Grasselli et al. describe the dynamic process of formation and interconversion of mono- and binuclear oxygen species on the surface of VPP, which is the complex basis for a deeper understanding of this reaction.

3.3.3.2 Temperature-Programmed Oxidation with $^{18}O_2$

Isotope labeling experiments are essential to understand the different roles of gas-phase, physisorbed, surface, or lattice oxygen species. The TPO temperature ramp with $^{18}O_2$ over VPO showed that the effluent isotope distribution is identical to the feed in a temperature range from 200 to 450 °C. The oxidized VPO catalyst does not undergo exchange reactions with gas-phase O_2 nor does O_2 desorb in measurable quantities in the temperature range that is relevant to the catalytic reaction. This is valid for the pure $^{18}O_2$/He feed as it is the case for SSITKA experiments with *n*-butane in the feed (see below), where mixed labelled $^{16}O^{18}O$ could not be observed either. This agrees well with the reaction scheme discussed above. Pulse studies and experiments inside a closed circulation setup with $^{18}O_2$ over VPO came to similar results[4c,10c]. The presence of superoxo species, which are formed from oxygen adsorption on vanadyl V^{4+} sites and stabilized by adjacent phosphate groups is discussed[25c]. 33 % of all surface vanadyl species are capable to adsorb one oxygen molecule, which is supported by recent NAP XPS studies[7c,26c]. These findings indicate an initial oxidation of 1/3 of surface vanadyl groups, which is irreversible. A feed of mixed labeled oxygen reveals that heteroexchange between O_2 molecules does not occur. Consequently, during the catalytic oxidation reaction bulk oxygen can only be functionalized by incorporation into the reaction products.

5.3.3 Isotope Scrambling of MAN with H_2O

Only a few studies correlate the abundance of gas-phase and bulk oxygen species with the formation of selective products like MAN and non-selective ones like CO_x. Vogel et al. described the problem of isotope scrambling with H_2O even for the selective oxidation of acrolein to acrylic acid[27c], where only small amounts of H_2O are formed due to the high selectivity of the reaction. In our case, the effect of oxygen exchange of H_2O with MAN must be considered due to the significant formation of H_2O in both selective and unselective reaction pathways. Studies by Abon et al. neglect the exchange inside a circulation reactor by removing MAN and H_2O after reaction[10c]. However, cofeed experiments of $H_2{}^{18}O$ and $MAN^{16}O_3$ in a PFR reactor together with 2 % *n*-butane reveal a strong exchange of oxygen atoms even after short contact times (Figure 26).

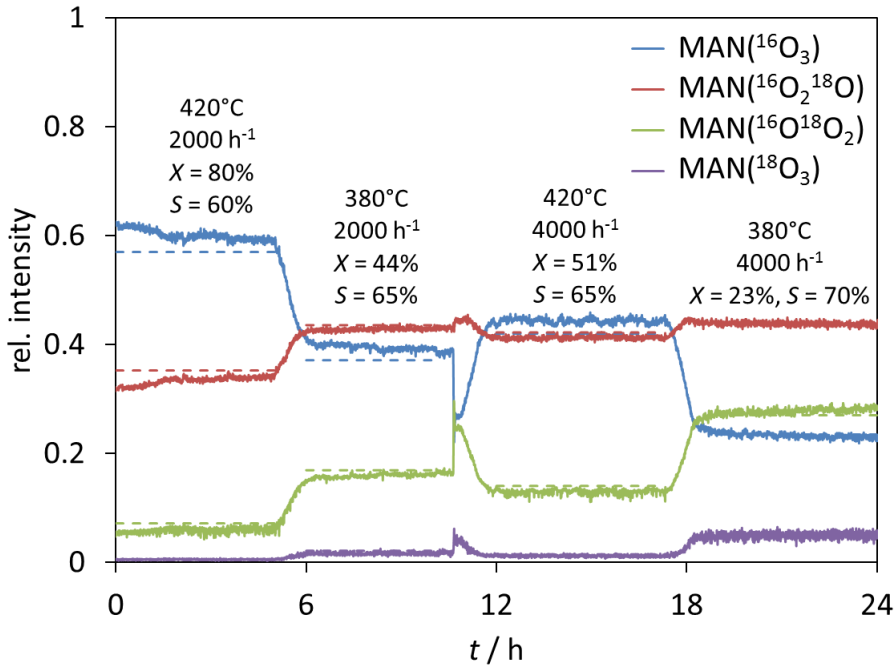

Figure 26 – . Distributions of MAN isotopes obtained over VPP in a feed of 2 % *n*-butane, 20 % 16 O_2, 0.5 % MAN($^{16}O_3$), and 3 % $H_2{}^{18}O$ at different temperatures and contact times, respectively, in comparison to the calculated equilibrium distribution (dashed lines).

Considering the fractions of ^{16}O and ^{18}O in the pool of exchangeable oxygen, *i.e.*, H_2O and MAN depending on *n*-butane conversion and MAN selectivity, the theoretical equilibrium distributions of MAN isotopes are indicated in Figure 26. It is seen that these equilibria are well approached in each case. Considering the fact that a significant part of MAN is only formed during the reaction, thus having available just a fractional part of the original residence time of the co-fed MAN, it is clear that the isotopic scrambling is much faster than the oxidation of *n*-butane. Further reference experiments under similar reaction conditions show that the isotope scrambling is negligible in an blank reactor (gas phase), and comparably high (to VPP) over PO_x-loaded SBA-15, indicating that the $^{16}O/^{18}O$ scrambling of MAN and H_2O isotopes might be facilitated by omnipresent (pyro)phosphate groups on the VPO catalyst surface.

5.3.4 SSITKA Experiment in the Dry Feed

The transient kinetic set-up gives access to the time resolved incorporation of ^{18}O (from gas phase $^{18}O_2$) into reaction products like MAN, CO, CO_2, H_2O, and acids. Ion traces of selected masses were corrected by background measurements and correlated with certain molecules. In particular, the following traces were analyzed: 18 ($H_2{}^{16}O$), 20 ($H_2{}^{18}O$), 32 ($^{16}O_2$), 34 ($^{16}O^{18}O$), 36 ($^{18}O_2$), 44 ($C^{16}O_2$), 46 ($C^{16}O^{18}O$), 48 ($C^{18}O_2$), 98 ($MAN^{16}O_3$), 100 ($MAN^{16}O_2{}^{18}O$), 102 ($MAN^{16}O^{18}O_2$), and 104

(MAN$^{18}O_3$). Further, a multi-component deconvolution was performed to account for multiply occupied ion traces.

The SSITKA experiment was performed without H_2O in the feed to reduce the consequences of post-catalytic $^{16}O/^{18}O$ scrambling of MAN and H_2O as much as possible. Note that the selective oxidation of *n*-butane to MAN as well as unselective side reactions produce H_2O as a by-product, thus we cannot totally exclude this disturbing effect. The experiment reveals the slow exchange of oxygen (Figure 27). The mass balance clearly indicates that subsurface oxygen is undoubtedly involved in the reaction. After 100 min of isotope exchange, MAN and CO_2 are still partially labelled with ^{16}O. These results agree with a report by Abon *et al.*, who found similar trends for VPP inside a circulation reactor at lower temperatures[10c]. In addition to the experimentally obtained ion traces Figure 27 also contains a statistical distribution with *y* being the degree of isotopic labelling in the respective compound.

$$y = {}^{18}O / ({}^{18}O + {}^{16}O) \qquad \text{(Eq. 14)}$$

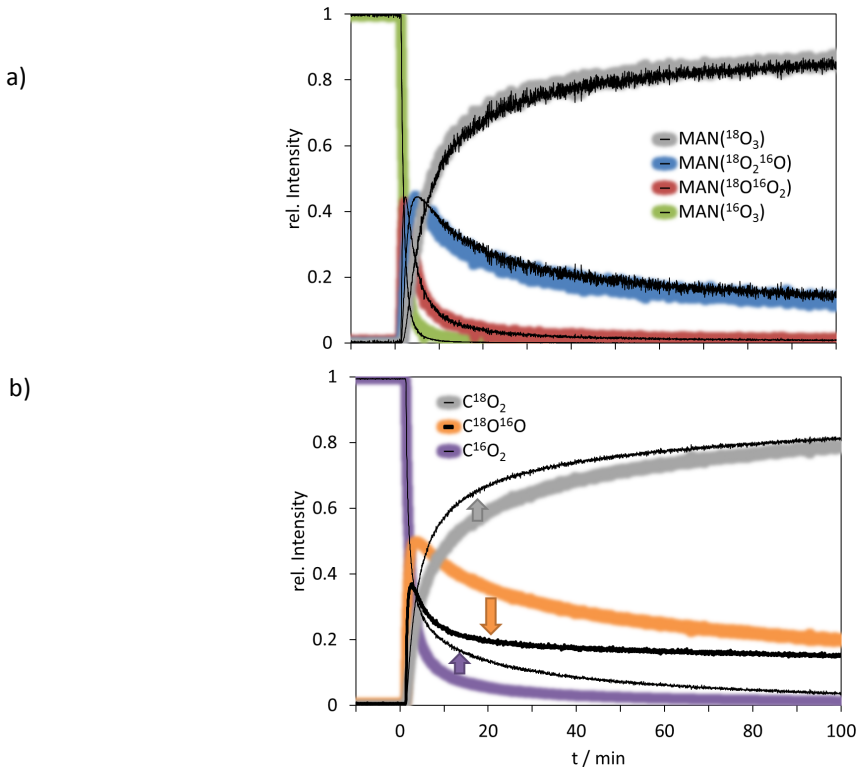

Figure 27 – SSITKA experiment without co-fed water (420 °C, 2000 h^{-1}, *X*(*n*-butane) = 72 %, *S*(MAN) = 67 %). Top: position of $^{16}O_2/^{18}O_2$ isotope switch while keeping *n*-butane constant. Traces of (a) MAN and (b) CO_2. The statistically expected distribution is given as a coloured shading, respectively.

Thus, according to Pascal's triangle[28c], the statistical model traces (coloured shading in Fig. 22) can be calculated as follows:

$MAN(^{18}O_3) = y^3$ (Eq. 15)
$MAN(^{18}O_2{}^{16}O) = 3\ y^2\ (1\text{-}y)$ (Eq. 169)
$MAN^{18}O(^{16}O_2) = 3\ y\ (1\text{-}y)^2$ (Eq. 30)
$MAN(^{16}O_3) = (1\text{-}y)^3$ (Eq. 31)
$C^{18}O_2 = y^2$ (Eq. 32)
$C^{18}O^{16}O = 2\ y\ (1\text{-}y)$ (Eq. 33)
$C^{16}O_2 = (1\text{-}y)^2$ (Eq.34)

Several mechanistic aspects are reflected in the traces. For MAN the experimental and statistical curves are almost congruent. We refer this to rapid post-catalytic scrambling of MAN isotopes with H_2O, as discussed above. However, unfortunately, this process likely masks deeper information of MAN isotopes if originally formed in a non-statistical distribution. Additionally, the congruency of experimental and theoretical statistical distributions of MAN isotopes in Figure 27 suggests that the exchange with the catalyst (*e.g.*, P-OH groups) in terms of isotope scrambling is comparably slow as compared to the intermolecular exchange. In contrast, for CO_2 the experimentally observed distribution of CO_2 isotopes clearly differs from the statistical prediction. Notably, VPO is not active for CO oxidation to CO_2[18c]. The amounts of doubly labelled $C^{18}O_2$ and unlabeled $C^{16}O_2$ are higher than statistically expected, respectively, on the cost of mixed labelled $C^{16}O^{18}O$ (orange arrow in Figure 27b). This confirms that CO_2 is inactive for post-catalytic isotope scrambling[10c] and the isotope pattern observed is a response to unselective surface reactions, *i.e.*, predominantly direct combustion of *n*-butane[18c] Thus a relative enrichment in $C^{18}O_2$ can be interpreted in a way that the unselective pathway of *n*-butane combustion involves an interaction with a binuclear [O_2] species[29c], *e.g.*, some electrophilic intermediates of gas phase O_2 activation on the VPP surface, which unselectively activate *n*-butane (or surface intermediates of MAN formation) finally leading to CO_2 (and CO). Consequently, both atoms of the dioxygen molecule end up in a single CO_2 molecule. This is in good agreement with the reaction scheme identified by model discrimination of the parameters field testing (Scheme 8), and the effect is clearly visible when rapidly oscillating $^{16}O_2$ and $^{18}O_2$ in the feed on a time scale that differentiates between surface O_2 activation and bulk-to-surface diffusion of [O] species (see below).

In return, the relative enrichment of $C^{16}O_2$ over the statistically expected value (purple arrow in Figure 27b) questions the established view on the reaction system, which assigns “bulk” oxygen exclusively to selective transformations[14c,30c]. In addition, the time constant of the MAN($^{16}O_3$) decay is much smaller than the time constant of the $C^{16}O_2$ decay, as is the total fraction of ^{16}O in MAN *vs.* CO_2 over time-on stream. Several reasons may serve as an explanation: First, the curves of $C^{16}O_2$ and MAN($^{16}O_3$) cannot be directly compared due to the different powers of (1-*y*) in Eqs. 22 and 26. The normalization significantly weakens the differences between both traces. Second, $C^{16}O_2$ is in parts a consecutive product, e.g., from ^{16}O bearing formed in primary pathways[18c] with “bulk” oxygen. Third, carbonaceous adsorbates as the intermediates of *n*-butane (and MAN) combustion may have a significantly longer lifetime on the catalyst surface than the duration of a catalytic cycle of selective MAN formation. Such ill-defined adsorbates are likely susceptible to deeper oxidation with “bulk” oxygen reaching the reaction site from the subsurface. Having discussed the pronounced tailing of $C^{16}O^{18}O$ and $C^{16}O_2$ traces, we put the focus back on the extremely short time constant of the MAN($^{16}O_3$) decay, which is unexpected when considering “bulk” oxygen as the dominating selective oxygen species of the VPO catalyst. The fact that the riser reactor concept gives exceptionally high MAN selectivities[30c] unquestionably proves the importance of the reservoir of subsurface oxygen for selective reaction on the catalyst surface. On the other hand, our SSITKA experiment indicates a higher fraction of ^{18}O in MAN as compared to CO_2. So what is the connection to the present observation? We assume that the initial steps of the selective oxidation of *n*-butane, which have been suggested to comprise predominantly dehydrogenation steps forming H_2O (Scheme 8), are realized by nucleophilic surface oxygen species, which are rapidly regenerated by ^{18}O in the SSITKA experiment. This is nicely confirmed by experimental evidence in Fig. 23, which compares the fractions of ^{18}O in H_2O and MAN. A clear delay of the y(^{18}O, MAN) response of approx. 30 s is visible and indicative for a short-term enrichment of ^{18}O in H_2O. The later steps, i.e., the insertion of oxygen atoms into the C_4 intermediate, may comprise both surface ^{18}O and subsurface ^{16}O atoms. The bulk-to-surface diffusion of the latter may be favored by a local reduction of the catalyst matrix in the near vicinity of the active site. The final result of this primary reaction sequence is a mixture of partially labelled MAN isotopes, whose composition follows the availability of oxygen on the catalyst surface. However, these MAN isotopes

immediately equilibrate with the abundance of $H_2{}^{18}O$ formed at the same time (notably, the unselective pathway of direct *n*-butane combustion produces high amounts of $H_2{}^{18}O$ as well), thus a significantly higher degree of ^{18}O incorporation into MAN molecules is seen in our experiment. Inversely, the amount of MAN($^{16}O_3$) sharply decreases by the fast secondary exchange.

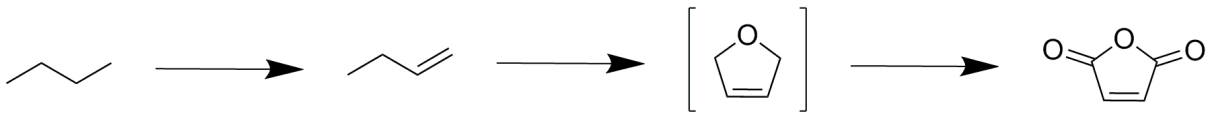

Scheme 9 – Postulated pathway of the selective oxidation of *n*-butane to MAN via gas-phase and surface intermediates[6c,22c]

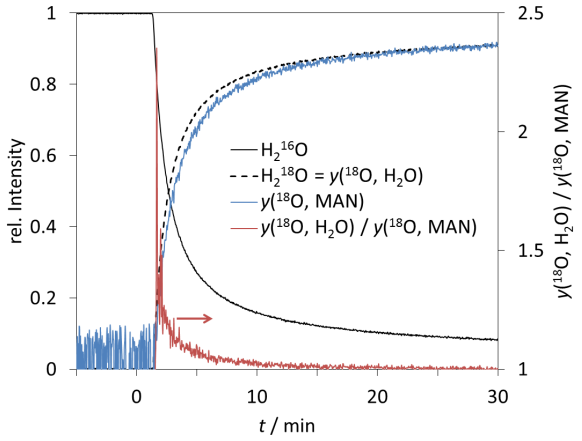

Figure 28 –Traces of H_2O and comparison of ^{18}O fractions *y* in H_2O and MAN, respectively.

5.3.5 Oscillation of $^{16}O_2/^{18}O_2$

It is expected that the time scale of diffusion of bulk oxygen to the surface is much slower as compared to reaction kinetics on the surface. Therefore, a gas phase oscillation between $^{16}O_2$ and $^{18}O_2$ has been performed under reaction conditions at two different frequencies (Figure 29). Based on the above discussion of oxygen species for different aspects on *n*-butane activation, we chose intervals of 10 and 30 s, which are in the range of the delay highlighted in Figure 29. Different times between gas-phase changes resulted in different responses of ^{18}O labeled MAN and CO_2 products. In general, the concentrations of ^{18}O labelled species increase in the number of $^{16}O_2/^{18}O_2$ cycles because the experiment starts from an unlabeled VPO catalyst. The surface layer, however, slowly enriches in ^{18}O during the oscillations because surface vacancies generated during the redox processes can be filled by gas phase $^{18}O_2$ or by sub-surface [^{18}O].

For the 10 s interval between $^{16}O_2/^{18}O_2$ switches (Figure 29a) the formation of $C^{18}O_2$ readily begins at the first switch and very shortly after the appearance of $^{18}O_2$ in the gas phase. The shift of the $C^{18}O_2$ pulses of approx. 0.25 min as compared to the originating respective $^{18}O_2$ cycles is due to the residence time (adsorption, multi-step surface reaction, and desorption) of the species on the catalyst surface, which by chance results in a contemporaneity of $C^{18}O_2$ and $^{16}O_2$ signals. Notably, fully labelled MAN (only MAN($^{18}O_3$) shown for clarity) is not formed during the first four $^{18}O_2$ pulses. It is clear evidence that gas phase oxygen and/or its intermediates of surface activation can be related to unselective reaction pathways, whereas the selective MAN formation proceeds *via* kinetically stable surface and sub-surface oxygen species. Here, the experiment does not differentiate between the direct combustion of *n*-butane to CO_x and the consecutive combustion of MAN.

The increase of the switching period to t = 30 s (Figure 29b) shows similarities and differences. Again, the shift of $C^{18}O_2$ *vs.* $^{18}O_2$ signals is approx. 0.25 min at half-maximum being indicative for the surface reaction. However, in contrast to the 10s oscillations the trace of MAN($^{16}O_3$) forms a very weak peak at the very first $^{18}O_2$ pulse and the normalized signal is closer to the $C^{18}O_2$ trace. However, MAN is still clearly enriched in ^{16}O during the first three $^{18}O_2$ pulses. Only at the 4th pulse a plateau is approached, indicating that a near surface O reservoir of the catalyst is filled with an amount of ^{18}O that is sufficient to enable the formation of comparable amounts of triply labelled MAN($^{18}O_3$). These results indicate that there are different pools of oxygen for MAN and CO_2. These oxygen species might be referred as nucleophilic and electrophilic oxygen, which are connected with each other (Eqs. 25). However, the exchange between both pools is slow compared to reaction kinetics, which indicates slow formation rates of *n*-butane to MAN or a slow oxidation of electrophilic to nucleophilic oxygen (Scheme 8). A fast exchange of nucleophilic surface and subsurface oxygen, which would also explain a delay in ^{18}O exchange, can be excluded due to the SSITKA studies. Taken the reaction order of oxygen with +0.42 into consideration, it looks that the reaction order for MAN formation is significantly smaller compared to *n*-butane oxidation.

a)

b)

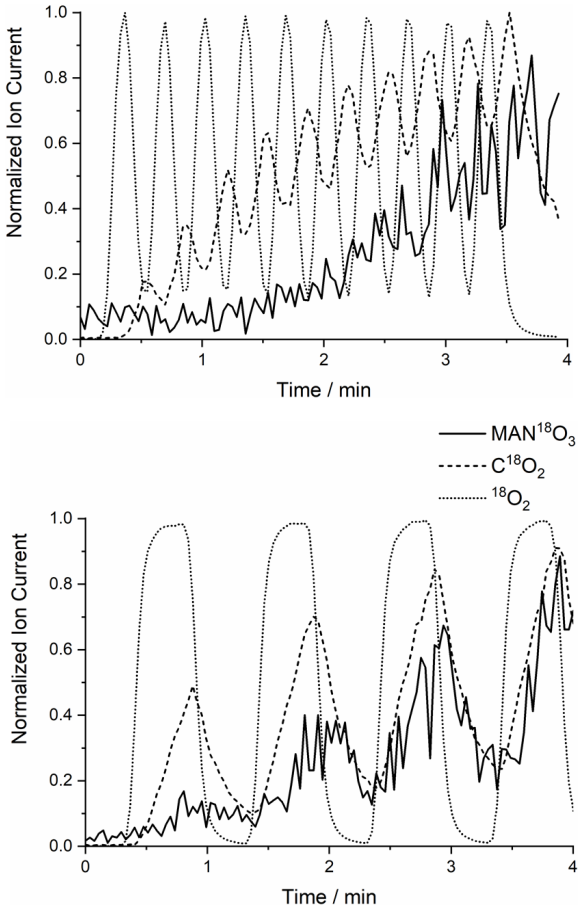

Figure 29 – Oscillating $^{16}O_2/^{18}O_2$ SSITKA experiments at 420 °C and 2000 h^{-1} (2 % *n*-butane, 20 % O_2, w/o H_2O) with switching times 10 s (a) and 30 s (b). $^{16}O_2$ (not shown) filling the gap between $^{18}O_2$ oscillations. Only selected traces are shown for clarity.

5.3.6 Quantification and Location of Exchanged Oxygen

For quantification of exchangeable oxygen, the ^{16}O content within all reaction products appearing after the SSITKA switch (dry feed, Figure 27) was determined. Bulk and gas-phase oxygen do not directly interact under reaction conditions as shown by the TPO experiment in $^{18}O_2$. Therefore, the respective ^{16}O fractions of the main reaction products MAN, CO, CO_2, H_2O, and acetic acid were summed up. Considering the given uncertainty of isotope quantification by MS the amount of oxygen detected in the products roughly corresponds to 5-10 % of the bulk oxygen in the VPO catalyst. After 8 h in the $^{18}O_2$ containing feed the further exchange is negligible, indicating that a full exchange of all oxygen atoms of the VPO catalyst cannot be reached in a reasonable timescale. In a schematic core-shell model, we can correlate the amount of exchanged oxygen to a fully labelled surface layer of a certain thickness (in contrast to the deeper bulk, which is considered as unlabeled). Based on the BET surface area of our material and the crystal structure of VPP[133c] (as an approximation it is assumed that the O bulk density of VPP is similar to the

real structure of the active surface layer), the amount of exchanged oxygen can then be assigned to a surface layer with a thickness of 0.5 – 1.0 nm. Such a surface layer, which is susceptible to the exchange of oxygen and, thus, isotopic labelling, coincides with the amorphous surface layer visible by TEM, which has been reported previously[9c].

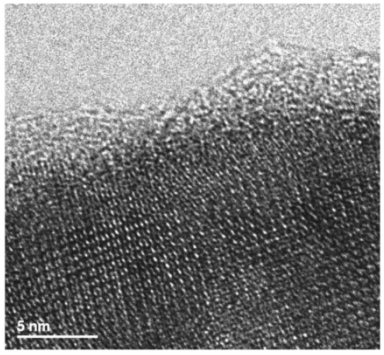

Figure 30 – TEM image of a VPO catalyst equilibrated for 100 h in feed[6c]. Reprinted with permission from Wiley-VCH.

Although the amorphous overlayer visualized in Figure 30 is in parts generated by electron beam damage, Schlögl *et al.* claim that at least half of the layer is an essential part of the working catalyst under reaction conditions. Its thickness well corresponds to the amount of oxygen atoms in our SSITKA studies. According to this concept, the semiconductive crystalline VPP bulk is less reactive in terms of oxygen exchange and rather serves as a pool of electrons to control the catalytic processes at the gas-solid interface as well as the structural and electronic dynamics of the amorphous overlayer. It is well known that the active catalyst surface is enriched with phosphorus and vanadium exists in different oxidation states (+4, +5). It has also been shown that the near surface concentration of V and P responds to the reaction conditions. Such structural dynamics corresponds to the oxygen exchange observed in our experiments.

5.5 Conclusion

The rich literature available for the selective *n*-butane oxidation over VPP documents the enormous effort investigated in the past to understand the formation pathway of MAN from *n*-butane. Questionably, all studies are based on the binuclear V_2O_8 structural motif as a characteristic of the crystal structure of VPP, although it is long known and widely accepted that the active surface of VPP is rather amorphous. However, the more important key for understanding and improving product selectivity is the activation of oxygen and the formation of active and selective surface species,

regarded as omnipresent in abovementioned studies. We contribute the following facts about catalytically active oxygen in the VPO catalyst: (i) the activation of gas phase O_2 occurs at least in two distinguishable steps via surface [O_2] and [O] species. [O_2] species initiate the combustion of *n*-butane, whereas nucleophilic [O] can selectively activate C-H bonds. (ii) H_2O in the gas phase likely promotes the dissociation of [O_2] into [O] sites, thus increases MAN selectivity. (iii) Oxygen exchange of the VPO catalyst based on VPP occurs exclusively over the reaction products and the amount of exchangeable O corresponds to a thin amorphous surface layer well-known from HRTEM studies. (iv) MAN can re-adsorb on surface PO_xH_y groups, which are active for rapid scrambling of oxygen isotopes within MAN and H_2O. Our model of O_2 activation, which is supported by kinetic analyses of a parameters field test as well as isotope labelling studies, may explain the apparent MAN selectivity limit near 60-70%, which has not been overcome for decades. Its origin could be the compulsory coexistence of selective and unselective oxygen species, as the latter are the precursor for the first ones. As has been realized very early, the concept of the riser reactor locally separating the reoxidation stage is a potential solution. Another approach might be the search for promotors of [O_2] dissociation. In the industrial process the co-feed of H_2O is an effective solution, however, limited by the stability of the catalyst at exceedingly high steam concentrations. A future research may focus on transition metal dopants, which could act in this direction as well.

5.6 Literature

[1c] N. Ballarini, F. Cavani, C. Cortelli, S. Ligi, F. Pierelli, F. Trifirò, C. Fumagalli, G. Mazzoni, T. Monti, Top. Catal. 38 (2006) 147–156.

[2c] a) G. Centi, Catal. Today 16 (1993) 5–26.; b) C.H. Bartholomew, R.J. Farrauto, Fundamentals of Industrial Catalytic Processes, John Wiley & Sons, Inc, Hoboken, NJ, USA, 2005; c) J.-C. Volta, C.R. Acad. Sci., Ser. IIc: Chim. 3 (2000) 717–723.; d) R. Glaum, C. Welker-Nieuwoudt, C.-K. Dobner, M. Eichelbaum, F. Gruchow, C. Heine, A. Karpov, R. Kniep, F. Rosowski, R. Schlögl, S.A. Schunk, S. Titlbach, A. Trunschke, Chem. Ing. Tech. 84 (2012) 1766–1779.

[3c] G. Centi, F. Trifiro, J.R. Ebner, V.M. Franchetti, Chem. Rev. 88 (1988) 55–80.

[4 M.A. Pepera, J.L. Callahan, M.J. Desmond, E.C. Milberger, P.R. Blum, N.J. Bremer, J. Am. Chem. Soc. 107 (1985) 4883–4892.

[5c] C.-K. Dobner, M. Duda, A. Raichle, H. Wilmer, F. Rosowski, M. Hoelzle (2006) US 2,008,227,992.

[6c] R. Schlögl, in: N. Mizuno (Ed.), Modern Heterogeneous Oxidation Catalysis, Wiley-VCH Verlag GmbH & Co. KGaA, Weinheim, Germany, 2009, pp. 1–42.

[7c] C. Heine, M. Hävecker, E. Stotz, F. Rosowski, A. Knop-Gericke, A. Trunschke, M. Eichelbaum, R. Schlögl, J. Phys. Chem. C 118 (2014) 20405–20412.

[8c] a) L.M. Cornaglia, E.A. Lombardo, Appl. Catal., A 127 (1995) 125–138.; b) Y. Suchorski, L. Rihko-Struckmann, F. Klose, Y. Ye, M. Alandjiyska, K. Sundmacher, H. Weiss, Appl. Surf. Sci. 249 (2005) 231–237.

[9c] W.C. O'Leary, W.A. Goddard, M.-J. Cheng, J. Phys. Chem. C 121 (2017) 24069–24076.

[10c] M. Abon, K.E. Béré, P. Delichère, Catal. Today 33 (1997) 15–23.
[11c] D. Wang, M.A. Barteau, Catal. Lett. 90 (2003) 7–11.
[12c] F. Cavani, G. Centi, F. Trifiro, Ind. Eng. Chem. Prod. Res. Dev. 22 (1983) 570–577.
[13c] V.A. Zazhigalov, Y.P. Zaitsev, V.M. Belousov, N. Wyustnek, H. Wolf, React. Kinet. Catal. Lett. 24 (1984) 375–378.
[14c] R.M. Contractor, H.E. Bergna, H.S. Horowitz, C.M. Blackstone, U. Chowdhry, A.W. Sleight, Stud. Surf. Sci. Catal. 38 (1988) 645–654.
[15c] E.W. Arnold, S. Sundaresan, Appl. Catal. 41 (1988) 225–239.
[16c] B. Frank, R. Fortrie, C. Hess, R. Schlögl, R. Schomäcker, Appl. Catal., A 353 (2009) 288–295.
[17c] F. Cavani, S. Luciani, E. Degli Esposti, C. Cortelli, R. Leanza, Chem. Eur. J. 16 (2010) 1646–1655.
[18c] C. Schulz, F. Pohl, M. Driess, R. Glaum, F. Rosowski, B. Frank, Ind. Eng. Chem. Res. (2018) accepted. DOI:10.1021/acs.iecr.8b04328.
[19c] a) J.S. Buchanan, S. Sundaresan, Appl. Catal. 26 (1986) 211–226. b) T.V. Malleswara Rao, G. Deo, AIChE J. 53 (2007) 1538–1549. c) D. Creaser, B. Andersson, Appl. Catal., A 141 (1996) 131–152. d) S.A. Al-Ghamdi, M.M. Hossain, H.I. de Lasa, Ind. Eng. Chem. Res. 52 (2013) 5235–5244.
[20c] U.S. Ozkan, R.B. Watson, Catal. Today 100 (2005) 101–114.
[21c] A. Bielański, J. Haber, Oxygen in Catalysis, Dekker, New York, NY, 1991.
[22c] P. Mars, D.W. van Krevelen, Chem. Eng. Sci. 3 (1954) 41–59.
[23c] M. Yan, Z.-Q. Huang, Y. Zhang, C.-R. Chang, Phys. Chem. Chem. Phys. 19 (2017) 2364–2371.
[24c] P.A. Agaskar, L. de Caul, R.K. Grasselli, Catal. Lett. 23 (1994) 339–351.
[25c] V.V. Guliants, J.B. Benziger, S. Sundaresan, Stud. Surf. Sci. Catal. (1996) 991–1000.
[26c] M. Eichelbaum, M. Havecker, C. Heine, A. Karpov, C.-K. Dobner, F. Rosowski, A. Trunschke, R. Schlögl, Angew. Chem. Int. Ed. 51 (2012) 6246–6250.
[27c] T. Petzold, N. Blickhan, A. Drochner, H. Vogel, ChemCatChem 6 (2014) 2053–2058.
[28c] B. Pascal, Traité du triangle arithmétique avec quelques autres petits traitez sur la mesme matière. Paris, France,1665.
[29c] O. Ovsitser, E.V. Kondratenko, Catal. Today 142 (2009) 138–142.
[30c] R. M. Contractor, Circulating Fluidized Bed Technology II. Butane Oxidation to Maleic Anhydride in a Recirculating Solids Riser Reactor, Elsevier, 1988.
[31c] S. Geupel, K. Pilz, S. van Smaalen, F. Büllesfeld, A. Prokofiev, W. Assmus, Acta Crystallogr., Sect. C: Cryst. Struct. Commun. 58 (2002) i9-i13.

6 Conclusion

6.1 Synthesis of Novel Catalysts for *n*-Butane Oxidation

Different mixed metal oxides were synthesized and tested for selective oxidation of *n*-butane based on $(VO)_2P_2O_7$ and $VOPO_4$. Transition metals like tungsten, molybdenum or iron were used for substitution of vanadium in bulk catalysts. Most materials were prepared by solution combustion synthesis[136].

The most promising catalyst was found by partial substitution of V by W, which leads to $V_{1-x}W_xOPO_4$ with α_{II}-$VOPO_4$ structure type (VWPO). The substitution by W leads to an equimolar reduction of V^V to V^{IV}. The amount of tungsten can be tuned in the range of $0.04 \leq x \leq 0.26$. XRD studies before and after catalytic testing revealed, that no by-phases are formed under reaction conditions. However, the specific surface area increases during the reaction. In general, the selectivity of MAN was lower in all cases compared to VPP. Nevertheless, it could be shown that the oxidation state of vanadium correlates with the selectivity for MAN. The selectivity for MAN over VWPO can go up to 31 %, which is significantly higher compared to β- $VOPO_4$.

The substitution of V with Mo in $(VO)_2P_2O_7$ and $VOPO_4$ shows different effects. In $VOPO_4$, V by Mo can be easily substituted leading to pure β- and γ-phases, which are more stable under reaction conditions compared to $V_{1-x}W_xOPO_4$. In case of $(V_{0.95}Mo_{0.05}O)_2P_2O_7$ there is no evidence in the XRPD that Mo is incorporated in the $(VO)_2P_2O_7$ lattice questioning the flexibility of the crystal structure for substitution. In both cases, the effect on catalysis is comparable. Selectivity for MAN and CO_x is reduced compared to the non-substituted catalysts. Further, addition of Mo strongly influences the C-C cleavage leading to the formation products like acetic and acrylic acid. The properties of vanadyl pyrophosphate synthesized by solution combustion synthesis are comparable to those of VPO from aqueous routes. The activity is lower compared to the industrial catalyst due to low surface areas. The selectivity for MAN is reduced, which might be explained by a lower ratio of P:V. Several studies showed that an excess of phosphorus enhances the selectivity[2]. The optimum ratio of P:V is around 1.1:1, whereby the ratio achieved by solution combustion synthesis is 1:1.

VPO_4-m1 is a new polymorph of VPO, which was introduced by removing the vanadyl oxygen atoms of β-$VOPO_4$. The reduction is reversible under reaction conditions and leads to formation of $(VO)_2P_2O_7$. Accordingly, the performance is comparable to VPO by SCS and stresses the importance of stable catalysts.

Complete substitution of V in $(VO)_2P_2O_7$ and $VOPO_4$ with iron or tungsten yields phase-stable materials that are not active in the selective oxidation of *n*-butane. These results indicate that V and P are crucial for the selective activation of *n*-butane. In general, the identification of novel $V_{1-x}W_xOPO_4$ materials with α_{II}-$VOPO_4$ structure type were a success for the first milestone of this thesis. The selectivity for MAN is lower compared to industrial VPP. However, the different oxidation state of the bulk vanadium is an interesting property. From the different VWPO catalysts, $V_{0.8}W_{0.2}OPO_4$ was chosen for a comparative study with VPP due to >30% selectivity for MAN.

6.2 Comparative Study of VPP and VWPO

The parameters field study inside a parallel test setup was found to be an advantageous method for acquiring steady state kinetic data in a short time scale. Mass and heat transfer limitations were tested and excluded for this study. The catalyst performance under reference reaction conditions was frequently checked to monitor the stability of the active site. A low activation with minor decrease in MAN selectivity was observed for VPP, whereas VWPO unexpectedly activates in the middle of the parameters field test while keeping the selectivity pattern. The data, which are unsuitable for kinetic fitting, could be easily identified by control experiments. For both catalysts VWPO and VPP the stability of crystal structure and specific surface area were confirmed by XRD and SEM measurements. The product spectrum and reaction network of the selective oxidation of *n*-butane appeared similar over both catalyst systems and is coherent with the reports published in literature with the exception of acetylene which was not reported so far. Notably, MAN appears to be more stable over VWPO, however, on the cost of a much lower initial selectivity. The assignment of these findings to electronic or structural properties of the model catalysts might lead to further improvements. The appearances of ethylene and acetylene, as well as acetic and acrylic acids were found to correlate with selectivity of MAN, indicating them (partially) as by-products of MAN decomposition. New reaction pathways for acetic and acrylic acids were proposed based on parameters field, pulse, and cofeed studies. Acrylic acid can be formed by hydrolysis of MAN, which is subsequently monodecarboxylated. Further, decarboxylation leads to ethylene. Ethylene is oxidized to acetic acid via ethanol and acetaldehyde. Another pathway of acetic acid formation is based on acetylene, which is formed from MAN. Hydrolysis of acetylene leads to acetaldehyde, which can be

selectively oxidized to acetic acid. Furan, 2,5-dihydrofuran and 1-butene are discussed as selective reaction intermediates in the literature. Pulse studies over equilibrated catalyst showed that MAN is formed from all assumed intermediates, but selectivites are lower than expected. The finding might be attributed to readsorption on the surface, which leads to non-selective pathways. Nevertheless, the results are in good agreement to the literature. Carbon monoxide is not readsorbed on the active site and cannot be oxidized to carbon dioxide. Temperature, water and *n*-butane partial pressure have a positive impact on *n*-butane concentration whereas oxygen partial pressure has none. We implemented a kinetic model which includes main reaction products MAN, CO, CO_2 as well as by-products like acetic acid and acrylic acid. Further, the role of oxygen activation is included and reflects experimental evidence.

As a very important result the success in kinetic modelling supports the reaction network proposed. The resulting model can now be used for further experiments, *i.e.*, advanced modelling of profile reactors as already done by Horn et al. [137], or extrapolation for the search of optimized reaction conditions. The straightforward discussion of kinetic parameters in terms of the reaction mechanism is not possible due to the formal character of the kinetic model. In general, the apparent activation energies for *n*-butane combustion (r_{0c}) as well as formation and combustion of MAN (r_{1f}, r_{1c}) are by approx. 15 kJ/mol lower for VWPO than for VPP, which is possibly due to the higher average oxidation state of VWPO. Such a phenomenon has recently been reported for the oxidative dehydrogenation over carbon-based catalysts[138]. In fact, the pre-exponential factors of VWPO are only by factor 3-4 smaller than those of VPP, although the specific surface area is by factor of 10 smaller, indicating that the net activity of VWPO could be substantially increased by increasing the specific surface area (3 m^2/g), e.g., by advanced synthesis protocols or by supporting the active phase. Notably, the apparent activation energies of acetic acid formation and combustion, respectively, are much higher than the values for the other reactions over VPP. As we discussed previously, acetic acid may also be formed in a secondary step from MAN. Thus, the exceptionally high apparent energies could point at a more complex reaction network as the basis for kinetic modelling. To solve this issue, dedicated co-feed studies with MAN and acetic acid are required. The apparent rate orders for most reactions lie in between 0.1 and 0.9, with the rate order of the carbonaceous compound being always higher that the rate order of O_2. This

can be tentatively interpreted as an indication that both steps, the catalyst oxidation and the hydrocarbon conversion, contribute equally to the overall rate with the catalyst being in a rather oxidized state. Mechanistic models to be developed and fitted to the dataset can possibly shed light on this aspect. MAN formation over VWPO (r_{1f}) is a single example with an almost first order reaction with respect to *n*-butane and zero rate order with respect to O_2. Here, we conclude that the surface-active site for the rate determining step is fully oxidized and the overall rate is only limited by the activation of *n*-butane. However, for all other reactions the situation is more complex.

Summarizing, the reaction network of VPP and VWPO is similar. The difference in bulk oxidation states is partly reflected in the difference of activation energy for *n*-butane activation. However, the difference in selectivity of MAN might be explained by two, different active sites responsible for selective and non-selective reaction pathways. If the reaction network and formal kinetics can be seen as a fingerprint for the active site, the nature of the active site does not correlate with the bulk crystal structure. It is more likely that amorphous surface species are important for the catalysis, which are stabilized on the crystalline bulk phase. Formation of such amorphous phases is well known in the literature and could be described by Schlögl[6] et al. for VPP by HRTEM studies. Therefore, VPP is chosen as a reference system for detailed analysis with ^{18}O isotope labeling studies, which gives a deeper insight in the participation of surface and subsurface oxygen as well as the contribution of bulk and amorphous phases.

6.3 Surface Dynamics of Oxygen for VPP

Enormous efforts were put in the understanding of the formation pathway of MAN from *n*-butane. Questionably, all studies are based on the binuclear V_2O_8 structural motif as a characteristic of the crystal structure of VPP, although it is long known and widely accepted that the active surface of VPP is rather amorphous. This finding is supported by the comparative study of VPP and VPWO. However, the more important key for understanding and improving product selectivity is the activation of oxygen and the formation of active and selective surface species, regarded as omnipresent in abovementioned studies. We contribute the following facts about catalytically active oxygen in the VPO catalyst: (i) the activation of gas phase O_2 occurs at least in two distinguishable steps via surface [O_2] and [O] species. [O_2] species initiate the combustion of *n*-butane, whereas nucleophilic [O] can selectively

activate C-H bonds. (ii) H_2O in the gas phase likely promotes the dissociation of [O_2] into [O] sites, thus increases MAN selectivity. (iii) Oxygen exchange of the VPO catalyst based on VPP occurs exclusively over the reaction products and the amount of exchangeable O corresponds to a thin amorphous surface layer well-known from HRTEM studies[6]. (iv) MAN can re-adsorb on surface PO_xH_y groups, which are active for rapid scrambling of oxygen isotopes within MAN and H_2O. Our model of O_2 activation, which is supported by kinetic analyses of a parameters field test as well as isotope labelling studies, may explain the apparent MAN selectivity limit near 70 %, which has not been overcome for decades. Its origin could be the compulsory coexistence of selective and unselective oxygen species, as the latter are the precursor for the first ones. As has been realized very early, the concept of the riser reactor locally separating the reoxidation stage is a potential solution. Another approach might be the search for promotors of [O_2] dissociation. In the industrial process the co-feed of H_2O is an effective solution, however, limited by the stability of the catalyst at exceedingly high steam concentrations.

7 Outlook

Although VPP is the best catalyst known, it has limited options for optimization due to the inflexible crystal structure and limited effect of promotors[114]. Therefore, mixed transition metal $V_xM_{1-x}OPO_4$ might be a good starting point for novel catalysts with higher potential for improvement. It could be shown that solid state synthesis methods like solution combustion synthesis might be a good way to access mentioned new materials/structure motifs for catalysis. However, surface areas are quite low. Consequently, other synthesis methods like hydrothermal routes should be considered as well as supporting of the active catalyst. Transition metals should be selected based on their catalytic performance in oxidation catalysis or by their potential for reduction of vanadium since recent NAP XPS studies of VPO showed that under working conditions the average oxidation state of surface vanadium is +4.3[33]. Therefore, it is also necessary to understand the change in surface area or accelerate the surface area change by ex-situ pretreatment until a steady state is reached. Also other transition metals might be of interest. So far, this thesis indicates that vanadium and phosphorus are indispensable. However, this would be a long-term study with a low chance for industrial relevant success.

If the product pattern and kinetic aspects of a catalyst under certain reaction conditions can be regarded as a sensitive fingerprint for the nanostructure of the active site of a catalyst, then the apparent similarities between VWPO and VPP point at a similarly structured active domain. This aspect should be discussed in terms of the novel mechanistic reaction model suggested recently by Goddard et al.[22-24] The ROA mechanism is based on the redox-transformation of reduced $(VO)_2P_2O_7$ and oxidized X1-$VOPO_4$ phases. Such transformation cannot easily be transferred to the α_{II} phase of our VWPO catalyst, although the surface composition and structure of both VPP and VWPO systems are still under debate and unknown, respectively. This apparent contradiction has to be addressed in future surface-sensitive studies. Nevertheless, our result show that the active site is located inside an amorphous layer and might be similar for both catalysts, which stresses the need for identification of amorphous vanadium phosphorus oxide species. The lack of precise characterization methods for amorphous species on crystalline “support” is the main challenge. Modelling approaches might be promising. A long-time goal would be the identification of these amorphous species and synthesize them as bulk catalyst or

supported ones. This approach is challenging but will be important for a better understanding of the mechanism.

Instead of a structural analysis of the amorphous layer, SSITKA experiments might help to understand the thickness of the layer. Different synthesis parameters and catalytic properties of VPP and other catalysts like VWPO should be correlated with the thickness of the layer. Effects of pretreatments and performance might be explained from these results.

Further development and validation of the kinetic model is crucial. Experiments including macro kinetics like heat and mass transport limitation are advisable based on this micro kinetic model. The reaction network is quite simple and should include all other by-products. Therefore, detailed reaction network studies are necessary. Reaction intermediates have to be introduced over equilibrated catalysts. The role of bulk oxygen is quite controversial, so more detailed isotope labeling studies should be taken into consideration. For VPP we identified the reaction temperature as the most important factor to realize changes in MAN selectivity. A lower reaction temperature, however, is accompanied by a significant loss of activity, thus future efforts should address structural factors like specific surface area, e.g., by supporting VPP, or developing templating techniques.

8 References

[1] G. Ertl, H. Knzinger, F. Schth, J. Weitkamp, Handbook of Heterogeneous Catalysis, Wiley-VCH Verlag GmbH & Co. KGaA, Weinheim, Germany, 2008.
[2] G. Centi, Catal. Today 16 (1993) 5–26.
[3] C.-K. Dobner, M. Duda, A. Raichle, H. Wilmer, F. Rosowski, M. Hoelzle (2006) US 2,008,227,992.
[4] R. Glaum, C. Welker-Nieuwoudt, C.-K. Dobner, M. Eichelbaum, F. Gruchow, C. Heine, A. Karpov, R. Kniep, F. Rosowski, R. Schlögl, S.A. Schunk, S. Titlbach, A. Trunschke, Chem. Ing. Tech. 84 (2012) 1766–1779.
[5] G.A. Olah, Hydrocarbon Chemistry (Second Edition), 2nd ed., Wiley-Interscience, S.I., 2003.
[6] R. Schlögl, in: N. Mizuno (Ed.), Modern Heterogeneous Oxidation Catalysis, Wiley-VCH Verlag GmbH & Co. KGaA, Weinheim, Germany, 2009, pp. 1–42.
[7] A. Bielański, J. Haber, Oxygen in Catalysis, Dekker, New York, NY, 1991.
[8] S.G. Jadhav, P.D. Vaidya, B.M. Bhanage, J.B. Joshi, Chemical Engineering Research and Design 92 (2014) 2557–2567.
[9] G.J. Sunley, D.J. Watson, Catal. Today 58 (2000) 293–307.
[10] H. Hock, S. Lang, Ber. dtsch. Chem. Ges. A/B 77 (1944) 257–264.
[11] G. Centi, F. Trifiro, J.R. Ebner, V.M. Franchetti, Chem. Rev. 88 (1988) 55–80.
[12] J.S.J. Hargreaves, S.D. Jackson (Eds.), Metal oxide catalysis, Wiley-VCH, Weinheim, 2009.
[13] P. Mars, D.W. van Krevelen, Chem. Eng. Sci. 3 (1954) 41–59.
[14] F. Trifirò, R.K. Grasselli, Top. Catal. 57 (2014) 1188–1195.
[15] N. Ballarini, F. Cavani, C. Cortelli, S. Ligi, F. Pierelli, F. Trifirò, C. Fumagalli, G. Mazzoni, T. Monti, Top. Catal. 38 (2006) 147–156.
[16] C.H. Bartholomew, R.J. Farrauto, Fundamentals of Industrial Catalytic Processes, John Wiley & Sons, Inc, Hoboken, NJ, USA, 2005.
[17] J.-C. Volta, C.R. Acad. Sci., Ser. IIc: Chim. 3 (2000) 717–723.
[18] M.A. Pepera, J.L. Callahan, M.J. Desmond, E.C. Milberger, P.R. Blum, N.J. Bremer, J. Am. Chem. Soc. 107 (1985) 4883–4892.
[19] G. Busca, J. Catal. 99 (1986) 400–414.
[20] N. BATIS, J. Catal. 128 (1991) 248–263.
[21] G. Poli, I. Resta, O. Ruggeri, F. Trifirò, Appl. Catal. 1 (1981) 395–404.
[22] F. Cavani, G. Centi, F. Trifiro, Appl. Catal. 9 (1984) 191–202.
[23] G.J. Hutchings, M.T. Sananes, S. Sajip, C.J. Kiely, A. Burrows, I.J. Ellison, J.C. Volta, Catal. Today 33 (1997) 161–171.
[24] J.W. Johnson, D.C. Johnston, A.J. Jacobson, J.F. Brody, J. Am. Chem. Soc. 106 (1984) 8123–8128.
[25] H. Morishige, J. Tamaki, N. Miura, N. Yamazoe, Chem. Lett. 19 (1990) 1513–1516.
[26] R. Naumann d'Alnoncourt, Y. V. Kolen'ko, R. Schlögl, A. Trunschke, Comb. Chem. High Throughput Screening 15 (2012) 161–169.
[27] C. Markert, Angew. Chem. Int. Ed. 44 (2005) 2183–2184.
[28] S.L. Shannon, J.G. Goodwin, Chem. Rev. 95 (1995) 677–695.
[29] C.O. Bennett, in: Elsevier, 1999, pp. 329–416.
[30] S.L. Shannon, J.G. Goodwin, Appl. Catal., A 151 (1997) 3–26.
[31] A. Drochner, P. Kampe, J. Kunert, J. Ott, H. Vogel, Appl. Catal., A 289 (2005) 74–83.
[32] G. Busca, G. Centi, F. Trifiro, J. Am. Chem. Soc. 107 (1985) 7757–7758.
[33] C. Heine, M. Hävecker, E. Stotz, F. Rosowski, A. Knop-Gericke, A. Trunschke, M. Eichelbaum, R. Schlögl, J. Phys. Chem. C 118 (2014) 20405–20412.
[34] P. Ruiz, P. Bastians, L. Caussin, R. Reuse, L. Daza, D. Acosta, B. Delmon, Catal. Today 16 (1993) 99–111.
[35] G.W. Coulston, Science 275 (1997) 191–193.
[36] F. Cavani, S. Luciani, E. Degli Esposti, C. Cortelli, R. Leanza, Chem. Eur. J. 16 (2010) 1646–1655.
[37] E. Bordes, Catal. Today 1 (1987) 499–526.
[38] K. Inumaru, M. Misono, T. Okuhara, Appl. Catal., A 149 (1997) 133–149.
[39] P.A. Agaskar, L. de Caul, R.K. Grasselli, Catal. Lett. 23 (1994) 339–351.
[40] M. Abon, K.E. Béré, P. Delichère, Catal. Today 33 (1997) 15–23.
[41] B. Schiøtt, K.A. Jørgensen, Catal. Today 16 (1993) 79–90.

[42]B. Schioett, K.A. Joergensen, R. Hoffmann, J. Phys. Chem. 95 (1991) 2297–2307.
[43]J.T. Cleaves, G. Centi, Catal. Today 16 (1993) 69–78.
[44]J.T. Gleaves, G.S. Yablonskii, P. Phanawadee, Y. Schuurman, Appl. Catal., A 160 (1997) 55–88.
[45]J.T. Gleaves, J.R. Ebner, T.C. Kuechler, Catalysis Reviews 30 (1988) 49–116.
[46]K. Miyamoto, T. Nitadori, N. Mizuno, T. Okuhara, M. Misono, Chem. Lett. 17 (1988) 303–306.
[47]C.J. Kiely, A. Burrows, S. Sajip, G.J. Hutchings, M.T. Sananes, A. Tuel, J.-C. Volta, J. Catal. 162 (1996) 31–47.
[48]L.M. Cornaglia, E.A. Lombardo, Appl. Catal., A 127 (1995) 125–138.
[49]M. Eichelbaum, M. Havecker, C. Heine, A. Karpov, C.-K. Dobner, F. Rosowski, A. Trunschke, R. Schlögl, Angew. Chem. Int. Ed. 51 (2012) 6246–6250.
[50]M. López Granados, J.L.G. Fierro, F. Cavani, A. Colombo, F. Giuntoli, F. Trifirò, Catal. Today 40 (1998) 251–261.
[51]V.V. Guliants, J.B. Benziger, S. Sundaresan, I.E. Wachs, J.-M. Jehng, J.E. Roberts, Catal. Today 28 (1996) 275–295.
[52]F. Cavani, F. Trifirò, Appl. Catal., A 157 (1997) 195–221.
[53]J.-C. Volta, Catal. Today 32 (1996) 29–36.
[54]Y. Schuurman, J.T. Gleaves, Ind. Eng. Chem. Res. 33 (1994) 2935–2941.
[55]T. Okuhara, M. Misono, Catal. Today 16 (1993) 61–67.
[56]G.W. Coulston, E.A. Thompson, N. Herron, J. Catal. 163 (1996) 122–129.
[57]U. Rodemerck, B. Kubias, H.-W. Zanthoff, M. Baerns, Appl. Catal., A 153 (1997) 203–216.
[58]U. Rodemerck, B. Kubias, H.-W. Zanthoff, G.-U. Wolf, M. Baerns, Appl. Catal., A 153 (1997) 217–231.
[59]H.W. Zanthoff, M. Sananes-Schultz, S.A. Buchholz, U. Rodemerck, B. Kubias, M. Baerns, Appl. Catal., A 172 (1998) 49–58.
[60]M.J. Lorences, G.S. Patience, R. Cenni, F. Díez, J. Coca, Catal. Today 112 (2006) 45–48.
[61]G.J. Hutchings, C.J. Kiely, M.T. Sananes-Schulz, A. Burrows, J.C. Volta, Catal. Today 40 (1998) 273–286.
[62]G. Centi, J. Catal. 89 (1984) 44–51.
[63]P. Amoros, M.D. Marcos, J. Alamo, A. Beltran, P. Beltran*, MRS Proc. 346 (1994).
[64]P. Amorós, M.D. Marcos, M. Roca, J. Alamo, A. Beltrán-Porter, D. Beltrán-Porter, Journal of Physics and Chemistry of Solids 62 (2001) 1393–1399.
[65]F. BENABDELOUAHAB, J. Catal. 134 (1992) 151–167.
[66]G.J. Hutchings, A. Desmartin-Chomel, R. Olier, J.-C. Volta, Nature 368 (1994) 41–45.
[67]B. Kubias, H. Wolf, G.-U. Wolf, N. Duvauchelle, E. Bordes, Chem. Ing. Tech. 72 (2000) 249–251.
[68]V.V. Guliants, J.B. Benziger, S. Sundaresan, I.E. Wachs, A.M. Hirt, Catal. Lett. 62 (1999) 87–91.
[69]B. HODNETT, J. Catal. 88 (1984) 43–53.
[70]B.K. Hodnett, P. Permanne, B. Delmon, Appl. Catal. 6 (1983) 231–244.
[71]F. GARBASSI, J. Catal. 98 (1986) 317–325.
[72]V.E. Strempel, R. Naumann d'Alnoncourt, M. Driess, F. Rosowski, The Review of scientific instruments 88 (2017) 74102.
[73]V.E. Strempel, K. Knemeyer, R. Naumann d'Alnoncourt, M. Driess, F. Rosowski, Nanomaterials (Basel, Switzerland) 8 (2018).
[74]Verena Strempel, In situ gravimetric monitoring of Atomic Layer Deposition on powders using a thermal magnetic suspension balance, Beijing, 2016.
[75]V.E. Strempel, D. Löffler, J. Kröhnert, K. Skorupska, B. Johnson, R.N. d'Alnoncourt, M. Driess, F. Rosowski, Journal of Vacuum Science & Technology A: Vacuum, Surfaces, and Films 34 (2016) 01A135.
[76]S. Sajip, J.K. Bartley, A. Burrows, M.-T. Sanane´s-Schulz, A. Tuel, J. Claude Volta, C.J. Kiely, G.J. Hutchings, New J. Chem. 25 (2001) 125–130.
[77]G.J. Hutchings, J.K. Bartley, J.M. Webster, J.A. Lopez-Sanchez, D.J. Gilbert, C.J. Kiely, A.F. Carley, S.M. Howdle, S. Sajip, S. Caldarelli, C. Rhodes, J.C. Volta, M. Poliakoff, J. Catal. 197 (2001) 232–235.
[78]G.J. Hutchings, J.A. Lopez-Sanchez, J.K. Bartley, J.M. Webster, A. Burrows, C.J. Kiely, A.F. Carley, C. Rhodes, M. Hävecker, A. Knop-Gericke, R.W. Mayer, R. Schlögl, J.C. Volta, M. Poliakoff, J. Catal. 208 (2002) 197–210.
[79]J.A. Lopez-Sanchez, J.K. Bartley, A. Burrows, C.J. Kiely, M. Hävecker, R. Schlögl, J.C. Volta, M. Poliakoff, G.J. Hutchings, New J. Chem. 26 (2002) 1811–1816.

[80]T. Shimoda, T. Okuhara, M. Misono, Bull. Chem. Soc. Jpn. 58 (1985) 2163–2171.
[81]L.M. Cornaglia, E.A. Lombardo, J.A. Andersen, J.G. Fierro, Appl. Catal., A 100 (1993) 37–50.
[82]G. Busca, G. Ramis, V. Lorenzelli, Journal of Molecular Catalysis 50 (1989) 231–240.
[83]L.M. Cornaglia, E.A. Lombardo, in: Acid-Base Catalysis II, Proceedings of the International Symposium on Acid-Base Catalysis II, Elsevier, 1994, pp. 429–440.
[84]M. Abon, J.-C. Volta, Appl. Catal., A 157 (1997) 173–193.
[85]G. Centi, G. Golinelli, G. Busca, J. Phys. Chem. 94 (1990) 6813–6819.
[86]M. Ai, J. Chem. Soc., Chem. Commun. (1986) 786–787.
[87]G. Centi, F. Trifiro', Chem. Eng. Sci. 45 (1990) 2589–2596.
[88]Z. Sobalik, S.G. Carrazan, P. Ruiz, B. Delmon, J. Catal. 185 (1999) 272–285.
[89]Z. Sobalik, S. Gonzalez, P. Ruiz, in: Preparation of Catalysis VI - Scientific Bases for the Preparation of Heterogeneous Catalysts, Proceedings of the Sixth International Symposium, Elsevier, 1995, pp. 727–736.
[90]Z. Sobalik, P. Ruiz, B. Delmon, in: 3rd World Congress on Oxidation Catalaysis, Proceedings of the 3rd World Congress on Oxidation Catalysis, Elsevier, 1997, pp. 481–489.
[91]Z. Sobalik, S. Gonzalez, P. Ruiz, B. Delmon, in: 3rd World Congress on Oxidation Catalaysis, Proceedings of the 3rd World Congress on Oxidation Catalysis, Elsevier, 1997, pp. 1213–1222.
[92]G. Centi, J. Lopez-Nieto, D. Pinelli, F. Trifiro, Ind. Eng. Chem. Res. 28 (1989) 400–406.
[93]E. Bordes, Catal. Today 16 (1993) 27–38.
[94]M.-J. Cheng, W.A. Goddard, J. Am. Chem. Soc. 135 (2013) 4600–4603.
[95]W.C. O'Leary, W.A. Goddard, M.-J. Cheng, J. Phys. Chem. C 121 (2017) 24069–24076.
[96]Z.-Y. Xue, G.L. Schrader, J. Phys. Chem. B 103 (1999) 9459–9467.
[97]M. Abon, J. Catal. 156 (1995) 28–36.
[98]M. Eichelbaum, R. Glaum, M. Hävecker, K. Wittich, C. Heine, H. Schwarz, C.-K. Dobner, C. Welker-Nieuwoudt, A. Trunschke, R. Schlögl, ChemCatChem 5 (2013) 2318–2329.
[99]J. HAPPEL, J. Catal. 65 (1980) 59–77.
[100] P. Biloen, Journal of Molecular Catalysis 21 (1983) 17–24.
[101] J. Bigeleisen, M. Wolfsberg, in: I. Prigogine, P. Debye (Eds.), Advances in Chemical Physics, John Wiley & Sons, Inc, Hoboken, NJ, USA, 1957, pp. 15–76.
[102] T. Petzold, N. Blickhan, A. Drochner, H. Vogel, ChemCatChem 6 (2014) 2053–2058.
[103] B. DMUCHOVSKY, J. Catal. 4 (1965) 291–300.
[104] R.I. Bergman, N.W. Frisch, United States of America Patent (1964) US 3,293,268.
[105] H. Raffelson, R. Lee, T. J. Dolan, US Patent (1973) US3907707A.
[106] F. Cavani, G. Centi, F. Trifiro, Ind. Eng. Chem. Prod. Res. Dev. 22 (1983) 570–577.
[107] R.O. Kerr, US Patent (1960) US 3156705.
[108] K. Blechschmitt, P. Reuter, W. Friedrich, H. Paul, US Patent (1975) US 4077984 A.
[109] B.C. Trivedi, B.M. Culbertson, Maleic Anhydride, Springer US, Boston, MA, s.l., 1982.
[110] R. Fischer, H.-J. Gosch, W. Harder, K.-D. Malsch, M. Eggersdorfer, L. Franz, H. Zimmermann, K. Brenner, K. Halbritter, W. Sauer, H.-J. Scheiper, US Patent (1987) US 4940805 A.
[111] H. E. Bergna (1988) US 4769477 A.
[112] G.K. Kwentus, M. Suda, US Patent (1982) US 4501907 A.
[113] E.C. Milberger, N.J. Bremer, D.E. Dria, US Patent (1981) US 4350639.
[114] G.J. Hutchings, R. Higgins, J. Catal. 162 (1996) 153–168.
[115] G.J. Hutchings, Appl. Catal. 72 (1991) 1–32.
[116] F. Ghelfi, G. Mazzoni, C. Fumagalli, F. Cavani, F. Pierelli (2004) US 7,638,457 (B2).
[117] V.A. Zazhigalov, J. Haber, J. Stoch, A.I. Pyatnitzkaya, G.A. Komashko, V.M. Belousov, Appl. Catal., A 96 (1993) 135–150.
[118] H.-Y. Wu, H.-B. Wang, X.-H. Liu, J.-H. Li, M.-H. Yang, C.-J. Huang, W.-Z. Weng, H.-L. Wan, Applied Surface Science 351 (2015) 243–249.
[119] T.A. Bither, US Patent (1982) US 4371702 A.
[120] J.G. Firth, A. Jones, T.A. Jones, Combustion and Flame 20 (1973) 303–311.
[121] R. Mallada, M. Menéndez, J. Santamaría, Catal. Today 56 (2000) 191–197.
[122] X. Yao, Y. Zhang, L. Du, J. Liu, J. Yao, Renewable and Sustainable Energy Reviews 47 (2015) 519–539.
[123] R.M. Contractor, H.E. Bergna, H.S. Horowitz, C.M. Blackstone, U. Chowdhry, A.W. Sleight, Stud. Surf. Sci. Catal. 38 (1988) 645–654.

[124] R. M. Contractor, Circulating Fluidized Bed Technology II: Butane Oxidation to Maleic Anhydride in a Recirculating Solids Riser Reactor, Elsevier, 1988.
[125] E. Müller-Erlwein, Computeranwendungen in der chemischen Reaktionstechnik, VCH, Weinheim, 1991.
[126] S. Geupel, K. Pilz, S. van Smaalen, F. Büllesfeld, A. Prokofiev, W. Assmus, Acta Crystallogr., Sect. C: Cryst. Struct. Commun. 58 (2002) i9-i13.
[127] C. Heine, M. Hävecker, E. Stotz, F. Rosowski, A. Knop-Gericke, A. Trunschke, M. Eichelbaum, R. Schlögl, J. Phys. Chem. C 118 (2014) 20405–20412.
[128] M. Abon, J. Catal. 156 (1995) 28–36.
[129] S.C. Roy, R. Glaum, D. Abdullin, O. Schiemann, N. Quang Bac, K.-H. Lii, Z. Anorg. Allg. Chem. 640 (2014) 1876–1885.
[130] S.C. Roy, B. Raguž, W. Assenmacher, R. Glaum, Solid State Sci. 49 (2015) 18–28.
[131] Subrata Chandra Roy, Thermodynamically stable and metastable solids: New approaches to the synthesis of anhydrous phosphates containing vanadium, molybdenum, and/or tungsten. PhD Thesis, Bonn, 2015.
[132] S.L. Wang, C.C. Wang, K.H. Lii, J. Solid State Chem. 82 (1989) 298–302.
[133] C. Dobner, M. Duda, A. Raichle, H. Wilmer, F. Rosowski, M. Hoelzle, EP Patent (2006) EP1915210 (A1).
[134] A.L. Alberton, M. Schwaab, M. Schmal, J.C. Pinto, Chemical Engineering Journal 155 (2009) 816–823.
[135] S.S. Bump, G.P. Campbell, J.C. Dille, US Patent (1996) US 5911238 A.
[136] A. Varma, A.S. Mukasyan, A.S. Rogachev, K.V. Manukyan, Chem. Rev. 116 (2016) 14493–14586.
[137] Y. Dong, M. Geske, O. Korup, N. Ellenfeld, F. Rosowski, C. Dobner, R. Horn, Chem. Eng. J. 350 (2018) 799–811.
[138] O.V. Khavryuchenko, B. Frank, J. Phys. Chem. C 121 (2017) 3958–3962.